MECHANICAL PROPERTIES OF A NEW CLASS OF MGO-C CASTABLES WITH EXTRUDED GRAPHITE PELLETS

MASTER THESIS FOR GRADUATION AT THE CHAIR OF CERAMICS AT UNIVERSITY OF LEOBEN

Gerhard-Horst PASCHEK **MONTRÉAL, JULY 2004**

The sientific investigations for this master thesis have been performed at École Polytechnique the Montréal under the guidance of Professor Michel Rigaud in the years 2003 and 2004.

EIDESSTATTLICHE ERKLÄRUNG

Ich erkläre an Eides statt, dass ich diese Arbeit selbstständig verfasst, andere als die angegebenen Quellen und Hilfsmittel nicht benutzt und mich auch sonst keiner unerlaubten Hilfsmittel bedient habe.

AFFIDAVIT

I declare in lieu of oath, that I wrote this thesis and performed the associated research myself, using only literature cited in this volume.

_____ _____

Datum Unterschrift

Acknowledgements

First of all I want to thank Professor Michel Rigaud, director of research, for his support and his advice throughout this project, and for the great opportunity he offered me to do this thesis at École Polytechnique. Big thanks go to Mr. Eugene Paransky, researcher in CIREP, for all his time and his invaluable help he gave me without counting.

Special thanks go to Professor Harald Harmut, who, with the exchange program between the Montanuniversität Leoben and École Polytechnique, made it possible to do this work in first place.

I also thank all the students, researchers and other members of the CIREP who, by their ideas and their answers took part in the orientation of this project. Especially I have to thank Mrs. Huiqing He and Mr. Jean-Philippe Bouchard, whose help was invaluable during my research and Mrs. Huguette Rioux and Mrs. Théresa Crisson, who helped me when ever they could.

A very special thanks goes to my parents and my family which did not only support me financially but also with there love and help.

Last but not least I have to thank all my friends in Austria and Canada who supported me in my decision to do my thesis in a country far away from home and who also helped me with there friendship during this time.

Abstract

The project's objective was to evaluate and compare mechanical properties of a new class of MgO-C castables with extruded graphite pellets to MgO-C castables containing flake graphite or fine carbon and to a conventional MgO-C brick. In order to achieve this goal, 15 castable compositions were designed containing different amounts and forms of carbon. One of those castables was defined as "reference" and was used for comparison; the others were divided in four groups. The "reference" castable consists of 89,5% MgO, 1,5% silica fume, 5% extruded graphite pellets and 4% silicon. The reason why this composition was chosen as "reference" is, that prior research (e.g. corrosion tests) was done on it, were it showed very good comparable results. In group one carbon was introduced in form of extruded graphite pellets of the 4th generation. The amount of graphite pellets, the maximum MgO grain size and the size of the pellets were varied in this group. Group two was produced with flake graphite. The amount of flake graphite varies in this group to make it possible to compare this group to group one and to see the different influence between pelleted graphite and natural flake graphite. In group three different amounts of fine carbon were introduced into the "reference" composition. Group four shows the influence of antioxidants in magnesia carbon castables. In this group the amount of Si varies between 0% and 4%. In order to compare the castables with a regular MgO-C brick, one MgO-C brick was tested too.

All castables were pre-fired and then cooled down for prior testing. The reference castables, were pre-fired at either 1100, 1300 or 1500°C for 5, 10 and 15h, with a heating and a cooling rate of 300°C/hour (5°C/min). Based on the results of the HMOR-tests for the reference composition at 1100, 1300 and 1450°C for all compositions, the wedge splitting tests, the hot E-modulus and the modulus of rupture tests were performed at 1300°C, after pre-firing in coke at 1300°C, for 5 hours. This temperature assured better homogenization of the microstructure and interaction between the components, than 1100°C, and provided highest values of HMOR, which remained almost unchanged after longer pre-firing at 1300°C.

X-ray, optical microscope and SEM analysis have shown that after firing at 1300°C the microstructure of the castables containing Si as an antioxidant consist of MgO, Mg_2SiO_4, C, SiC and SiO_2 phases. The inner layer contains more SiC and less Mg_2SiO_4 than the outer layer. The carbon in the outside layer can be explained from secondary carbon formation during pre-firing. Another analysis showed that there is still some free Si in the sample pre-fired and tested at 1100°C.

Porosity plays a major role on all the properties of refractory materials, and particularly the mechanical properties. The comparison of the porosity of the castables has shown that the porosity is increasing with increasing carbon content. However, castables with EG pellets show an overall lower porosity than castables with flake graphite as carbon source.

Many macrostructural observations were carried out on the castables throughout the project. The observations were all made on pre-fired samples after testing either on bars or on wedge splitting test specimen. Especially different amounts of EG pellets and the extremes of the other groups compared to the "reference" sample were investigated. Different degrees of oxidations due to pre-firing and testing at different temperatures (1100°C, 1300°C and 1500°C) were observed as well as the formation of MgO whiskers on the outside of the castables after pre-firing and testing at 1500°C. The responsibility of Si for the secondary carbon formation is shown. It was found that the pellets are covered with a bright layer. It was observed in SEM that this is due to thin coating on the pellets. Also the darker outside layer and the brighter inside layer can be distinguished by visual observation.

The mechanical behaviors of the materials were assessed according to the linear and non-linear fracture mechanics theories. The parameters were measured and/or calculated using the 3-point bending test and the so-called wedge-splitting test.

By testing the hot modulus of rupture (HMOR) it could be observed that by increasing amount of Si the HMOR increases. This is true for samples with and without carbon. Introduction of EG pellets has a small, but negative influence in the strength; on the contrary the modulus of rupture is highly impacted by flake graphite. The higher porosity due to high water content in castables using flake graphite as well as weak bonding lead to very low values of HMOR. The addition of fine carbon lowers the HMOR values very slightly.

The modulus of elasticity is an important property of the materials, which makes it possible to strongly highlight their behaviour. It was found that within the margin of errors the E-modulus is higher for high Si amounts. The E-modulus decreases with increasing amount of EG pellets. The introduction of smaller maximum MgO grain size (<3 mm) has a positive effect and increases the E-modulus. The application of long EG pellets slightly increases the E-modulus. For flake graphite the modulus of elasticity decreases from low to high amounts. Fine carbon has almost no influence on the modulus of elasticity.

The study of the fracture behaviour (wedge splitting test) shows one of the key results of this work. First of all, all materials exhibit a marked non-linear behavior. A higher amount of Si has a positive influence on the work of fracture. With increasing amount of EG pellets, the work of fracture decreases. It can also be seen that the introduction of long EG pellets or the use of a smaller maximum grain size has almost no influence on the stress level necessary for the crack initiation. The same behaviour as with increasing amount of EG pellets can be observed with increasing amount of flake graphite or increasing amount of fine carbon, it also lowers the work of fracture.

The observed differences in high temperature properties of different castables evaluated in this work follow from the different microstructures formed in those castables

upon firing. The high strength levels (especially in castables with EG pellets and 4% Si) are due to extensive formation of Mg_2SiO_4 bonding phase, in part through reactions in vapour phase. The overall negative influence of carbon in the matrix on the bonding and, consequently, the strength, is significantly reduced when carbon is agglomerated in pellets without sacrifice in oxidation resistance.

Overall one can say that the introduction of EG pellets have a positive effect on the properties of MgO-C castables compared to castables with flake graphite as carbon source.

Résumé

L'objectif du projet est d'évaluer et de comparer les propriétés mécaniques d'une nouvelle classe de béton MgO-C constituée de granules de graphite extrudé (EG) avec celles de deux autres types de matériaux MgO-C, un béton à base de graphite naturel (en flocons) ou de carbone fin et une brique conventionnelle de MgO-C. Pour ce faire, 15 bétons de compositions différentes furent élaborés, dans lesquels la forme ainsi que la quantité de carbone utilisées variaient. Un béton de référence (dont la composition est 89,5% MgO, 1,5% fumée de silice, 5% granule de graphite et 4%Si) fut choisi parmi ces 15 compositions pour effectuer des comparaisons internes. Le choix de ce béton comme « référence » fut effectué en fonction de résultats préliminaires indiquant une excellente reproductibilité. Tous les autres bétons furent divisés en 4 groupes. Le premier groupe comprend des bétons dont le carbone est incorporé sous forme de granule de graphite. À l'intérieur de ce groupe, la quantité de carbone, la taille maximale des granules ainsi que la taille maximale des agrégats de MgO sont variées. Le second groupe comprend des bétons constitués de flocons de graphite. La quantité de graphite naturel fut ajustée d'un béton à l'autre de manière à pouvoir comparer les bétons de ce groupe avec ceux du premier et d'analyser l'influence de chaque type de graphite sur les propriétés des bétons. Dans le groupe numéro 3, différentes quantité de carbone fin furent introduites dans le béton de référence. Enfin, le groupe quatre a permis d'analyser l'effet des antioxydants dans les bétons magnésie-carbone. Dans ce groupe, la quantité de Si varie de 0% à 4%. Enfin, une brique MgO-C fut également étudiée dans le but de comparer les bétons aux briques.

Tous les bétons furent cuits et refroidis avant les essais. Le béton de référence fut cuit soit à 1100°, 1300° ou 1450°C pendant 5, 10 ou 15 heures avec une montée en température équivalente à 300°/heure (5°C/min). Sur la base des résultats obtenus lors d'essais de flexion à 1100, 1300 et 1450°C sur le béton de référence, les essais d'écartement par enfoncement d'un coin, ainsi que la mesure du module de rupture et celle du module d'élasticité, furent effectuées à 1300°C pour tous les échantillons, après

une pré-cuisson de 5 heures sur un lit de coke à 1300°C. Cette température permet en outre d'assurer une meilleure homogénéisation de la microstructure ainsi que de meilleures interactions entre les différents constituants. De plus, cette température permet d'obtenir des résistances en flexion plus élevées qu'une cuisson à 1100°C, les modules de rupture ne variant presque plus pour des températures de cuisson supérieures à 1300°C.

Les analyses effectuées en microscopie optique et électronique, ainsi qu'aux rayons-X, ont montré que la microstructure des bétons contenant du silicium comme antioxydant et cuits à 1300°C était constituée de MgO, Mg_2SiO_4, C, SiC et SiO_2. La couche interne est essentiellement constituée de MgO, Mg_2SiO_4, SiC, C et SiO_2, alors que MgO, Mg_2SiO_4, SiC et C composaient l'essentiel de la couche externe. La présence de carbone dans la couche externe est due à la formation de carbone secondaire pendant la cuisson. Une autre analyse montre par ailleurs qu'une certaine quantité de Si est toujours présente dans les échantillons cuits et testés à 1100°C.

La mesure de la porosité des bétons montre que celle-ci augmente avec la proportion de carbone présent dans les bétons. Cependant, les bétons contenant des granules EG présentent une porosité globale plus faible que ceux contenant du graphite naturel.

Plusieurs observations macrostructurales furent également effectuées sur les bétons durant ce projet. Les observations furent toutes effectuées sur des échantillons pré-cuits et après les essais mécaniques. L'investigation porta plus spécifiquement sur les comparaisons entre le béton de référence et des bétons contenants différentes quantités de granule EG ainsi que des bétons des autres groupes présentant des compositions « extrêmes ». Différents degrés d'oxydation dus à la cuisson ainsi qu'aux essais à haute température (1100, 1300 et 1500°C) furent observés en plus de la formation de tricluiters de MgO sur la face externe des bétons après cuisson à 1500°C. L'effet de Si dans la formation de carbone secondaire fut démontré. Par ailleurs, les granules sont toutes

recouvertes d'une couche très claire que l'observation au MEB permet d'identifier comme étant le résultat d'un mince dépôt. Enfin, la couche externe, plus sombre, était facilement distinguable à l'œil nu de la couche interne, plus claire.

Le comportement mécanique des matériaux fut étudié à l'aide des concepts de la mécanique de la rupture linéaire et non-linéaire. Les paramètres furent mesurés et/ou calculés à partir d'essais de flexion 3-points et des essais dits « d'écartement par enfoncement d'un coin » (WST).

La mesure du module de rupture à chaud (HMOR) permit de démontrer les points suivants. D'abord, le module de rupture augmente avec l'augmentation de la teneur en silicium des bétons, que l'échantillon contienne du carbone ou non. L'introduction de granule EG à par ailleurs une influence négative, quoique faible, sur la résistance mécanique des bétons alors que celle-ci est fortement influencée par l'ajout de graphite naturel. La porosité plus élevée de ces matériaux (due à une plus grande utilisation d'eau) ainsi que les faibles liaisons entre les constituants sont à l'origine des très faibles valeurs de résistance. L'ajout de carbone fin n'a à peu près aucun effet sur la résistance, les valeurs de HMOR obtenues n'étant que très légèrement plus faibles.

Le module d'élasticité est une propriété importante des matériaux et permet en outre de mettre clairement en évidence leur comportement. D'abord, le module d'élasticité des bétons est plus élevé (à l'intérieur des marges d'erreurs) lorsque la teneur en Si est plus élevée. De plus, le module d'élasticité diminue lorsque la quantité de granule EG augmente. L'utilisation de granules EG allongées permet cependant d'augmenter légèrement le module d'élasticité. Dans le cas du graphite naturel, le module d'élasticité diminue lorsque la teneur en graphite augmente alors que le carbone fin ne présente à peu près aucun effet. Enfin, une taille de grain maximale de MgO plus faible (< 3 mm) conduit à des valeurs du module d'élasticité plus élevées.

L'étude du comportement des bétons en fissuration (par WST) est l'un des résultats clé de ce travail. Tout d'abord, tous les matériaux présentent un comportement non-linéaire marqué. Une teneur plus élevée en Si conduit à une influence positive sur le travail de rupture. Une augmentation de la quantité de granules EG cause quant à elle une diminution du travail de rupture. Le même comportement est également observé dans le cas du carbone fin et du graphite naturel. De plus, l'introduction de granules allongées ou l'utilisation d'une taille de grain maximale plus faible n'ont à peu près aucune influence sur le niveau de contrainte requis pour l'initiation des fissures.

Les différences observées quant aux propriétés mécaniques à haute température des différents bétons étudiés dans le cadre de ce projet sont essentiellement dues aux différences existant dans les microstructures (formées lors de la cuisson) de ces bétons. Les résistances mécaniques élevées sont dues à la formation, en partie en phase gazeuse, de Mg_2SiO_4, lequel agit comme une phase liante (particulièrement dans les bétons contenant des granules EG et 4%Si). L'influence globale négative du carbone sur les liaisons dans la matrice et, conséquemment, sur la résistance mécanique, est réduite de manière significative lorsque le carbone est aggloméré en granules, sans pour autant sacrifier la résistance à l'oxydation.

Globalement, on peut donc dire que l'introduction de granules EG a une influence positive sur les propriétés des bétons MgO-C comparés au graphite naturel comme source de carbone.

Table of Contents

List of Tables

List of Figures

Introduction

The role of castable refractory materials for the steel industry as compared to bricks, has become more and more important in the last two decades. The advantages of castables are shorter manufacturing cycles, reduced energy consumption and manpower and simplified installation procedure. The physical, thermo-mechanical and thermo-chemical properties of castables have improved significantly due to improvement of raw materials, binders, bonding systems and additives. The development of castable refractories started with alumina-based systems and more recently magnesia-based systems are being used. To meet the demand of the modern steel industry, nowadays the emphasis is shifted towards carbon containing castable materials.

Carbon containing refractories for the slag-line of steel making ladles are in use in form of magnesia-carbon bricks since more than a decade. Their advantages are superior slag penetration resistance, excellent thermal shock resistance due to the non-wetting properties of carbon with the slag, good thermal conductivity, low thermal expansion and satisfactory toughness. Those properties have to do with the introduction of carbon in refractories and hence it is obvious to introduce this carbon into castables. However, it is more complicated to insert carbon into castables than into bricks.

The carbon source, which performs best in bricks because of its high crystallization, purity, oxidation resistance and corrosion resistance, is natural flake graphite. However, it becomes the worst solution to insert into castables, because of its non-wetting and anisotropic properties. It causes poor dispersibility in the castable mix and hence leads to high water demand and higher porosity of the material, lack of bonding with oxides and in consequence high oxidation rates at elevated temperatures.

The advantages of using carbon-bonded refractories are based on the presence of carbon. When carbon or graphite oxidizes, the porosity increases and hence the penetration of aggressive slag is bigger. Since castables are already more porous than

bricks, due to a higher water content (about 18% for castables and about 12% or less for common bricks), the oxidation will happen easier in castables than in bricks. Due to those reasons, protecting carbon from oxidations becomes even more important for carbon containing castables.

A way to protect carbon from oxidation in carbon containing bricks is to add various kinds of antioxidants: metallic additives or metal alloys and non-metallic additives, in particular borides. Several antioxidants used in MgO-C bricks cannot be used in carbon containing castables. The present of water and water vapour during the drying constitute a real challenge to the antioxidant additions.

Two important factors regarding the oxidation of basic carbon containing castables are the nature of carbon and hence graphite in relation with water and the selection of the right antioxidant agent. The challenges are the difficulties of inserting graphite into castables, the limitation of using antioxidants and the minimization of the porosity. Rigaud et al. (CIREP, Ècole de Polytechnique de Montrèal) found a way to insert graphite in form of pellets into the castable. In this way one can circumvent the non-wetting nature of graphite flakes and lower levels of porosity can be achieved. As the result of continuous research in this field and at the beginning of this thesis extruded graphite pellets of the 4^{th} generation were produced, which incorporate silicon as antioxidant.

The objective of this work is to investigate the physical and mechanical properties of a new class of carbon containing castables for steel ladle lining, which uses agglomerated graphite pellets as the source of carbon.

The particular goals of this thesis have been set as follows:

1. To measure the physical properties of the castables with extruded graphite (EG) pellets of the 4th generation such as porosity and the linear variation after firing.
2. To study the macrostructure of various castables with different amount of EG pellets compared to castables with flake graphite and fine carbon.
3. To measure the mechanical properties of the castables at high temperature with emphasis on fracture mechanical parameters, evaluated by the wedge-splitting test.
4. To study the microstructure of various castables with different amount of EG pellets compared to castables with flake graphite and fine carbon.

This thesis has been divided into 4 chapters as follows:

In chapter 1 a literature review on current refractories and MgO-C containing refractories in steelmaking has been made in order to establish the framework for this thesis. It covers a description of the different carbon sources, the manufacturing of carbon containing refractories as well as a short overview onto physical and mechanical properties of carbon containing refractories and also an overview on antioxidants and their properties.

In the chapter 2 the mechanical behaviour of refractory materials is reviewed. It starts from the fracture of the structures in general and concentrates on the mechanical behaviour of refractory materials. The most important mechanical parameters, which will be described, are the modulus of elasticity, the mechanical resistance and the crack initiation, the crack propagation and thermal shock parameters.

Chapter 3 describes the materials and the experimental techniques employed in this work.

The last chapter reports the results of all performed experiments. Initially, the physical properties of the castables are presented. The next section is used to describe

preliminary tests, which were used to plan all the following testing. In the section three the macrostructure of various castables is described. The last section is devoted to the mechanical properties and the presentation of the microfractographic study of the samples from the four different groups of castables, as well as that of the reference MgO-C brick.

Chapter 1. Refractories and MgO-C based Refractories

1.1. General information on refractory materials

Refractories are broadly defined as materials that have been engineered to withstand high temperatures and corrosive environments. Since the early days of mankind – after fire was discovered – the ability of certain minerals to resist fire is well known. Ancient people used them to produce goods like cement or pig iron to facilitate growth of their industries and further development of their civilizations.

Since the industrial revolution the importance of refractories in many different industries increased dramatically. People soon understood the crucial significance of refractory use for the industry refractory producing companies were established. Refractory producers knew the necessity of further development of their products concerning properties as well as production, which in return increased the variety of applications for refractories.

Constant improvements of refractories lead to increasing sales and growing consumption by the industry. Refractory producers still had to improve the properties of their products constantly to be able to fulfill the needs of their customers, which are generally the reduction of replacement and increased productivity.

Unfortunately for refractory producers the constant improvements of refractories in the end lead to decreasing specific refractory consumption in all fields. With the competition between refractory producers increasing and sales decreasing refractory producers (or at least the ones that are still in business) soon understood that a different approach was needed. Refractory companies could not sell refractories any more; they had to start selling ‘properties’.

In order to put the right properties in their bricks different technologies for refractory production were investigated and today's state of the art refractory producer needs a vacuum brick press to be competitive in shaped refractories. This sophisticated equipment leads to high production costs of refractory bricks due to the high capital cost of the vacuum press.

By looking at their process refractory producers realized that by producing unfired bricks for high temperature applications they could save some money avoiding the drying and firing in their furnaces. Hence drying and firing would be 'outsourced' to the customers who themselves use high temperatures in their processes anyway. Furthermore if unshaped refractories could be sold in order to even outsource the shaping process, savings would be even bigger. However this development would lead to greater competition due to less capital costs for equipment, which could lead to more producers of unshaped refractories.

Unshaped refractories have been on the market for a long time, but their use was limited due to the lack of good installation methods as well as properties of the refractories. In most cases they were only used for short time repairs. Hence refractory producers were constantly trying to improve the properties of their unshaped refractories and at the same time trying to find installation methods for them. If unshaped refractories could make the step from repairing materials to replace bricks, savings for refractory producers would make a significant difference. At the same time those unshaped refractories have to have the same properties in order to make them attractive to the customer.

Today unshaped refractories are not only broadly used as repairing materials but are already replacing bricks in many different applications. The installation methods used today also lead to cost savings. However installation of unshaped refractories and their

treatment before the first use are crucial to the performance while in operation. Hence different technology is needed and research is still an ongoing issue.

The main customer of refractories is the steel industry with approximately 70%, followed by the cement and lime industry, the ceramics industry, the glass industry, the chemicals industry, the non-ferrous industry and other industries. However the refractory consumption is not equally distributed all over the world. The biggest consumer is the Asian and Pacific region followed by Eastern Europe, Western Europe, the NAFTA and Latin America.

The steel industry is also one of the most challenging applications for refractories due to a big variety of processes, thermal, chemical and mechanical environments, vessel shapes and other logistic constraints.

In order to be able to have refractories available to satisfy all these different conditions, a lot of effort was put into research by refractory producers as well as some steel producers that realized the impact of refractories on the steel production. Still refractory materials are modified continuously to meet the evolving needs of the steel industry.

As new processes and procedures are deemed advantageous and therefore adopted, refractory modifications or new developments are required. Once the improved refractory has been engineered to withstand the service conditions, steel procedures make additional changes to further increase productivity, improve cleanliness or reduce costs, requiring further modifications to the refractory. This cycle has been repeated for decades leading ultimately to the steel processes and associated refractory materials that are considered standard today. So long as improved steel making processes are developed and improved refractory materials are available, this trend will almost certainly continue indefinitely.

Steel producers today face a very tough competition and even tough the refractories they use only make a small fraction of the total costs for steel production they try to save where they can

The primary advantage of monolithic refractories is that they can be used without the need of joins. These joins increase heat loss, gas permeability and are a week point for thermal stress forces.

Another factor is the easier installation of castables compared to bricks, in terms of labour and time requirements. Furthermore castables can be installed in almost any shape and hence zoning in the ladles lining can be easily performed and can be changed from one lining to the other one.

The big advantage of castables is the possibility of easy repair (even hot repairing of ladle linings by shotcasting is performed already today) which results in cost savings for refractories and reduction of waste material to a minimum.

Generally monolithic expansion is lower than that of bricks, which corresponds to less thermal stress and also higher thermal shock resistant.

However a disadvantage of castables is that they need to be cured after installation. This curing takes a multiple of the time for preheating the newly installed brick lining and hence is more expensive. Also the equipment for regulation of the temperature for the curing step – generally not yet implemented in a steel shop – is an important cost factor and needs to be considered.

In the first part of this study, one proposes to define the refractory material class, as well as the processes used to characterize it. One will stick then more particularly to

the interest, specificities and the stakes of magnesia carbon castables. The last part will be devoted to the properties of such refractory materials.

1.2 Status of carbon and graphite containing refractories

1.2.1 Background and early history

Carbon and graphite variously described as either black lead or plumbago have been well known to impact superior properties to refractories. More than 200 years ago Gousse Bonnin was granted a patent by George III for a crucible superior to those commonly known as “Black Lead Crucibles”. The crucible was comprised essentially of equal parts of clay and graphite. Joseph Dixon, in 1827, founded a factory in the USA to produce crucibles of black lead. He subsequently claimed that they were the first reliable melting pots ever made. He warranted every crucible to work with perfect safety “without regard to the degree of heat or sudden change of temperature” pointing here to one of the major advantages of graphite as a constituent in refractory bodies (Cooper, 1980). Percy’s *Metallurgy* (1875) describes a process for making plumbago crucibles resulting from the offer of a prize from the Society of Arts in 1828. Reference to Percy shows that at the time of publication black lead or plumbago crucibles were a well established product for the melting of a wide range of metals including gold, silver brass, copper and iron. This early supremacy of graphite in refractories has for many specific applications continued through to the present day.

References to the Refractories Bibliography published by the American Ceramic Society yields about 120 papers or patents relating to graphite and graphite containing refractories in a 20 years period from1928 to 1947. Most of these refer to graphite as a mineral or it’s processing but crucibles, nozzles, stoppers are referred to as well as its use in zircon refractories (Cooper, 1984). Using the internet as a modern data retrieval system using the keywords graphite and refractory more than 60.000 hints can be found. This is a reflection of the importance of graphite in modern refractories.

A considerable proportion of the total world production of graphite is made up of so called “amorphous” graphite, a misnomer for a micro-crystalline form which is not

sought after for the graphite refractories discussed here, principally because it is far less effective in engendering thermal shock resistance (Cooper, 1980).

1.2.2 Graphite as a raw material

Graphite can be found naturally in many parts of the world. The major raw material suppliers are China, Canada, South Africa, Brazil, Mexico and Korea. Graphite was built in metamorphic rocks as a result of thermal alteration of carbonaceous materials.

The graphite is conventionally mined crushed and graded before it goes through some refining processes to raise the graphite content. The main differences between the different suppliers of the raw material are the flake size and the level of impurities. Impurities are normally silicates, as would be expected from a natural mineral. The problem with the impurities is, that they are often pact between the cleavage planes of the graphite, which makes them mostly unrecoverable without braking down the flakes.

As mined, graphite exhibits a natural flake size and in the trade is described loosely as coarse, medium and fine flake and amorphous. Beneficiation is given sometimes to increase the yield of coarse flake of material supplied (Cooper, 1980).

As commonly known, graphite has a very special morphology. It is plate-like, with pronounced cleavage in the basal planes, which are responsible for its efficiency as a lubricant. Graphite has a hexagonal structure with a carbon-carbon distance of 1,42 Å in the layer and an interlayer separation of 3,35 Å (see figure 1.1).

To fully understand the unique function of graphite in refractory materials it is necessary to take a closer look on its chemistry. In molecular orbital terms, the carbon in graphite is hybridized in sp^2. This means that 3 of the electrons around the nucleus take up 3 equivalent orbits at 120° in a plane (Cooper, 1980). This accounts for the ability to

build a hexagonal planar structure, which means that there is no bonding ability perpendicular to the plane. This means that the surface of a graphite flake has a very low energy. Hence the reactivity is very low and the surface is not wetted by aqueous materials, organics or slags. Aqueous and organics are of interest during fabrication of refractories where it is necessary to attain adequate distribution of binders and their subsequent cohesion, but of course slags are of prime interest in terms of refractory performance.

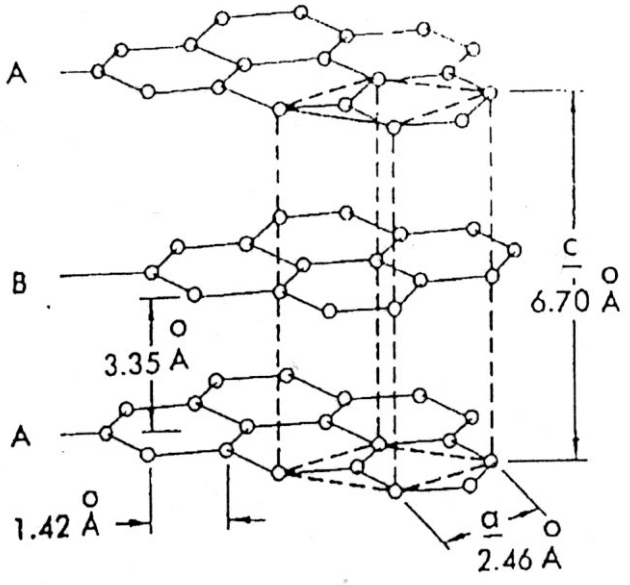

Figure 1.1. Crystallographic structure of graphite

The planar hybrid, which is covalent in nature has no miscibility with oxide slags. The only free bonding availability to the carbon atoms exists on the edge of the planar covalent structure.

The remaining electron from the carbon atom joins its neighbours and stays as an electron cloud between the layer planes. This is the main reason for exceptionally high electrical and thermal conductivity in the plane of the flake. Table 1.1 shows some of these properties of graphite compared to other forms of carbon and some common

refractory materials. Refractory oxide phases are invariably insulators at room temperature. At high temperature they can achieve a kind of semiconduction properties. The only electrical conductors with comparable properties would be carbides and hard metals. Of these two groups silicon carbide and molybdenum disilicide are really the only two with high temperature capability for general use as a refractory and in terms of thermal conduction only BeO amongst the oxides can compare in any way. Other forms of elemental carbon are more electrically resistive and not good thermal conductors which brings graphite to its important role in the refractory industry.

Table 1.1. Typical properties of graphite and other refractory materials

	Thermal Conductivity		**Resistivity**	
	cal/sec/cm2/°C/cm		ohm - cm	
	100°C	1000°C	20°C	1000°C
Natural Graphite	0,1 - 0,5	0,1 - 0,2	0,0005 - 0,002	
Synthetic Graphite	0,1 - 0,3		0,0001	
Pyrolytic Carbon	0,1 - 1,2			
Carbon	0,001 - 0,02		0,004	
Anthracite	0,0005 - 0,0008		10^{10} - 10^{14}	
Alumina	0,07	0,014	$> 10^{14}$	10^{7}
Beryllia	0,5	0,05	$> 10^{14}$	10^{8}
Zirconia	0,005	0,005	10^{8}	500
Mullite	0,013	0,008	$> 10^{14}$	
Silicon Carbide (dense)	0,17	0,22	10	4
Porcelain	0,004	0,005	$> 10^{14}$	10^{4}
Glass	0,005		$> 10^{14}$	

Even if this properties cannot be defined readily in scientific terms, graphite as a layered structure is very flexible and much like fibres which yields a certain toughness to the body.

Even with his highly refractory nature and its great thermal and mechanical properties, graphite can not operate alone in a large number of hostile environments. This is due do the relative ease with which it is oxidized and also because of its solubility in iron which is unsaturated with carbon.

The biggest disadvantage of graphite, since it is carbon, is, that it is capable of being oxidized. In comparison to less ordered carbon like cokes and blacks the oxidation resistance of graphite is quite good since its active parts in the structure are only around the flake edges. The oxidation, in a significant rate, starts between 600 and 700°C. To avoid oxidation and protect graphite in a non-protective atmosphere it needs to be formulated into a composite, or two-phase system.

There is no limitation on the use temperature of carbon on a physical point of view, since all forms of carbon do not melt. Carbon sublime at very high temperatures well in excess of 2500°C. However, the disadvantage for this high stability is that carbon is not able to achieve atom mobility which means that it is not possible to sinter carbon under practicable conditions. Hence the mineral must be with a second phase to bind together.

Graphite has no solubility for copper and aluminium which makes it highly suitable for those two metals. It is well known that there is of course a solubility in iron but as it will be shown this does not disqualify its use in the iron and steel industry.

Against this background of the properties of graphite it is possible to develop its use in refractories and to show how its unique properties contribute to the performance of bodies of which it comprises a part.

1.2.3 The manufacture of graphitic refractories

As outlined above, it is not possible to sinter graphite under practicable conditions. Hence graphite needs at least one second phase as binder. Traditionally this was clay, which is still in use for certain products. However, in today refractory bricks pitch or tar is used for a wide range of materials providing initially a viscous, cohesive phase which permits a binding of the particulate material and subsequently provides a carbon bond, not truly graphitic, to hold the body together after pyrolysis. The extent of this bond depends on the binder and the carbon yield it provides on degradation (Cooper, 1980). The value of such organic binders has long been known and Percy (1875) refers to the use of fatty matter to make carbon crucibles. Today sophisticated chemicals such as phenol-formaldehyde are used as carbon precursors even in the manufacture of commercially practicable refractories.

Because of the non-wetting behaviour of the low energy graphite surfaces the mixing of the various binders is sometimes very complicated, since the liquid phases do not have a natural tendency to spread. Hence mixing can be seen more as a “buttering” or shearing process in which deep experience and understanding are of value. Surfactants although considered are seldom of any real value in improving the wetting.

As mentioned before graphite has a very poor oxidation resistance. To provide some measure of oxidation resistance one mixes graphite with an oxide or second phase. This second phase than also requires consideration with respect to the binder. If this is an oxide or clay there is a virtual incompatibility in bond terms between the covalency of the graphite and the ionicity of the oxide. It is a well known state of the art that an addition of silicon is made to graphite containing refractories. This silicon provides a bridge between the two bond types. The silicon normally reacts to silicon carbide, silica and, depending on firing conditions and body size, as silicon nitride or oxynitride (Cooper, 1980).

Graphite, being plate-like in morphology, behaves anisotropically in fabrication. It has to be taken care of avoiding lamination, which, if occur, can lead to major failure. On the other hand, because the physical properties of the flake are anisotropic, it is possible to design the properties of products to a degree since it is possible to make products with controlled orientation. It is possible to overcome this anisotropy by milling the graphite flakes to a small particle size. However, the superior thermal properties of graphitic refractories are dependent to an extent on flake size. To achieve best properties a compromise between smaller flakes, which means superior densities and strengths, and a good thermal shock resistance, which is lower for smaller flake sizes, has to be found.

The flake-like nature and the bad wettability of the graphite also leads to a tendency to give a more open texture, and in absence of a true sintering process the higher porosity is a problem which has to be solved. On the other side, due to no sintering, the shrinkage during firing of the refractory products is very low.

Because of the poor oxidation resistance of graphite at high temperature firing is crucial and hence has to be done neutral, protective, glazed or buried in coke dust or some similar protective medium. Firing temperatures are usually limited because of the protective atmosphere requirements and also because in the presence of oxide phases reductive reactions will occur at very high temperatures. Hence firing temperatures for graphitic refractories are usually in the range of 1100°C to 1500°C.

Some graphite containing refractories, especially bricks and special products are glazed as a final finishing process to give oxidation resistance. Here again the problem is that the surface of the refractory to be glazed consists of a certain part of graphite which again brings up certain wetting problems with typical oxide glazes. Controlled firing cycles to oxides just the graphite on the surface of the product and glazes which contain silicon are two of the methods to overcome these difficulties.

1.2.4 Physical and mechanical properties of carbon containing refractories

As already explained carbon in the form of graphite must be judged unique. It does not fit into any of the periodic group similarities as do most elements. The nearest equivalent of carbon is the compound boron nitride which is isostructural with graphite and is composed of the elements either side of carbon in the periodic table. Graphite is electrically and thermally highly conducting compared with all other non-metallics. It is highly anisotropic and, with a melting point of about 3500°C (under pressure) it is arguably the most refractory element.

With the exception of iron in which graphite will dissolve it is inert to many metals. It is insoluble and through an oxidation – reduction process it reacts with all oxide systems at high temperatures. The only weakness of graphite is its big tendency to oxidation at temperatures above 600°C.

a) Physical Properties:

Thermal expansion:

Cooper (1987) described the expansion of this kind of multiphase systems roughly by a mixtures law, if it is assumed that the graphite does not contribute to the expansion. Hence, there is a close relationship between expansion and graphite content as can be seen from figure 1.2, with an increase in graphite causing a pronounced drop in thermal expansion. The importance of the thermal expansion is that it markedly influences thermal shock and is a factor in all thermal shock parameters. Within the limits of accuracy, after a few percent addition, there is a proportionality relationship and the expansion of the composite α_c can be reasonably accurately predicted from the mixture law assuming that the graphite expansion is zero, that is the expansion is directly proportional to the volume fraction V_f of the oxide phase and its thermal expansion α_o:

$$\alpha_c = V_f \alpha_o \tag{1.1}$$

One can use this relationship for other carbon bonded composite systems, but it is less valid for ceramic bonded systems. Even if, with those results, it is hard to show the effect of graphite flake size, it is clear that if there is one it is very small.

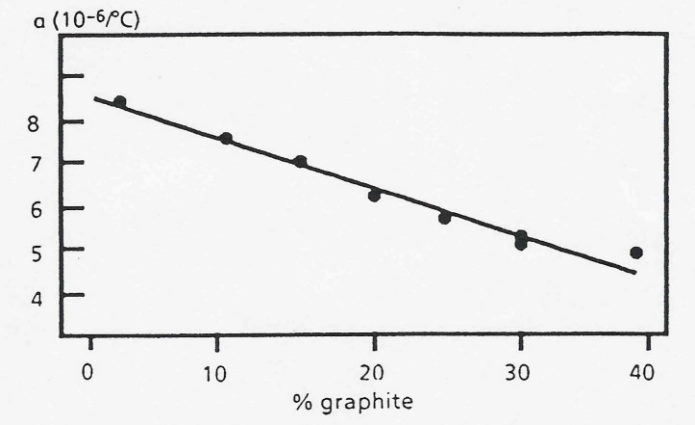

Figure 1.2. Relationship between thermal expansion and graphite content for an alumina-graphite (Cooper, 1986)

Thermal conductivity:

The thermal conductivity of a two phase system to a first approximation is described by a mixture law (Cooper, 1994). Although graphite has a high thermal conductivity it is highly anisotropic. Observations on compacted natural graphite gave results in the direction of the plane layer in the region of 100-300 W/mK, and normal to the plane layer of 10-20 W/mK. Thus the anisotropy was in the range 10 to 35:1, the higher figure deriving from coarser graphite with higher aspect ratios. Thus graphite will significantly affect that of the body into which it is incorporated, particularly because the conductivity of a typical fired oxide refractory will be only a few W/mK. Figure 1.3 presents the conductivity quoted in some commercial literature representative of various magnesia-graphite.

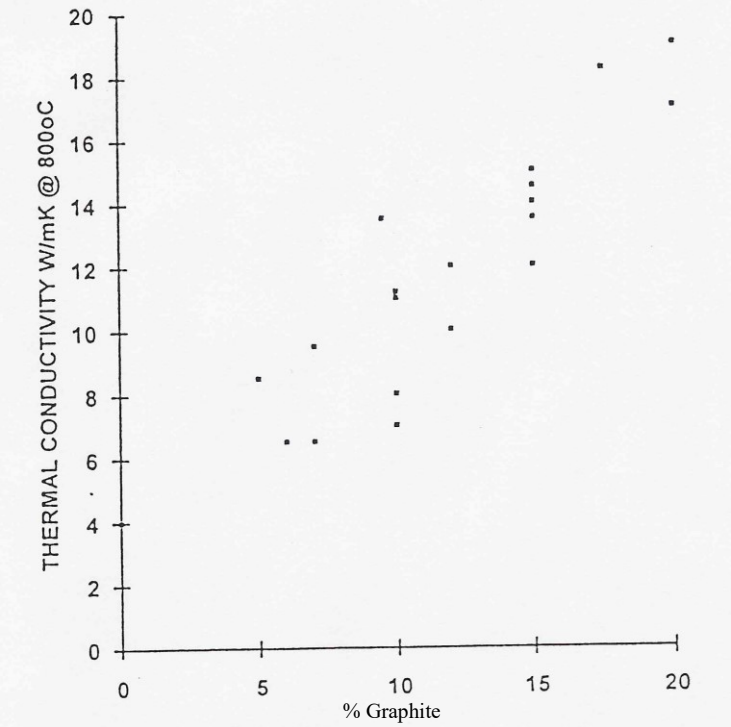

Figure 1.3. Thermal conductivity MgO-C versus graphite (Cooper, 1994)

Electrical resistivity:

More than any other non-metallic element or compound, graphite is highly electrically conducting. In its layer plane its conductivity is as good as many metals. In refractories it will provide a conductive path through the system, a feature which is enhanced by the forcing of the flakes into alignment around the grains during pressing. Thus with this alignment and the lenticular nature of the graphite, low resistivities can be achieved at relatively low graphite contents. There is some indication that the flake size affects resistivity, an effect which is more pronounced at low graphite levels, presumably because of a greater number of resistive links reducing the continuity to a greater degree than at high concentrations, where such factors might be masked(Cooper, 1994).

There is no other refractory, which is economically viable, which can give such levels of conductance, in combination with both the corrosion resistance and thermal shock resistance required for this purpose.

b) Mechanical Properties:

Modulus of rupture:

The strength of a refractory is often an indicator of the bonding in the body. Since there is no bonding between graphite and the ceramic matrix/grain, graphite does not contribute to the strength. With increasing graphite content the strength drops and different literature shows that with an addition of 50% graphite the strength is lowered by an order of magnitude. There is also an indication that the strength drops with increasing in flake size, perhaps doubling as coarse graphite is replaced by fine (Cooper, 1994).

Young's Modulus:

The Young's modulus is not greatly affected by graphite content, but is possibly lower in carbon bonded systems, and increases with decrease in flake size, which would be expected if there is less disruption of the structure. It is also clear that graphite containing bodies have much lower moduli (5 to 20 GPa) than conventional fired refractories (30 to 100 GPa), suggesting poor structural coherence (Cooper, 1994).

What is more significant in respect of graphite is the stress – strain curve. Such a curve for a ceramic bonded alumina-graphite is shown in figure 1.4. What can be seen is that the stress – strain curve is not linear, and there is still some structural coherence after peak stress. Similar curves are appropriate to carbon bonded systems.

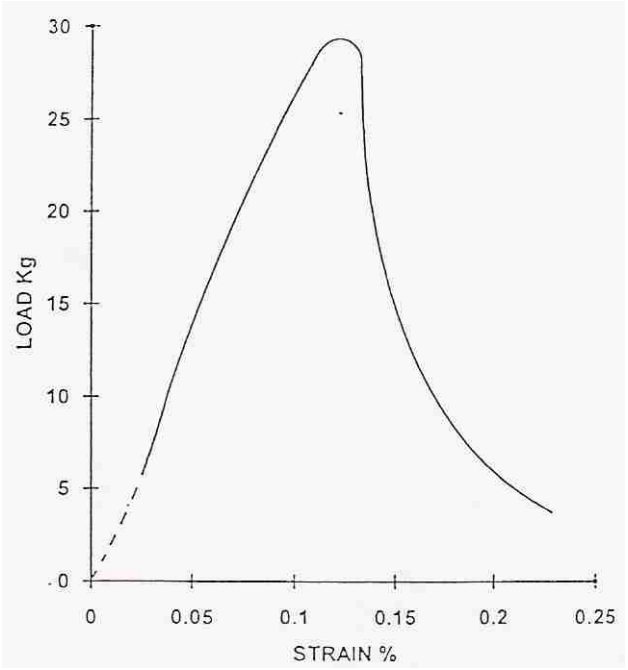

Figure 1.4. Stress-strain to fracture for ceramic bonded alumina-graphite (35% graphite; Cooper, 1994)

Work of fracture:

The area under a stress – strain curve is a measure of the work of fracture. With increasing graphite content, the work of fracture increase (figure 1.5). Cooper (1994) also showed that coarse graphite gives higher work of fracture than fine graphite for given graphite content. More detailed information to the measurement and calculation of the work of fracture are given in chapter 2.

c) Thermo Shock Resistance:

Cooper (1986) pictured that the outstanding attribute of graphite is its thermal shock resistance, recognized by the earlier manufacturers of graphitic refractories. It has generally been ascribed to the high thermal conductivity of the composite body produced by the incorporation of graphite, coupled with a moderately low thermal expansion. This is to Cooper almost certainly too simplistic an approach. Indeed, if one applies the

modern theories of Hasselman (1969), then the important features are seen to be a high work of fracture value, a low modulus of elasticity and low thermal expansion.

Hasselman defined a number of thermal shock parameters which might be applied to refractories; the one that is judged relevant to the graphitics is:

$$R_{ST} = \sqrt{\frac{\gamma_{wof}}{E\alpha^2}} \tag{1.1}$$

Where γ_{wof} is the work of fracture, E is the Young's modulus and α is the thermal expansion.

Cooper (1986) also showed that the work of fracture has a direct dependence upon graphite content (figure 1.5).

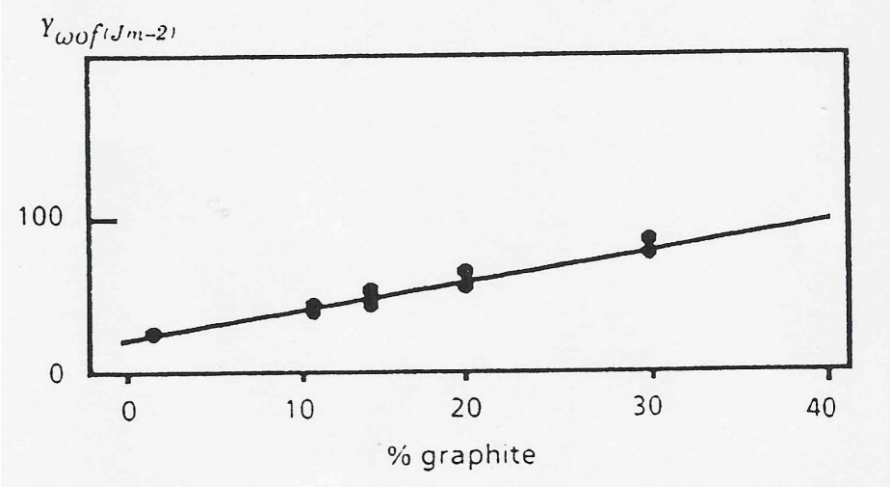

Figure 1.5. Influence of graphite on work of fracture (Cooper, 1986)

It is also influenced by factors such as bonding system, but generally graphitic materials have high values of work of fractures in relation to many of the more conventional refractories. The high values can be explained by a number of factors. For

example, graphite can give a complex crack path and cause crack branching. It has the ability to absorb energy through slip and it can act as a plate-like reinforcement, absorbing energy either through pull-out or actual flake fracture.

A low modulus of elasticity is common to most graphitics containing coarse flake graphite and is probably due to its poor bonding to the other phases.

Thus, if the Hasselman parameter R_{ST} is accepted as measure of thermal shock resistance, then graphite influences it to advantage by engendering low thermal expansion, high work of fracture and low elasticity modulus.

d) Corrosion Resistance:

Graphite, being a covalent material, has a little or no affinity for oxide phases which, when molten, are primarily ionic in nature. Therefore graphite refractories have long been recognised for their resistance to wetting by slags and some metals. In respect of some metals a similar incompatibility of bond type results in a resistance to dissolution. Hence any reaction with slags probably takes place through an oxidation – reduction step.

Because of its inability to actually dissolve in slags, the graphite phase of any composite refractory is highly inert relative to the oxide constituents. Conversely, the oxide phases in these composites are insoluble in metal. The two phases can therefore be said to be mutually protective, the graphite protecting the oxide in a slag environment. Where the slag removes the oxide phase, exposing the graphite, it can no longer wet or penetrate to attack more deeply in the structure. Conversely, material which has been immersed in steel, for example, has the graphite removed, exposing a surface which is all oxide phase and no longer soluble.

For flux resistance, the refractory as a whole probably requires no more than about 10% by weight of graphite. However, in respect of thermal shock resistance, there is often a need for 25-30% (Cooper, 1986).

e) Oxidation and anti-oxidants:

Refractories containing graphite have been shown to have exceptional properties deriving from its presence. It is therefore appropriate to ask why it is not used on its own. The principal answer is of course that it will readily oxidize above 400 – 500°C. This is the weakness of graphite refractories and one which needs techniques to be adopted to prevent or reduce oxidation. These are primarily the use of glazes, both external and internal, oxygen getters and pore blockers. There are also peculiar situations relating to MgO-C, where due to internal reactions, a dense zone of magnesia forms which reduces the ingress of oxidizing gases.

Oxidation Kinetics:

The oxidation of graphite is most unusual in that it occurs with an extreme of anisotropy. In a perfect crystal it is believed that oxidation takes place only at the edge. A perfect layer plane would offer no site for oxygen to react with the carbon. In reality this is not the case and some attack does take place through the layer plane via, almost certainly, points of imperfection. This can be seen in oxidation pits which are negative crystals of graphite with holes with a hexagonal outline (Cooper, 1994). Some oxidation effects are shown schematically in figure 1.6.

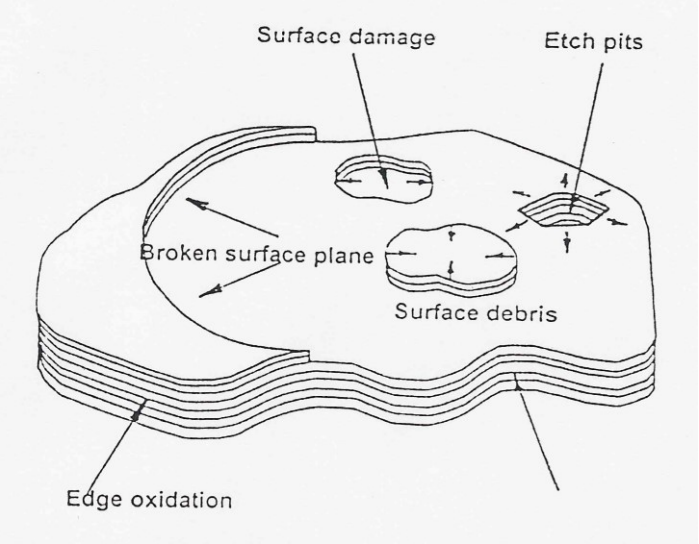

Figure 1.6. Schematic of oxidation mechanisms operative in the oxidation of a graphite flake (Cooper, 1994)

Antioxidants:

Many types of antioxidant additions to graphitic refractories are in use. Either metals such as silicon, aluminium or magnesium, or compounds such as boron carbide. There are two main mechanisms to explain the way of operation of those antioxidants. Either the material may act as a getter and take the oxygen preferentially, or the oxidation causes an increase in size of the addition as the oxide is formed, thus working as pore blocker. Additionally boron and silicon compounds may give rise to some internal glazing.

It must be realised that in some systems, one of the prime requirements is to protect the carbon bond, since its destruction would destroy the coherence of the structure even if the graphite, as such, was largely untouched. The carbon bond is far more reactive than the graphite and probably represents only 1-2% of the material by weight. Thus the potential of small metal additions to preferentially consume the oxygen is there, although it must be seen as only a transient, since once the metal is consumed, the bond will be again exposed to oxidation.

Carbides or nitrides will generate gaseous oxidation products such as carbon oxides or nitrogen. These will build up a protective atmosphere in the system which can only be removed by diffusion of the reaction products out of the system.

1.2.5 Packing carbon into castables

In the last years the most promising way to overcome the difficulties of using flake graphite in castables, is, to introduce graphite in extruded graphite pellets.

The making of the meanwhile four generations of extruded graphite pellets were described by Rigaud et al. (2003). The pellets which were used for this work are from the 4th generation (EG-4). The efforts for these pellets have been concentrated on improving the strength of the pellets and their ability of withstanding strong mechanical mixing, which would be required in industrial scale production. A resinous hydrocarbon binder, dissolved in an organic solvent, was used to replace the original organic binder after the heat treatment of the pellets. The new binder contributed to the final strength of the pellets, and also modified the surface of the pellets, making them more easily dispersible in water based castables. The antioxidants in the EG-4 pellets were based on Si.

From pellets of the first generation to EG-4, not only the strength but also porosity, density and oxidation resistance were improved. Figure 1.7 shows the pore size distribution of EG pellets of the 3rd and 4th generation by mercury porosimetry measurement.

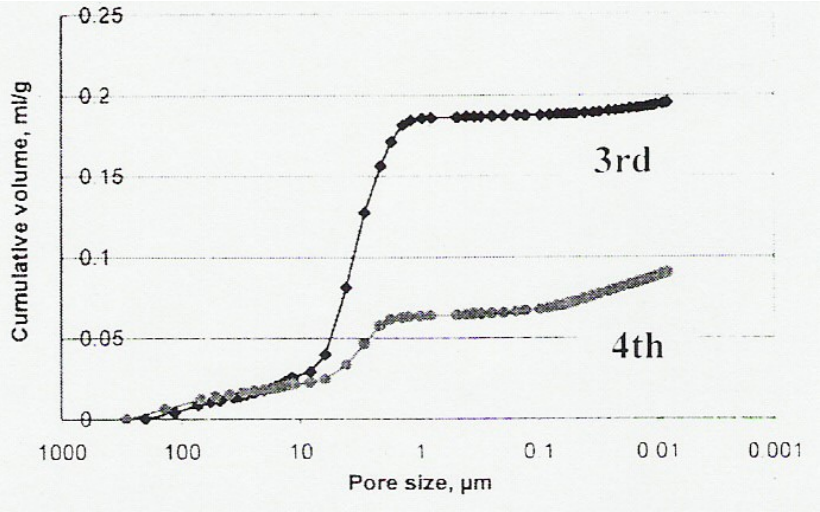

Figure 1.7. Pore size distribution of EG pellets of the 3rd and 4th generation by mercury porosimetry measurement (Rigaud, 2002)

Using the new pellets, it was possible to reduce the water addition needed in the $MgO\text{-}SiO_2$ castables from 6% H_2O in the 3rd generation to 4,8% in the 4th, and to improve the flowability. Figure 1.8 illustrates the effects of pellets of the 3rd and 4th generation on the rheology of $MgO\text{-}SiO_2$ castables.

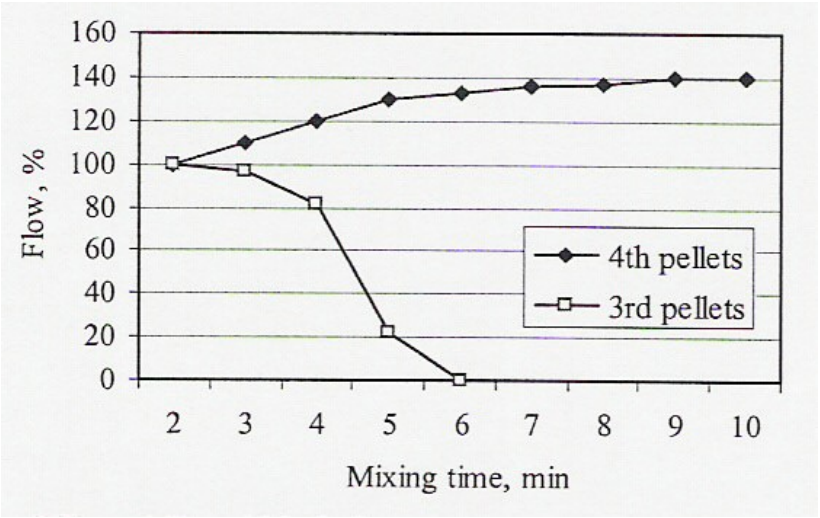

Figure 1.8. Flowability of MgO-C castables with EG pellets (5%) of the 3rd and the 4th generation (Rigaud, 2003)

Other improvements, like better oxidation resistance and corrosion resistance of EG-4 pellets as well as secondary carbon formation could be observed during development. Figure 1.9 shows the oxidation index of MgO-C castables with different carbon sources and EG-antioxidant pellets (6% C). Mechanical and physical properties are furthermore tested and explained during this work.

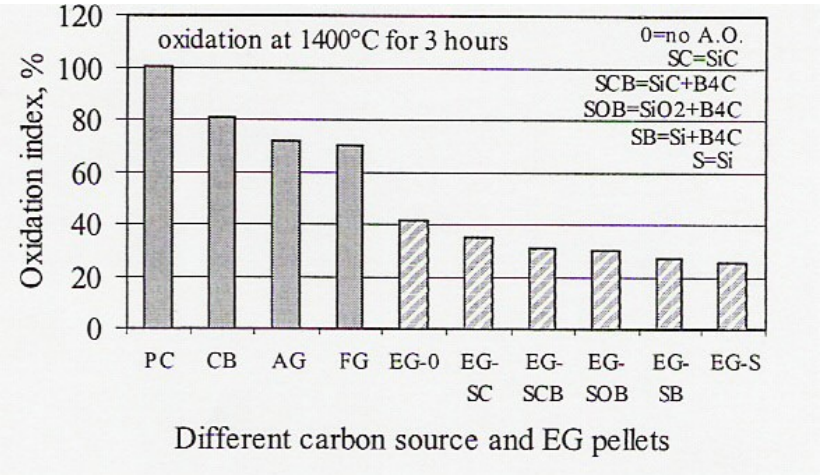

Figure 1.9. Oxidation index of MgO-C castables with different carbon sources and EG-antioxidant pellets (6% C; Rigaud, 2003)

Chapter 2. Mechanical behaviour of refractory materials

2.1. Fracture of the structures

The way in which the structures in service behave depends largely on the properties of the materials used, in particular of their mechanical behaviour at the time of the request. The choice of materials generally depends on the application and on the geometry of the structure but especially on the stress during the service (Shah et al., 1995).

The majority of structural materials can be divided into three categories according to their mechanical behaviour: fragile, ductile or "quasi-fragile" materials. The fragile materials are materials in which a crack will be propagated in a catastrophic way (at speeds close to that of the sound) as soon as the stress anywhere in the material reaches its mechanical resistance. Glass and certain fine ceramics are the best examples of this type of materials. In ductile materials (like metals), the stress, as it increases, can be redistributed in the structure by plastic deformation. In tension, this characteristic makes it possible for ductile materials to maintain certain integrity without catastrophic rupture even if the local stress becomes higher than the yield stress. Rupture occurs when the stress in all the sections becomes higher than the resistance of the material. The quasi-fragile materials are characterized by behaviour completely different from the two first. When the local stress reaches the value of the mechanical resistance of the material, one generally observes the appearance of a crack and a reduction in the load which supports the material. However, the crack is not propagated in a catastrophic way, it stops or is propagated in a stable way depending on the applied load. The important point is that a material of this kind can continue to fulfill its role even if it is cracked, since it always has a certain remaining resistance. The best examples of this type of materials are the concretes (civil engineering), certain advanced ceramics (e. g. stabilized zirconia) and the refractory materials. Figure 2.1 schematizes each of these behaviours. In each case, the

distribution of the stress around the defect (or at the head of a crack) at the time of the rupture will depend on the mechanical behaviour of the material.

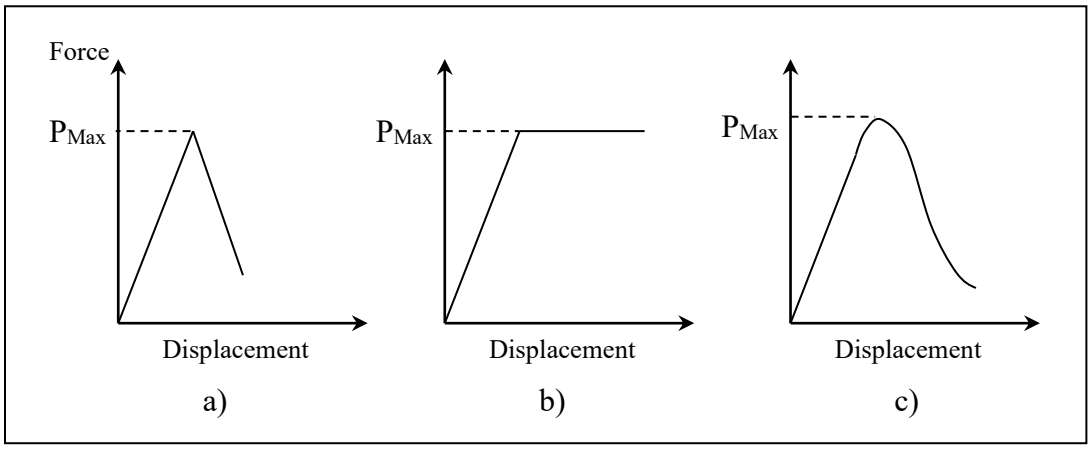

Figure 2.1. Mechanical behaviour of various types of materials. a) fragile materials, b) ductile materials, c) quasi-fragile materials.

The design of the structure and the choice of the materials in addition require the definition of selection criteria, based on the properties of the materials, which in return consider their capacity to achieve their task. With the natural defects in each material, and with the particular geometry of certain structures, the simple knowledge of the mechanical resistance of a material is insufficient to make an adequate choice. The need for reliable criteria led to the development of the theories of the linear elastic rupture mechanics, which makes it possible to study and determine the capability of a material to resist a certain load with a given geometry. In the case of fragile materials and ductile materials (in plane deformation), a criterion based on resistance (or an energy balance) is generally sufficient to describe their behaviour, since there will be catastrophic rupture primarily when the maximum stress is reached locally or when a crack has reached a critical length. In the case of quasi-fragile materials, the initiation of a crack is not balanced by a catastrophic propagation, but rather by a more or less slow propagation corresponding to an increasing drop of the resistance of the material. For this reason, at least two criteria of rupture must be defined, one for the initiation of the crack, the other for the propagation.

2.1.2. Elements of the linear elastic rupture mechanics

The linear elastic rupture mechanics are of interest, particularly in the moment when the conditions of sudden rupture are met in a material. The important parameters for sudden rupture are critical size of the defect or critical intensity of the stress. The definition of the criterion can be done according to two equivalent approaches: a mechanical approach based on the analysis of the stress area at the head of the crack and an approach based on the energy balance of a system at the time of cracking.

The mechanical approach starts from the fundamental relations of elasticity, to determine the distribution of the stress at the head of a crack, depending on the opening method of the crack. In case of an opening in tension (Method I), Westergaard (1939) developed the following relations for an infinite plate with an elliptic crack inside with the length 2a (see also Figure 2.2 for the definition of the variables):

$$\sigma_x = \frac{K_I}{\sqrt{2\pi r}} \cos\frac{\theta}{2}\left(1 - \sin\frac{\theta}{2}\sin\frac{3\theta}{2}\right) \tag{2.1}$$

$$\sigma_y = \frac{K_I}{\sqrt{2\pi r}} \cos\frac{\theta}{2}\left(1 + \sin\frac{\theta}{2}\sin\frac{3\theta}{2}\right) \tag{2.2}$$

$$\tau_{xy} = \frac{K_I}{\sqrt{2\pi r}} \sin\frac{\theta}{2}\cos\frac{\theta}{2}\cos\frac{3\theta}{2} \tag{2.3}$$

One defines the stress intensity factor K_I the following way:

$$K_I = \lim_{r\to 0} \sqrt{2\pi r}\,\sigma_y\left(r, \theta = 0\right) \tag{2.4}$$

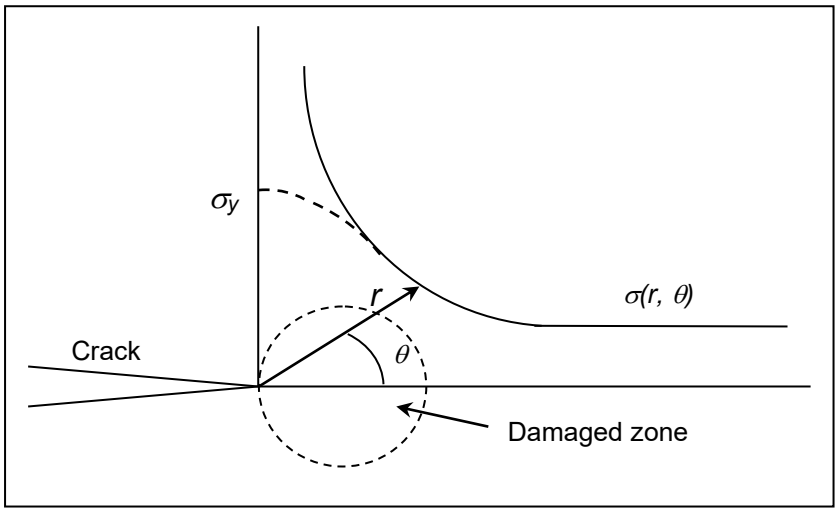

Figure 2.2. Stress field and zone of damage at the head of a crack (Brisson, 2002)

In a general way, one obtains:

$$K_I = Y\sigma\sqrt{a} \tag{2.5}$$

where Y is the form factor which depends on the geometry of the sample and the load. For the infinite plate, one defines:

$$K_I = \sigma\sqrt{\pi a} \tag{2.5}$$

The value of K_I shows a special characteristic in the stress field at the head of the crack (Figure 2.2). Indeed, for r $\rightarrow$ 0 following equations 2.1 to 2.3, the stress tends towards infinity. Since such a stress is impossible for an actual material, a deformed zone develops in the materials (e.g. plastic deformation in metals) to adapt this stress. In quasi-fragile materials like refractory materials, a zone similar, known as "zone of damage" leads to the same result. This zone will be described in detail further in this chapter.

When the stress intensity factor reaches a critical value (noted K_{IC}), the crack is propagated in a catastrophic way in the material. On the basis of the linear elastic rupture mechanics, K_{IC} is a property of the material and can be used as a criterion for crack initiation.

The whole problem can also be considered according to an energy approach, originally suggested by Griffith (1922). Generally, this approach corresponds to make an energy balance on a plate containing a crack length *a* and a tension *P*. the potential energy of the subjected system can be written (Shah et al., 1995):

$$\Pi = U - F + W \tag{2.6}$$

In equation 2.6, *U* corresponds to the elastic energy stored in the structure, *F* is the work carried out by the external forces and *W* is the necessary energy for the formation of a crack. For a projection "*da*" of the crack, the system will be in balance when:

$$\frac{\partial \Pi}{\partial a} = \frac{\partial}{\partial a}\left(U - F + W\right) = 0 \tag{2.7}$$

At forced dislocation, the work, which is carried out by the external forces, is zero and equation 2.7 becomes:

$$-\frac{\partial}{\partial a}\left(U(a,u)\right) = \frac{\partial W}{\partial a} \tag{2.8}$$

The term *U(a, U)* is a term which depends on the length of the crack and the deformation. One defines the term on the left of equation 2.8 as being the rate of energy relaxation (noted *G*), whereas the term on the right side is defined as being the critical rate of relaxation of the energy (G_C). This term represents the energy which is necessary

to advance the crack to a distance "*da*" and is a property of the material. In the case of fragile materials, since the start of the crack leads invariably to the catastrophic rupture, G_C can be used as criterion of rupture, the crack is being propagated when $G \geq G_C$. The rate of relaxation of the energy can be calculated from the load – displacement curve according to the following equation:

$$G = \frac{1}{2} P^2 \frac{dC}{da} \tag{2.9}$$

The parameter *C* is the compliance of the sample, defined as: $\delta = CP$.

Since both, the stress intensity factor (K_I) and the rate of relaxation of the energy (G) describe the necessary driving force to initiate the crack propagation, one can show that there is a relation between K_I and G_I. This relation is independent on the geometry and is often indicated as the "relation of similarity" of Irwin, to whom the paternity of the stress intensity factor is generally recognizes (1950). This relation is represented by the following equation (in plane stress):

$$G_I = \frac{K_I^2}{E} \tag{2.9}$$

In plane deformation, one replaces the factor *E* (modulus of elasticity) by $E/(1-\nu^2)$, where ν is the Poisson's ratio. Since the relations are higher developed on the basis of the fundamental equation of elasticity, so that they remain valid and applicable, several conditions must be met by the material. Initially, the material must be a linear rubber band, i.e. its modulus of elasticity must remain constant until the rupture, according to the applied load. Moreover, no residual deformation must remain in the material after crack propagation when the stress is decreasing. Lastly, the linear elastic rupture mechanics implies that at the time of the propagation, energy is only consumed at the head of the

crack, and only converted into surface energy. In cases of real materials, these conditions are observed very seldom. However, one generally assumes real materials by limiting the size of the plastic zone at the head of the crack compared to the length of the none broken part. For very rigid metals, for example, one obtains such a plastic zone in plane deformation. For the other types of materials, corrections on the linear elastic rupture mechanics must be made to describe their mechanical behaviour in an adequate way.

2.2. Mechanical behaviour of refractory materials

Refractory materials are one of the main parts in the category of quasi-fragile materials. After the initiation of a crack, it can be propagated in a catastrophic way (complete rupture of the material, which becomes fragile in a matter of fact), in a "semi-stable" way or a stable way. The mechanical behaviour of these materials is strongly related to their microstructure (described in chapter 1). In fact, the majority of the authors regard these materials as composites, rather than just ceramics, which originally was the case. Indeed, their heterogeneous microstructure, formed of fragile grains dispersed in a porous matrix, strongly interacts with the crack at the time of the propagation. This mainly explains their non-linear and non-elastic behaviour when cracking occurs. Moreover, the same microstructure is the origin of other mechanisms, occurring before and during the propagation, which make it possible to adapt the material to important displacements in tension without completely cracking. On the load – displacement curve, one notes that several "sections" can be identified (Phillips et al., 1993) (figure 2.3), each one being in general associated to a particular mechanism. The phenomenological approach will be presented in the following section.

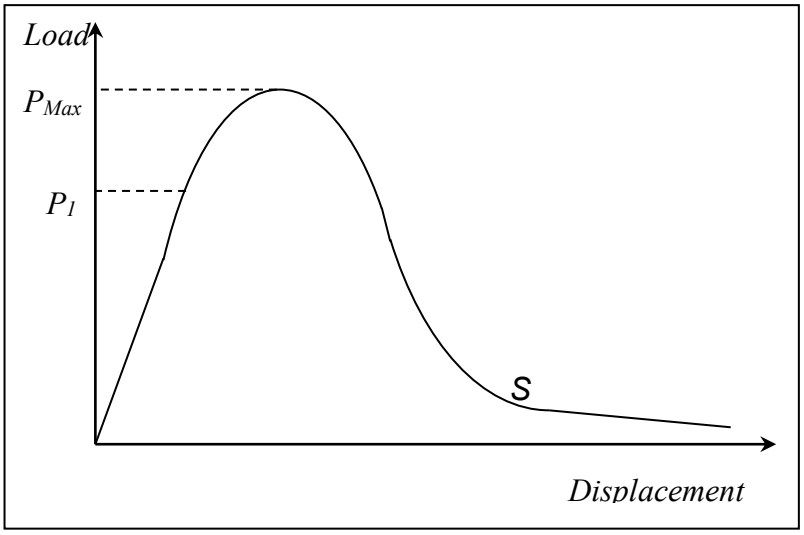

Figure 2.3. Description of the cracking curve of a quasi-fragile material.

2.2.1. Modulus of elasticity

The first section of the curve (Figure 2.3, until P_1) corresponds to the linear part of the material. This section of the curve can be characterized by the modulus of elasticity (E), which expresses the relation between the applied stress and the resulting deformation (let us note that in the case of a test with notched samples, the slope of the curve does not directly result in the modulus of elasticity, the compliance associated with the notch is exaggerating the measured deformation). The modulus of elasticity as such is related to several factors like: the nature of the phases, the connections between the various components, the porosity of the material and the presence of microscopic cracks in the matrix and between the interface aggregates/matrix. These are the most important factors (Carniglia and Barna, 1992, Bradt, 1993). Besides several attempts were tried to calculate the modulus of elasticity starting from the micro structural characteristics and the modulus of elasticity of materials "without defects". The most common calculations are the relations which only use porosity or the microscopic cracks (see Bradt, 1993, which makes a review on the subject).

After the point indicated P_1 on figure 2.3, the modulus of elasticity is not constant any more and the material shows variations within the linearity. Several mechanisms can be the source of this phenomenon generally with accordance to the temperature. Thus, with ambient and relatively low temperatures, the formation of microscopic cracks and/or the already existing propagation of the cracks are the conventional mechanism which occur in general (Venkateswaran et al., 1988). One then speaks about the damage of the material. These microscopic cracks can develop in a homogeneous way in the material (undefined damage) or localized (generally around a macroscopic notch). At high temperatures, the presence of viscous or liquid phase contributes to decrease the rigidity of the material. The involved mechanisms can be viscous flow (or creep) as well as the formation of microscopic cracks, associated this time with cavitations at the time of the dislocation of the aggregates.

The non-linearity of the modulus of elasticity, according to the applied load, also introduced problems for both, its measurement and its definition. Indeed, the modulus of elasticity is increasingly weaker in tension than in compression, because of the effect of the opening of the cracks. Moreover, the modulus of elasticity measured by dynamic methods (by velocity measurement of the ultrasounds in materials or the resonance frequency) is increasingly higher than for the two other methods. In the last case, the very weak strain of the material at the time of the measurement is responsible that no (or very little) micro cracking is influencing the explanation of the results. The disadvantage of the dynamic methods is that they do not make it possible to highlight the non-linear character of refractory materials. Nevertheless, certain authors consider that it is the only, truly valid method (Bradt, 1993) whereas others consider it unacceptable, precisely because it leads to too high values of *E* for the design of these materials (Schacht, 1993). In fact, in the study of the mechanical behaviour of refractory materials, the two methods should rather be used in a complementary way, which makes it possible moreover to better understand what occurs at the time during the loading (Lee and Moore, 1998, Simonin, 2000).

Let us notice that the modulus of elasticity as such can be considered constant for a given material. The variations with the linearity observed at the time of the loading are thus selected to deformations known as "irreversible", a little like the manner of the plastic deformation of metals. This approach is, at the base of the technique, known as "dimensionless" analysis of non-linear materials developed by Sakai and Bradt (1993) and Sakai and Inagaki (1989).

According to the temperature, one often observes a light reduction in the modulus of elasticity followed by an increase at intermediate temperatures then followed by a final fall at high temperatures (see for example Taniguchi and Ishikawa, 1988). The increase in the modulus of elasticity is generally associated with the closing of the micro cracks at

the time of the temperature increase, whereas the decrease at high temperatures is often connected to the appearance of a liquid phase or the presence of a vitreous phase.

In the end, let us note that the position of the point P_1 on the curve can be at very low stress, in particular at high temperatures, where it becomes impossible to observe any initial linear section.

2.2.2. Mechanical resistance and crack initiation

The mechanisms which occur between the point P_1 and P_{Max} on the curve presented at figure 2.3 are still relatively poorly understood. Shah et al. (1995) give the following interpretation of this phenomenon for concretes used in civil engineering (very similar to castables).

Immediately after the point P_1, the microscopic cracks develop in a diffuse way into the material until a certain stress, where they start to be localized. This localization of the microscopic cracks leads to the formation of a discrete and measurable crack, probably through the connection of several microscopic cracks. Sakai and Ishikawa (1992) also identifies that "the initiation" of the crack appears before the top of the curve. This "macro-crack" is propagated in a stable way, only when the applied pressure increases. At the top of the curve, the crack reaches a critical length and is propagated even if the applied pressure decreases. In fact, in forced loading, the crack would be propagated in an unstable way (i.e. catastrophic) when the level of stress would be equivalent to P_{Max}. This section of the curve will be discussed further.

When the tests are done with plane test-bars, i.e. without notch, the maximum force (and the associated stress) observed are regarded as being the mechanical resistance of the material. In general, one measures the mechanical resistance of refractory materials by a 3-point deflection test (infrequently in compression). The maximum stress measured at rupture is then called "modulus of rupture" (mechanical resistance). However, since the

method of load of these materials is generally in forced deformation, the value of the deformation corresponding to the maximum stress is also very important for the choice of the material. Figure 2.4 illustrates this fact (Schacht, 1993). One notices on this figure that material A presents a mechanical resistance higher than that of material B, but that its stress appears for a weaker deformation. In forced deformation, the rupture of the material A will thus occur before that of the material B.

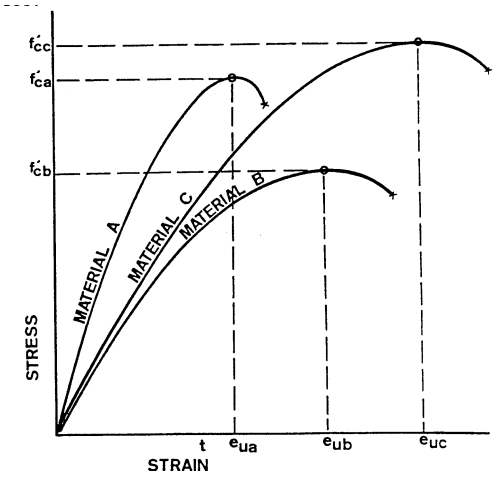

Figure 2.4. Comparison of the modulus of rupture of various refractory materials. According to Schacht, 1993.

Several micro structural mechanisms were discussed in the literature to explain the proceedings in quasi-fragile materials after the initiation of a crack until the top of the load – displacement curve. Figure 2.5 present some of these mechanisms. These mechanisms highlight the effect (and the importance) of the various micro structural parameters. For example, the aggregates can be the origin of the connection and of the deviation of the crack, and also play an important role in micro cracking. The very rough surfaces of the crack can also influence the resistance to the propagation, by effect of friction between the facets and/or by decreasing the intensity of the stress at the head of the crack. The pores can also act like brakes within cracking. Indeed, when the crack intercepts porosity, the effect of the latter is to blunt the bottom of the crack locally, thus

reducing the concentration of the stress. An additional force is thus necessary to continue cracking at this place.

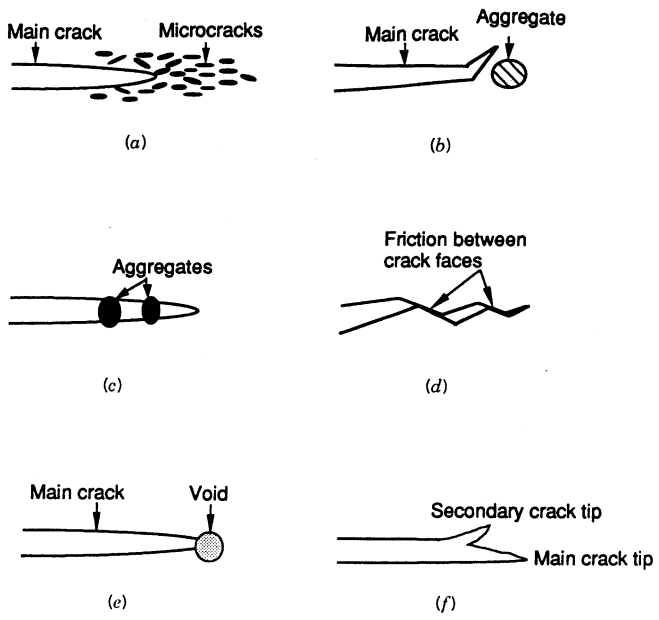

Figure 2.5. Possible mechanisms of strengthening and cracking resistance of a refractory material (Shah et al., 1995)

In a general way, these mechanisms can occur either in front of the crack (zone of damage, or *fracture process zone*) or behind the face of cracking (weak region). In fact the interaction of the crack with the microstructure of the material involves an increase in its strength, which continues even after the top of the load – displacement curve. This characteristic of refractory materials is important for the data of the *R*-curve concept which will be presented later.

2.2.3. Crack propagation

At the point P_{Max} on the load – displacement curve (figure 2.3), the crack initiated earlier is propagated in a critical way. The "critical" term is used here, meaning that this crack is able to be propagated in a quasi-stable or stable (controlled) way (depending

mainly on the geometry of the sample, the working conditions under stress/strain and the properties of the material).

The zone located between the P_{Max} point and the point *S* on figure 2.3 was named by Phillips (1993) "zone of fast softening" (Simonin, 2000). Indeed, the force which is necessary for the extension of the crack after the critical point decreases more or less quickly as the length of the crack increases. The propagation of the crack during this stage is relatively fast. Moreover, the interaction of the crack with the microstructure starts to become dominating.

However, in many fragile materials, the resistance to crack propagation continues to increase according to the length of the crack. The identified mechanisms which are responsible for this phenomenon are primarily the same as those described previously. Sakai et al. (1988), for example, identified the bridging of the aggregates as being the dominating factor for the increase in the strength of polycrystalline graphite samples after the top of the curve. This mechanism is regarded besides as one of the most important concerning this behaviour. However, other mechanisms can also act, forming a synergy whose result is the increase in the resistance to the propagation. Let us note that the resistance to cracking generally reaches a constant value for a given length of the crack. This constant value can however be observed only when the crack is in a "steady mode" of propagation, i.e. when the mechanisms of cracking and the dissipation of the energy are fully developed. One can observe this value only when the sample is adequately large to obtain this steady mode (Sakai and Ichikawa, 1992).

The last part of the curve (from the point *S* up to zero) can be regarded as a zone of slow softening. In fact, it is extremely possible that this zone is strongly influenced by the sample size. Indeed, the size of the zone of damage is very large in this type of materials. The foreseeable effects on the boundaries lead to a very low value of the measured stress, together with a very large deformation.

2.3. Characterization of the mechanical behaviour of refractory materials

2.3.1. Resistance against crack initiation

It was shown that the refractory materials generally present a non-linear behaviour in tension, which forces to modify some of the equations of the linear elastic rupture mechanics. The description of the behaviour of refractory materials generally requires the use of at least two criteria (often more). This is necessary for the initiation of the crack and for its propagation.

The initiation of the crack can be characterized in a mechanical way by the determination of the critical factor of stress intensity K_{IC}. As defined by the theory of Griffith-Irwin, this parameter corresponds to the intensity of the stress at which the crack is propagated in an unstable way. In fact, since the stability of a crack depends on the variation of the free energy of the whole system, the value measured for K_{IC}, according to its definition, will vary according to the geometry of the test-sample and the used method. According to this definition, it is always debatable to regard K_{IC} as a property of the material (Sakai, 1988). On the other side, the mechanical approach selected from Irwin defines this parameter as "being the critical level of stress intensity" at which the stress in the bottom of the notch (or crack) is sufficient to break the atomic connections. In this direction, K_{IC} becomes a property of the material. However, the size of the zone of damage, at the time of the measurement of this parameter, must be low compared to the sample size. In the contrary case, one will observe an increase in this parameter according to the length of the crack. This makes the phenomenon of the increasing *R*-curve values reasonable. With this explanation, one can define the following term:

$$K_R(a) = Y\left(a/W\right)\frac{P_C}{B\sqrt{W}} = F\left(a/W\right)\sigma_C\sqrt{\pi a} \qquad (2.10)$$

The value of P_C used in this equation represents the critical load necessary to start a crack with the length a. Note that $K_R = K_{IC}$ when $\Delta a = 0$, i.e. when the extension of the crack is zero. Figure 2.6 schematizes a typical K_R curve according to Δa for a refractory material. This type of curve is called R-curve, although the term R as such is the energy equivalent of K_R. Besides to limit confusion between the two terms, certain authors prefer to use the term "T-curve" when K_R is used (Wachtman, 1990).

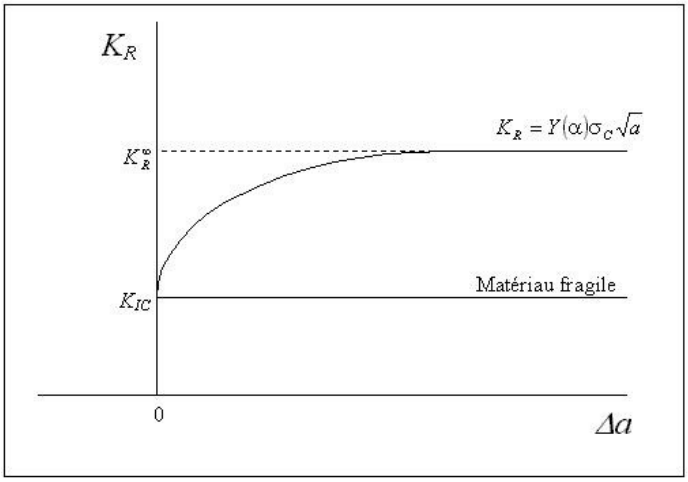

Figure 2.6. Diagram of a *R*-curve of a quasi-fragile material

In the literature the value of K_{IC} is very often calculated using the measured maximum load. However, for refractory materials, the crack is generally initiated before the top of the curve, which implies that the measured value of K_{IC} does not represent the stress intensity at the initiation of the crack, but the K_R value for which the crack is propagated in a critical way does. K_{IC} is obtained in a accurate way by precise measurement (using extensometers or visually measurement) of the point P_C on the load – displacement curve corresponding to the initiation of the crack before the top of the curve (Sakai and Bradt, 1993). The difficulty in measuring this value is probably due to the origin of this confusion in the literature. Let us note that Tang et al. (1992) uses K_{IC}^S to indicate the K_R value equivalent to the top of the curve. To avoid any confusion we will also use this term in the rest of this thesis.

The energy equivalent to the previous approach is similar with that developed within the outline of the linear elastic rupture mechanics. Thus, by doing an energy balance on the material under stress, one obtains a relation identical to equation 2.8. To identify the non-linear behaviour, the rate of the energy relaxation is marked as G_q (according to the document of Shah et al., 1995) and the crack resistance of the material is marked R. In the case of a linear material, $G_q = G$ and $R = G_C$. Non-linear materials are contrary to linear materials, wherefore G_C is a constant, R is generally a function of the crack length. One can thus write (Sakai and Ishikawa, 1992):

$$R(a) = \left(\frac{d\Pi}{dA} \right)_{Equilibrium} \tag{2.11}$$

Equation 2.11 means that the resistance to cracking of the material is equal to the variation of the potential energy of the system for the creation of a new surface dA during cracking in equilibrium. The R-curve is obtained by tracing the value of R according to Δa, the projection of the crack. This curve is similar with that presented in figure 2.4. The methods of determination of this curve will be presented in chapter 3.

The critical value of R (R_C) corresponds to the critical rate of relaxation of the energy at the time of crack initiation. R_C is equivalent to the definition of the J-integral given by Rice (1968) and can be calculated according to the same approximation:

$$R_C^{init} = \frac{2\Pi_{init}}{S} \tag{2.12}$$

The term Π_{Init} in equation 2.12 corresponds to the energy stored in the system at the time of the initiation of the crack, i.e. the surface under the load – displacement curve

is 0 at P_{Max} in forced displacement. S is the total not broken surface of the crack at the beginning of the test.

One of the most important points at this stage is that for non-linear materials, the relation of the similarity of Irwin (equation 2.9) is not true. Since R_C is not necessarily equal to G_C, it is not either equal to K_{IC}^2/E. Indeed, for this relation to be true, the relaxation of the load on the sample must be accompanied by the return to the origin *without remaining deformation*. In the case of refractory materials, this situation is met very seldom. Figure 2.7 illustrates this difference.

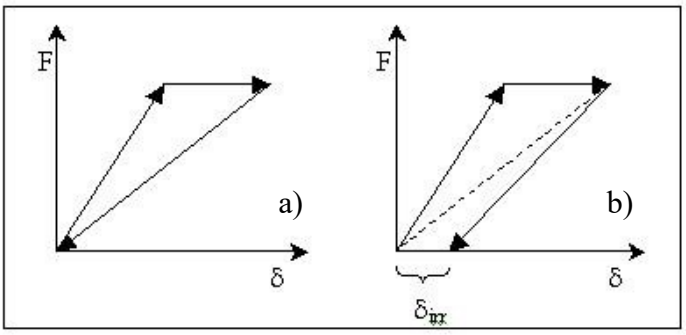

Figure 2.7. Illustration of the crack propagation.
a) elastic linear material, b) non-linear material.

Thus, the dissipated energy during crack propagation in a non-linear material (surface under the curve) is higher than the necessary energy to create two new surfaces. To explain this difference, the relation of similarity of Irwin becomes (Sakai and Ishikawa, 1992):

$$R(a) = G(1 + 2\eta(a)) = \frac{K_R^2(a)}{E}(1 + 2\eta(a)) \tag{2.12}$$

The term η is defined (for propagation in equilibrium) like:

$$\eta(a) = \frac{d\delta_{irr}/da}{d\delta_{elastic}/da} \tag{2.13}$$

Obviously, if the unrecoverable deformation is zero, the factor η is equal to zero and equation 2.12 is summarized in equation 2.9 for $R_C = G_C$.

2.3.2. Resistance to crack propagation

The *R*-curve allows to visualize the resistance of a material to the initiation of a crack and to see its propagation, since the term *R* varies according to a function of Δa. *R* is one, if not the, parameter used to characterize the resistance of a material to crack propagation, which was developed by Nakayama in 1964. This parameter, named "work of rupture (γ_{wof})" (or energy of cracking, G_F), represents the sum of all the energy dissipated during the complete cracking of a sample, returned to the projection of the surface of the crack. One can thus write:

$$\gamma_{wof} = \gamma_{Surface} + \gamma_{microcracking} + \gamma_{grain-bridging} + \ldots \tag{2.14}$$

The work of rupture is equal to the total surface under the load – displacement curve, divided by 2*S*, the new created surface out of two surfaces:

$$\gamma_{wof} = \frac{W_{wof}}{2S} = \frac{1}{2S}\int_0^{\delta} P d\delta \tag{2.15}$$

Sakai and Ichikawa (1992) showed that the work of rupture was in fact closely related to *R(a)* and K_R. Initially, since elastic energy is completely relieved when cracking is complete, the total variation of the potential energy of the system after cracking can be written as:

$$\Delta\Pi = -W_{wof} \tag{2.16}$$

However according to equation 2.11:

$$-\Delta\Pi = \int_0^S R(a)dA = \langle R \rangle S \tag{2.17}$$

where $\langle R \rangle$ is the average value of *R(a)* for the complete rupture. Therefore, according to equation 2.16: $\gamma_{wof} = \langle R \rangle / 2$.

Finally, for non-linear materials:

$$\gamma_{wof} = \frac{\langle K_R^2(a) \rangle}{2E} + \frac{\langle K_R^2(a) \cdot \eta(a) \rangle}{E} \tag{2.18}$$

The first difficulty for the experimental measurement of the work of rupture is associated to the fact that the relation load – displacement must be known at any time during the propagation of the crack. This requires that the crack is propagated in a stable (or controlled) way in the sample, and that the used equipment is capable to measure the load and displacement at any time. The conditions of obtaining a stable crack were studied in a very rigorous way by Harmuth (1995). Hence, stable cracking is favoured when the machine used is very rigid, also the sample should have a sufficiently large rough surface and the material should presents a high γ_{wof}/R ratio. This last condition is generally obtained by materials presenting an increasing *R*-curve. Let us note that stable cracking is obtained relatively easily for refractory materials by the use of the wedge splitting test, which will be described in chapter 3.

It is possible to combine the criterion of crack initiation with that for crack propagation to obtain a performance parameter only based on the properties of the

material. One then defines the "characteristic length" in the following way (Harmuth, 1996):

$$l_{ch} = \frac{G_F E}{\sigma_C^2} \tag{2.19}$$

This parameter makes it possible to compare various materials quickly with each other, and it also allows to estimate the "brittleness" of the material. When we have a large characteristic length, it means that only little energy is necessary to initiate a crack, but that the crack propagation will be stopped quickly. The material will also preserve a certain integrity. In the contrary case, the quantity of the necessary energy to initiate the crack will be sufficient so the propagation will be almost catastrophic in the material.

2.3.3. Strength and thermal shock resistance

The thermal shock represents one of the most critical stresses for refractory materials. Hasselman (1969) developed a theory to try to explain the resistance of ceramic materials (regarded here as linear rubber band) to thermal shock. This study had been started earlier by Kingery (1955), but it has been restricted to the initiation of the crack, by thermal shock, according to a thermo elastic approach. Primarily, it is recognized that thermal shock stresses the materials with forced deformation. The amplitude of the deformation is a function of the gradient of the stress which effects the material, depending on its thermal properties, α, such as:

$$\varepsilon = \alpha \Delta T = \frac{\sigma}{E} \tag{2.20}$$

α is the thermal extension coefficient of the material. There will be crack initiation when the deformation associated with the differential of the temperature ΔT is equivalent to the

mechanical resistance of the material. Hence, one can define a parameter of crack initiation, according to Kingery:

$$\Delta T_C = R = \frac{\sigma_C}{\alpha E} \tag{2.21}$$

According to an energy approach, one obtains:

$$R_{st} = \sqrt{\frac{G_C}{\alpha^2 E}} \tag{2.22}$$

Equation 2.22 makes it possible to quantify the resistance of one material to crack initiation by thermal shock. Let us note that this relation is only true when the Biot number β tends towards the infinite (i.e. $\beta = Wh/2k \to \infty$, were h is the heat transfer coefficient and k is the thermal conductivity of the material). This criterion means that the surface temperature will reach the temperature of the medium instantly, whereas the internal temperature of the material remains unchanged. In practice, it is considered that this is the case for $\beta \approx 100$.

Hasselman was interested in the propagation of cracks in a material exposed to thermal stresses. Figure 2.8 illustrates his theory. Primarily, this graph shows that the propagation of a short crack initiated by thermal shock will continue until the crack reaches a certain length where the rate of elastic energy relaxation will be lower than the energy of cracking of the material. This condition is possible since the thermal shock occurs in forced deformation. Hence, the presence of a crack in the material decreases the value of the effective modulus of elasticity, which reduces much of the stored elastic energy (regarded as the driving force for cracking). The crack then will be propagated in a "quasi-static" way, i.e. increasingly larger temperature differentials will be necessary to initiate a new propagation.

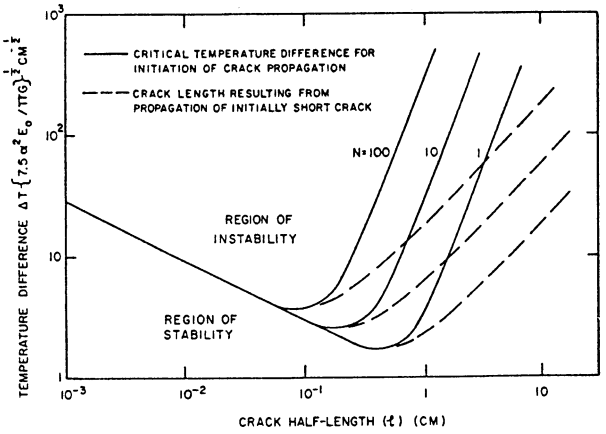

Figure 2.8. Effect on the length of a crack. On the resistance to crack propagation by thermal shocks (according to Hasselman, 1963).

Hasselman also developed a parameter which makes it possible to estimate the resistance of one material to the propagation of a crack per thermal shock. This parameter is equivalent to the characteristic length presented before:

$$R'''' = \frac{\gamma E}{\sigma_C^2} \tag{2.23}$$

Here, γ is the surface energy of the material, comparable with G_F for the characteristic length, which is related to the total energy dissipated during the cracking. Hence, the relation between the characteristic length and the strength parameter to crack propagation by thermal shock is $l_{ch} = 2R''''$.

Equations 2.21 and 2.23 imply a fundamental result for the resistance of refractory materials to the thermal shock: it is impossible to maximize their resistance to crack initiation at the same time with their resistance to crack propagation. Indeed, the mechanical resistance of a material, the numerator of equation 2.21, shows that one could increase the resistance of crack initiation by increasing the mechanical resistance of the

material. By doing this, one however decreases his resistance to crack propagation, since σ_c is the denominator of equation 2.23.

This result is of great importance for refractory materials, because it highlights the fact that the choice of a refractory material for a given application is a question of compromises between all its properties.

Chapter 3. Materials and experimental techniques

3.1. Description of the materials being used

Four main groups of castables based on MgO-SiO_2-C were tested within the framework of this project. The nature of carbon and its amount vary from one group to the other. Also, for the rest of this thesis, we will refer to a "reference" composition. This "reference" composition was used for comparison in all four groups. It consisted of 89,5% MgO, 1,5% Silica fume, 5% carbon in form of extruded graphite pellets and 4% silicon. The reason why we have chosen this composition as "reference" is, that prior research (e.g. corrosion tests) was done on it, were it showed very good comparable results. In group one carbon was introduced in form of extruded graphite pellets of the 4th generation. The amount of graphite in form of these pellets, the maximum grain size of MgO grains and the size of the pellets varies in this group. Group two was produced with flake graphite. The amount of flake graphite varies in this group to make it possible to compare this group to group one and see the different influence between pelletiesed graphite and natural flake graphite. In group three different amounts of fine carbon were introduced into the "reference" composition, which will be explained later. Group four shows the influence of antioxidants in magnesia carbon castables. In group four the amount of Si varies between 0 and 4%. In order to compare the castables with a regular MgO-C brick, one MgO-C brick was tested too. Table 3.1 presents the composition of the castables.

The raw materials consisted of four fractions of sintered magnesia aggregates from 6,7 – 3,35 to 0,3 – 0,05 mm, and one ball mill fine magnesia (<0,075 mm). Silica fume (≥98%, <1,0µm, 971U Elkem Materials, Norway) and metallic silicon (≥99%, <10µm, J-99 Elkem ASA Materials) were used as a bonding agent and metallic silicon was used as antioxidant. The different carbon sources which were used are extruded graphite pellets of the 4th generation, flake graphite and fine carbon. Table 3.1. presents a overview of the various raw materials used.

Table 3.1. Composition of the castables

Group	Castable	Magnesia	Silica	EG-Pellets	Flake Graphite	Fine Carbon	Silicon
Group 1	1	94,5	1,5	0	-	-	4
	2	91,5	1,5	3	-	-	4
	3, Reference	89,5	1,5	5	-	-	4
	4	87,5	1,5	7	-	-	4
	5	85,5	1,5	9	-	-	4
	6	89,5 <3mm	1,5	5	-	-	4
	7	89,5	1,5	5 long	-	-	4
Group 2	8	93,5	1,5	-	1	-	4
	9	92,0	1,5	-	2,5	-	4
	10	90,0	1,5	-	4,5	-	4
Group 3	11	88,5	1,5	-	-	1	4
	12	87,5	1,5	-	-	2	4
	13	85,5	1,5	-	-	4	4
Group 4	14	98,5	1,5	-	-	-	-
	15	91,5	1,5	5	-	-	2
Brick	16, Brick	90,4	3,5	-	4,8	-	-

The quantity of water added to each castable was kept constant at 5%. However, since the bad wettabillity of graphite the samples with flake graphite needed a higher amount of water up to 7,5%.

The castables were initially dry mixed for 4 minutes, followed by another 4 minutes after the addition of water. Once cast (on a vibration plate), they were left in the moulds during 24h, then unmoulded and dried at room temperature during 24h. Drying was continued at 110°C for another 24 hours.

For the hot modulus of rupture (HMOR) the pre-firing of the castables of the reference composition was carried out at 1100, 1300 and 1500°C for 5, 10 and 15h, with a heating and a cooling rate of 300°C/hour (5°C/min). Based on the results of the HMOR-tests for the reference composition at 1100, 1300 and 1450°C for all compositions the wedge splitting tests and the modulus of rupture tests were performed at 1300°C, after pre-firing in coke at 1300°C, for 5 hours. This temperature assured better homogenization of the microstructure and interaction between the components, than 1100°C, and provided highest values of HMOR (see results in chapter 4), which remained almost unchanged after longer pre-firing at 1300°C.

3.2. Experimental Techniques

3.2.1. Characterization of the physical properties, the composition and the microstructure

The apparent porosity and the apparent density of the castables were measured on bars by the "Archimede" method, in accordance with the ASTM C810 standard. Because of the low reactivity of the castables, water was used as medium.

The permanent linear variation of the castables after sintering was measured on bars (40x40x160 mm) by comparison of the dimensions before and after firing.

X-ray diffraction was used to perform a qualitative mineralogical characterization of the castables. A Phillips "X'pert" powder diffractometer with monochromated Cu-k_α radiation was used, operating at 40 kV and 50 mA. The powdered specimens were scanned in a step mode, typically 0,025°/second, with 10 seconds exposure.

Microstructural characterization was carried out employing a scanning electron microscope JMS-840 (JEOL, Japan), equipped with detectors for secondary and back scattered electrons.

The observations were made on the fracture surfaces and on polished samples of the castables in secondary and back scattered electrons. The first approach makes it possible to examine the fine details of the matrix of the castables, with an excellent resolution. The second technique makes it possible to obtain additional information on the distribution of different phases in the matrix.

The polished samples were prepared according to the ceramographic techniques standards, which consist in sequentially operation of coarse polishing on SiC papers, followed by fine polishing using diamond paste of 6, 3 and 1 μm.

Phase identification was carried out by energy-dispersive X-ray spectroscopy (EDS), using LINK ISIS detector and software from Oxford Instruments, England. This spectrometer allows a reliable detection of the X-rays of all the elements starting from boron. Measurements were taken by using a tension of acceleration of 20 kV and a current from 1 to 10 nA, at a working distance of 39 mm. The direct comparison of the spectra of a reference with those obtained for the castables, under the same operating conditions, allowed a reliable identification of the involved phases (magnesia, graphite, forsterite, silicon-carbide and silica=.

3.2.2. Measurement of mechanical properties

Initially, the mechanical resistance (or "modulus of rupture") of the castables was measured at 1100, 1300, 1450°C by three point bending tests, while following the method described by ASTM (ASTM C100, 1990). The dimensions of the samples were 40x40x160 mm.

An Instron machine (model 5581), including a load cell 0 - 30 kN was used to break the samples. The modulus of rupture is calculated starting from the equation (3.1):

$$MOR = \sigma_{Max} = \frac{3FL}{2bh^2} \tag{3.1}$$

In this equation, b is the width of the sample, h the height and L the distance between the supports (126,85 mm). It has to be noticed moreover that only the intensity of the maximum force (force at rupture) is sufficient to calculate this parameter.

The modulus of elasticity for each composition was measured at 1300°C. With this intention, the load - displacement curve was established by three point bending tests

on samples of 40x40x160 mm using the Instron machine. The extension was measured by using a LVDT-type extensometer, measuring the force with a load cell of 0 - 30 kN.

The modulus of elasticity as such was determined by calculation of the slope (by linear regression on several points) of the elastic range of the curve. Due to non-linearity of certain curves (see chapter 4), the modulus of elasticity was evaluated as the highest slope of the curve before the rupture of the material. The modulus of elasticity is obtained by the following relation:

$$E = \left(\frac{F}{\delta} \right) \frac{L^3}{48I} \tag{3.2}$$

In the equation above, the F/δ ratio corresponds to the slope of the forces (F) – and the displacement (δ), L is the width between the support rollers, (here: 126,85 mm) and I is the second surface moment of the sample.

Also the measurement of the cold dynamic Young modulus was carried out. When one works in a dynamic way, it is a question of measuring the elastic module, either by determining the resonance frequency of the sample subjected to a shock (grindosonic), or by measuring the propagation speed of a wave within the material (microsonic).

For this work, measurements were made mainly with the second method because it allowed the automation of measurements amongst other things and because it had also a more powerful operating system.

The sample dimensions were 40x40x160 mm as mentioned before. The sensitivity and the intensity of the request are regulated. Then, one sets the sample under a shock. A computer equipped with a microphone collects and analyzes the signal and calculates a

certain speed value. This procedure has to be done several times to obtain an average value according to the standard deviation and the number of repetitions.

At the time of acquisition, one tests the sample in three different ways in order to collect the propagation speed in flexion, longitudinal and torsion. One receives than, thanks to the *EMOD-grindosonic* software, the values of the Young modulus E_{ij} and the Poisson's ratio. For example, in the case of an isotropic material the propagation speed v_x is calculated as shown in the equation (3.3) :

$$v_x = \sqrt{\frac{E_{ij}}{\rho}} \tag{3.3}$$

The precision obtained with this method is a function of the presence of defects (lack of homogeneity) in the sample and is expressed by the standard deviation of the calculated values. It was tried to carry out the measurements in a way to maximize the precision. For that, on certain samples which present defects or cracks which considerably reduce the propagation speed of the waves, it is essential to analyze the spectrum received in order to see whether the received values are not an average of two propagation speeds. In this case the special software makes a correction by applying either a filter to remove incorrect speeds, or by changing the level of sensitivity of the microphone.

3.2.3. Measured parameters of the rupture process: Wedge splitting test

The two principal parameters of the breaking process (K_{IC} and γ_{wof}) were measured by using the test known as "Wedge splitting test". All the other parameters calculated in this thesis result from one or the other of these two parameters. The wedge splitting test was initially proposed by Tchegg (1991). Harmuth (1995, 1996) further developed the test and made some improvements to it. This test allows the controlled

propagation of a crack in a quasi-fragile material. Figure 3.2. schematically represents the necessary assembly to perform the test. The geometry as well as the dimensions (in mm) of the sample are presented in figure 3.3. One defines the factor *B* as being the width of the not broken zone (*B* = 61 mm) and *W* the length of this same zone before the test (*W* = 65 mm). The side notches are primarily used to make sure that the crack will be propagated in the desired way.

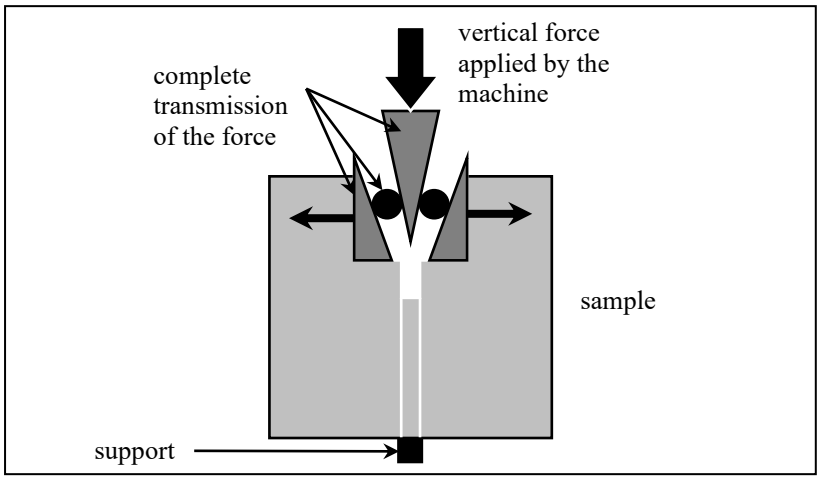

Figure 3.2. Schematic representation of the wedge splitting test

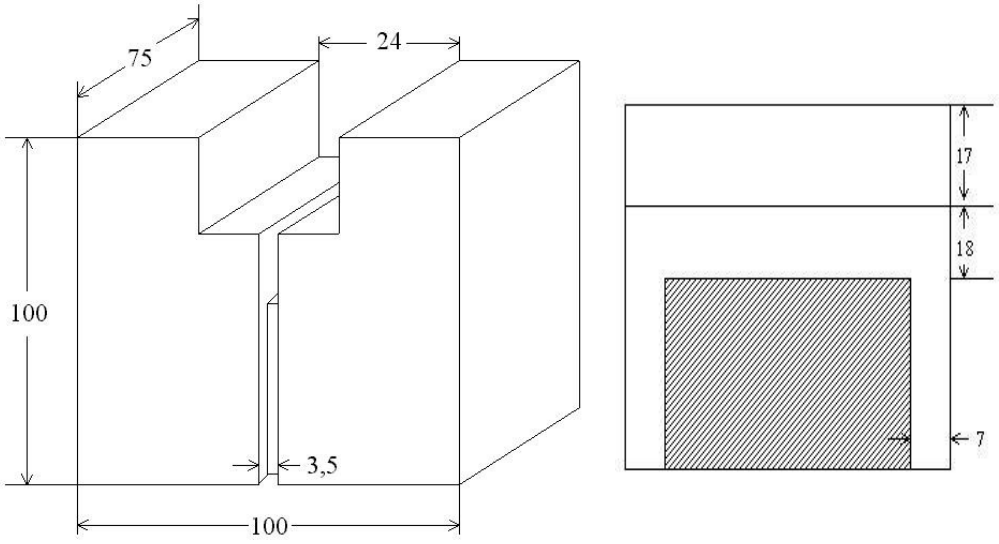

Figure 3.3. Sample dimensions for the wedge splitting test. (dimensions are in mm).

The vertical force applied to the sample by the piston is transmitted horizontally by a wedge slipping between two rollers. These rollers are supported with two side supports (inclined plane) installed on both sides of the principal notch (the one with 24 mm). The relation between the vertical force (the one applied by the machine) and the horizontal force which results from the vertical one is given by equation 3.3.

$$F_H = \frac{F_V}{2\tan(\beta/2)} \tag{3.3}$$

The parameter β is the angle formed by two surfaces of the wedge. In this project, this angle is 10°, which gives a F_H/F_V ratio of approximately 5,7. Let us note that the angle of the supports compared to the vertical must be precisely equal to β/2, primarily to prevent that the force is not applied in an unequal way, which could lead to significant measurement errors.

Displacement, i.e. the deformation and the opening of the sample during cracking, are calculated in a similar way as equation 3.3 and is based on the vertical displacement of the span of the machine (equation 3.4).

$$\delta_H = 2\tan(\beta/2)\delta_V \approx 0.175\delta_V \tag{3.4}$$

The modulus of elasticity can also be calculated starting from the right load - displacement slope in the elastic range, by using the following relation:

$$E = \frac{\lambda(0)}{B}\left(\frac{dF_H}{d\delta_H}\right) \tag{3.5}$$

The term $\lambda(0)$ is the dimensionless compliance before crack initiation for the given geometry (Figure 3.3) and is equal to 15,4 (which is determined by finite element simulation by Harmuth (1996).

However, the modulus of elasticity will not be measured during this test. In fact, the measurement of the opening of the sample was not taken in a precise way with an extensometer, partly because of the complexity of the assembly at high temperature. At crack initiation the error is zero and it is very low for the energy of cracking, since the total deflection at the time of the test is much larger than the elastic strain.

Stress for the rupture is obtained by the summation of the existing flexion and tension loads in the sample during the test. It is given by the following relation:

$$\sigma_{Max} = \frac{F_{H,Max}}{BW}\left(1 + \frac{6y}{W}\right) \tag{3.6}$$

The variable y corresponds to the distance between the centric section and the point of the load application. For the geometry given in figure 3.3, y = 66 mm before the propagation of the crack.

For such a geometry, the critical factor of intensity of stress is equal to:

$$K_{IC}^{S} = kF_{H,Max} \tag{3.7}$$

Constant k is equal to 354,5 $m^{-3/2}$ and was obtained by finite element simulation (Harmuth, 1996). Harmuth also provides the values of $Y(\alpha)$ and $\lambda(\alpha)$ for the geometry presented in figure 3.3. In a general way, one can write:

$$K_{IC}^{S} = Y\left(a/W\right)\frac{F_{H,Max}}{BW^{1/2}} \tag{3.8}$$

Here, W = 100 mm, B = 61 mm and a = 35 mm (α = 0,35). This expression, as well as the values of $Y(\alpha)$ and $\lambda(\alpha)$, is very useful for the calculation of the R-curves. The numerical values of $Y(\alpha)$ and $\lambda(\alpha)$ are presented in the appendices.

Finally, the energy of rupture, or work of rupture, is obtained by numerical integration of the load - displacement curve. The boundaries of the integrations used are $\delta_1 = 0$ (F_{VI} = 30N) and $\delta_2 = \delta$. The test conditions, described below, will determine the reasons of these choices.

$$G_F = \frac{1}{B(W - a_0)}\int_0^{\delta} F d\delta \tag{3.11}$$

The tests were carried out at 1300°C using an Instron machine (model 5581). A vertical preload of 30 Newton was applied to the assembly during the heating. Two principal reasons explain this choice. Initially, the preload makes it possible to maintain the moving parts (wedge, rollers and supports) in place and balance on the sample. Secondly, it makes it possible to limit the negative effect at the beginning of loading, related to the adjustment of the various parts. For this test, the loading rate was optimized by Harmuth (1996) and Paransky (2000). The speed (vertical) used for this project will be the same as that determined by these authors and is equal to 0,5 mm/min. This speed makes it possible moreover to ensure the stable propagation of the crack for the majority of refractory materials, while making it possible to carry out the test within reasonable times (30 to 45 min) and to limit the deformations related to creep. The tests were stopped when the horizontal displacement (δ_H) reached 3mm (17,03mm vertical displacement). Indeed, some preliminary tests allowed us to conclude that at this stage of the very advanced crack the force on the specimen decreased very slowly with the

displacement. The result is that the tail of the curve becomes almost horizontal. As the result, the contribution of this stage to the work of fracture will be overestimated. As it is also quite possible that at this final stage of rupture, the zone of damage has already reached the edge of the sample (what could cause strong affects on the results), it was decided to stop the test at 3mm horizontal displacement to avoid this problem.

In opposition to other standard tests for the fracture toughness, the wedge splitting test offers the advantage of minimizing the force applied by the machine, at the same time decreasing the energy stored in the machine. This situation makes it possible to support a stable crack propagation. The fact that the force is multiplied by ten, due to the geometry of the wedge splitting test, makes it possible to test samples much more massive, and in the case of heterogeneous materials like refractories, much more representative of their microstructure. Lastly, the preparation of the sample is relatively simple and requires only the cutting of the notches in the cast specimen.

A remark is essential however with regard to the principal notch. Starting from the wedge splitting test, Rieder et al (1998) studied the effect of the width of the notch to the measures of K_{IC} of various refractory materials. Indeed, the value of K_{IC} measured by standard tests of the rupture process often depends on the radius of curvature at the base of the notch. However, for a radius larger than a certain breaking value (which depends on the material), the value of K_{IC} is generally constant. This implies that errors of the measurement can occur during the tests when the notch is too wide. In fact, Rieder et al demonstrated that the value of K_{IC} increased by 15% for notches which width is higher than 3,5 mm. The results then presented a much more significant distribution. In general, these authors suggest that the critical notch radius should be approximately equal to the half of the diameter of the largest aggregates (considering that the maximum size of the defects is related to these aggregates). Hence, since the castables studied here contain aggregates of 6 mm, the width of the notch will be maintained at around 3 mm.

Chapter 4. Results and discussion

This chapter presents the main part of the results obtained throughout the project. The chapter as such is divided into four sections. Initially, we will present the physical properties of the castables, such as porosity and the linear variation after firing. The next section is used to describe preliminary tests, which were used to plan all the following testing. In the section three the macrostructure of various castables is described. The last section will be devoted to the mechanical properties and the presentation of the microfractographic study of the samples of the four different groups of castables, as well as of the MgO-C brick.

4.1. Characterization of the castables

4.1.1. Composition and mineralogy of the castables

The mineralogical composition of the tested castables was performed by X – ray diffraction (XRD). Figure 4.1 shows a XRD spectrum of castables, fired at 1100°C, 1300°C and 1450°C for 10 hours. It is seen, that after firing at 1100°C some of the Si metal is still present in the microstructure. Firing at 1300 or 1450°C reveals in complete reactions of Si and formation of SiC and, also, Mg_2SiO_4 (forsterite) phase.

Figure 4.2 shows XRD spectra for the “reference” castable with 5% EG pellets and 4% Si after pre-firing for 5 hours and testing at 1300°C. Two different layers were analysed: a dense outer layer and an inner layer.

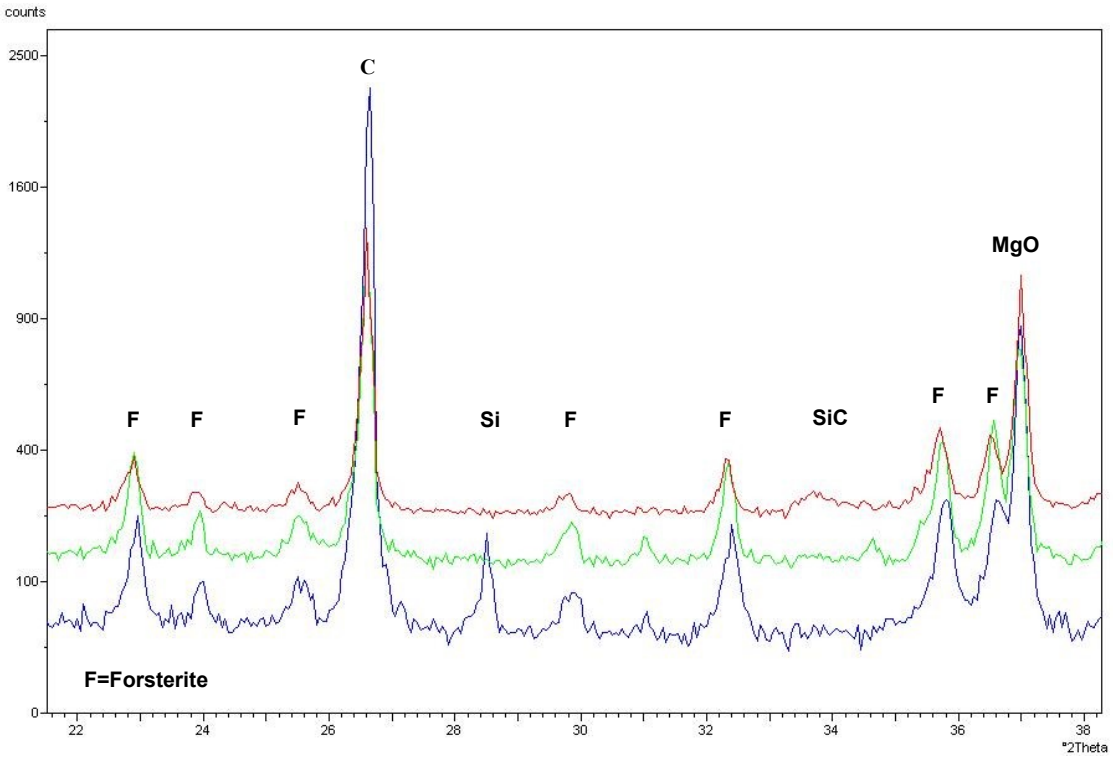

Figure 4.1. XRD spectra for the reference castable (5% EG pellets, 4% Si) after testing at 1100°C, 1300°C and 1450°C

For the dense outside layer the main components are MgO, Mg_2SiO_4, C and SiC (figure 4.2). The carbon in the outside layer is due to the present of graphite in the pellets and to the secondary carbon coating on the surface. A detailed explanation for the formation of secondary carbon follows later in this section.

The mineralogy of the inner layer is very close to that of the outer layer, but it contains more of SiC and less of Mg_2SiO_4 (figure 4.3).

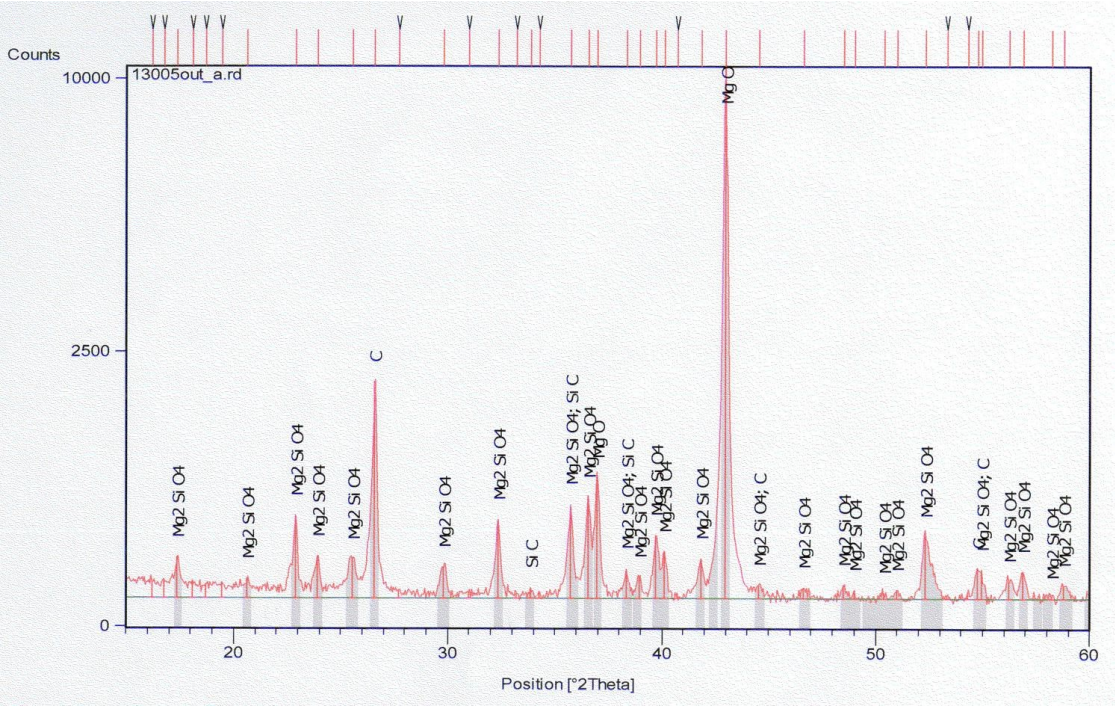

Figure 4.2. XRD spectra for the outer layer of the reference castable (5% EG pellets, 4% Si) after testing at 1300°C

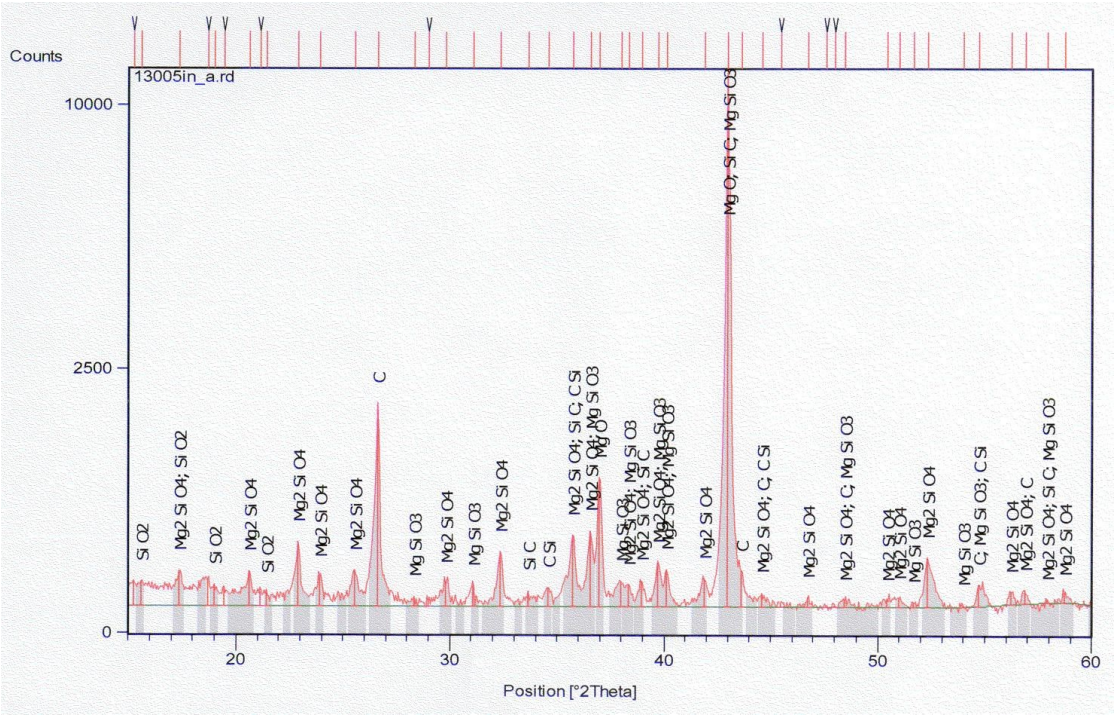

Figure 4.3. XRD spectra for the inner layer of the reference castable (5% EG pellets, 4% Si) after testing at 1300°C

4.1.2. Bulk density, porosity and linear variation

Porosity plays a major role on all the properties of refractory materials, and particularly the mechanical properties. The results obtained by the method of Archimede for the apparent porosity and the bulk density of the castables are thus presented in the table 4.1.

Table 4.1. Density, apparent porosity and linear variation of the castables

Nr.	Castable	Bulk density (g/cm^3)		Porosity	Linear variation
		before firing	after firing	after firing	(%)
1	**0% P, 4% Si**	2,93	3,00	12,27	0,21
2	**3% P, 4% Si**	2,83	2,90	14,57	0,11
3	**Reference (5% P, 4% Si)**	2,68	2,74	18,14	-0,03
4	**7% P, 4% Si**	2,67	2,72	17,74	0,09
5	**9% P, 4% Si**	2,60	2,64	19,30	-0,19
6	**5% P, 4% Si, MgO<3**	2,66	2,71	18,20	-0,11
7	**5% LP, 4% Si**	2,77	2,79	15,78	0,01
8	**1% FG, 4% Si**	2,85	2,90	13,71	0,04
9	**2,5% FG, 4% Si**	2,66	2,75	17,93	0,04
10	**4,5% FG, 4% Si**	2,55	2,58	21,24	0,06
11	**5%P, 1% fc, 4% Si**	2,70	2,73	17,80	0,02
12	**5%P, 2% fc, 4% Si**	2,70	2,72	16,45	0,08
13	**5%P, 4% fc, 4% Si**	2,62	2,68	16,88	0,07
14	**0% P, 0% Si**	2,93	2,92	15,11	-0,18
15	**5% P, 2% Si**	2,76	2,77	16,19	0,12
16	**Brick (5% C)**	n.a.	n.a.	11,00	n.a.

P=Pellets, LP=Long Pellets, FG=Flake Graphite, fc=Fine Carbon, C=Carbon, Si=Silicon

Several observations due to the different levels of porosity follow:

1. Lowest porosity is observed in castable 1 (without carbon) since there is better sintering and bonding.
2. Highest porosity is observed in castable 10 (with 4,5% flake graphite) due to the non-wetting properties of flake graphite, poor sintering and higher water content.
3. It is remarkable that castable 5 (9% pellets) has a lower porosity than castable 10 (with 4,5% flake graphite).

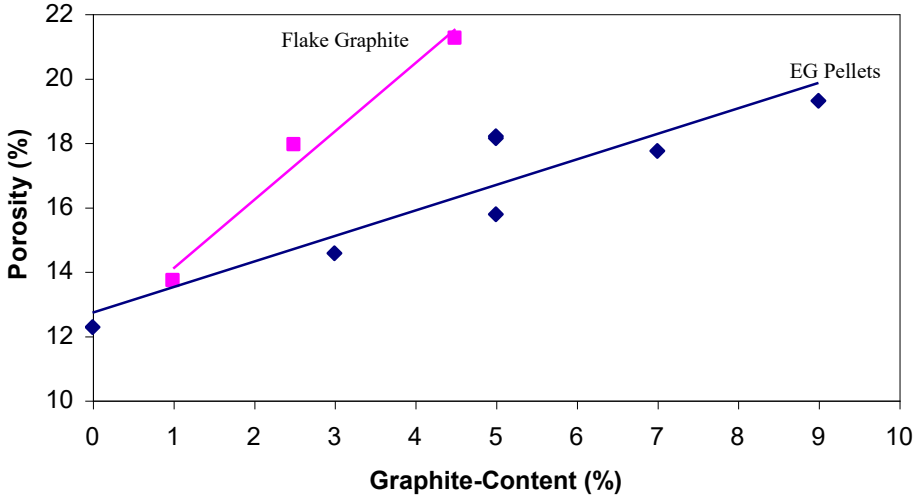

Figure 4.4. Comparison of the level of porosity between castables containing flake graphite or EG pellets

Table 4.1 shows that the porosity after firing is highest for samples with a high amount of graphite. This is due to the poor wettability of graphite which was mentioned earlier. As can be seen in figure 4.4 the porosity increases with graphite content. It is important to notice that the porosity for 4,5% flake graphite is even higher than the porosity of 9% EG pellets. These EG pellets are produced from agglomerated graphite and the 9% pellets equal approximately 8,5% graphite content. This shows clearly that the new EG pellets have a positive influence on the porosity.

The simplest method to characterize sintering is to measure the dimensional variations of the castables after sintering. The results measured on the castables pre-fired with 1300°C for 5h are presented in table 4.1 (the negative signs indicate a reduction in size). As can be seen, the linear variation is very low and hence the microcracking due to thermal stresses during firing is expected to be very small.

4.2. Preliminary HMOR tests

In this section the testing methods are explained. Tests were performed in different atmospheres (coke or argon), at different temperatures (1100°C, 1300°C and 1500°C) and with different holding times (5, 10 and 15 hours). All those preliminary tests were performed with the "reference" sample, hence a castable with 5% EG pellets and 4% Si.

The modulus of rupture is indisputably the most often measured mechanical property for refractory materials. This property makes it possible to quickly compare materials between each other and to classify them. Moreover, the measurement of the modulus of rupture at several temperatures makes it possible to have a good idea of the effect of the temperature on the mechanical resistance of materials, and thus, in an indirect way, to follow the evolution of their microstructure.

Figure 4.5 shows the results of HMOR at 1100°C, 1300°C and 1500°C for 5, 10 and 15 hours holding time. In order to explore the mechanical properties of MgO-C castables at relative high temperatures and since the strength variations between 5 and 10 or 15 hours of firing were rather small, it was decided to use 5 hours of pre-firing at 1300°C.

To show the importance of a carbon protective atmosphere during pre-firing, one test was directly performed with pre-firing in an argon atmosphere. The result of this experiment, which are shown in table 4.2 and figure 4.6 can be explained due to two main points: First, the argon atmosphere does not completely prevent the oxidation of the castable. On the other hand, a dense surface layer containing secondary carbon is formed during firing in carbon atmosphere. This results in a 50% higher strength of the sample which was pre-fired in carbon atmosphere compared to the sample pre-fired in argon atmosphere.

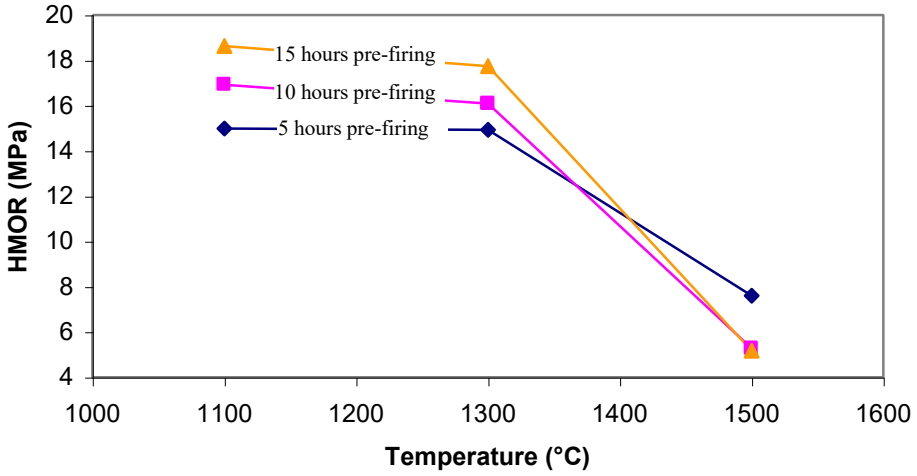

Figure 4.5. HMOR at different pre-firing temperatures and holding times

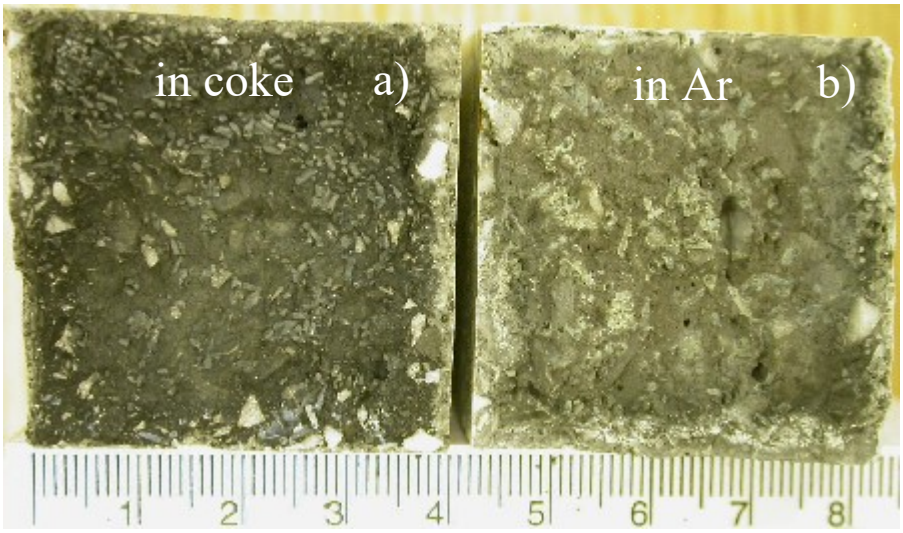

Figure 4.6. Macroscopic appearance of samples after pre-firing in a) coke protected atmosphere, b) in argon protected atmosphere

The existence of secondary carbon deposition (layer) on the fracture surface was confirmed by the following evidence: a) distinctive black colour at the outer layer (see figure 4.8), b) detection of the carbon peak in the areas of the outer layer by microprobe (SEM/EDS) and c) detection of carbon reflections in XRD spectrum at carbon-free castable 1 after prefiring in coke (see figure 4.7)

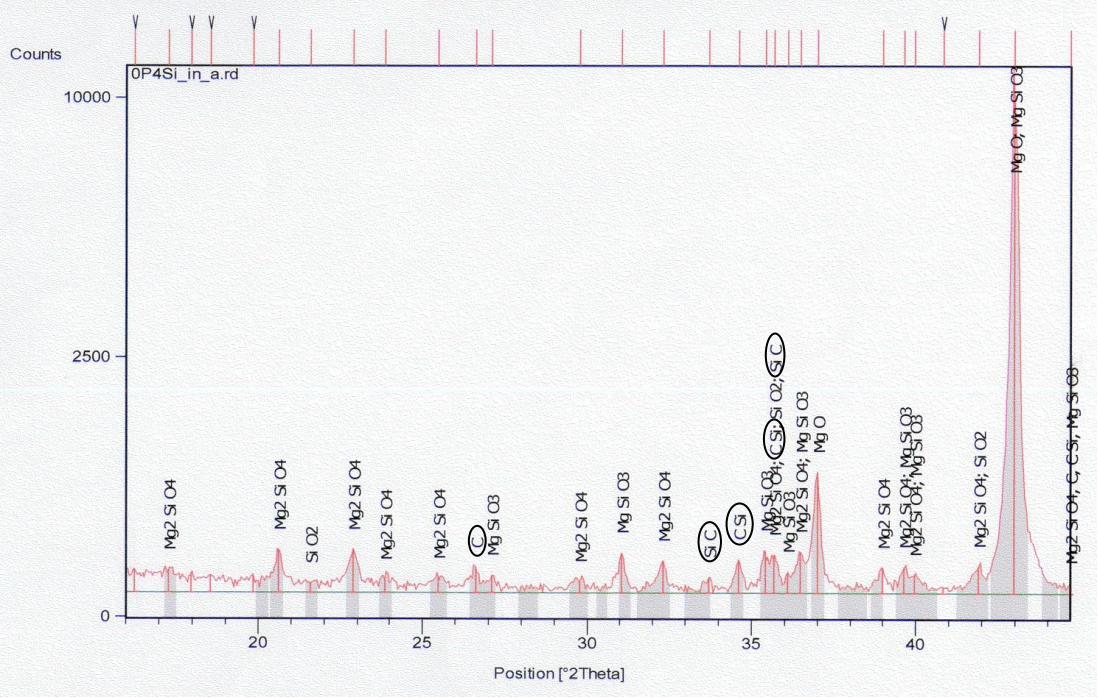

Figure 4.7. X-ray analysis of castable 1 (0% EG pellets, 4% Si) after testing at 1300°C

To preserve this dense layer which contributes to high strength, it was decided to cut the wedge splitting test specimen before pre-firing. Due to the low linear variation this did not lead to a higher risk of microcracking on firing. The advantage of pre-cutting is illustrated in table 4.3.

Table 4.2. Pre-firing in coke protected atmosphere and argon

	reference	**direct test**
Temperature (°C)	1300	1300
Atmosphere pre-firing	coke	argon
Atmosphere test	argon	argon
HMOR (MPa)	14,9	10,0

Table 4.3. Comparison between the strength of the pre-cut and the pre-fired castables

Castable	pre-cut	pre-fired
HMOR (MPa)	7,9	6,1
K_{IC} (MPa (m)$^{1/2}$)	1,6	1,2
WOF (J/m^2)	475	475

To further demonstrate a lack of oxidation protection in argon atmosphere, the results of testing with argon at 1500°C and testing the same specimen at room temperature (no protection needed) are shown in figure 4.7 and table 4.4.

Table 4.4. Pre-firing in coke protected atmosphere and test with/without argon protection

	argon protection	without argon
pre-firing Temperature (°C)	1500	1500
Atmosphere pre-firing	coke	coke
testing Temperature (°C)	1450	RT
Atmosphere test	argon	no protection

In figure 4.8 b) one can easily see the dense outside layer which is formed during pre-firing in coke. During the test in argon this layer is partially oxidized (from the outside), due to the pressure of oxygen in the furnace atmosphere.

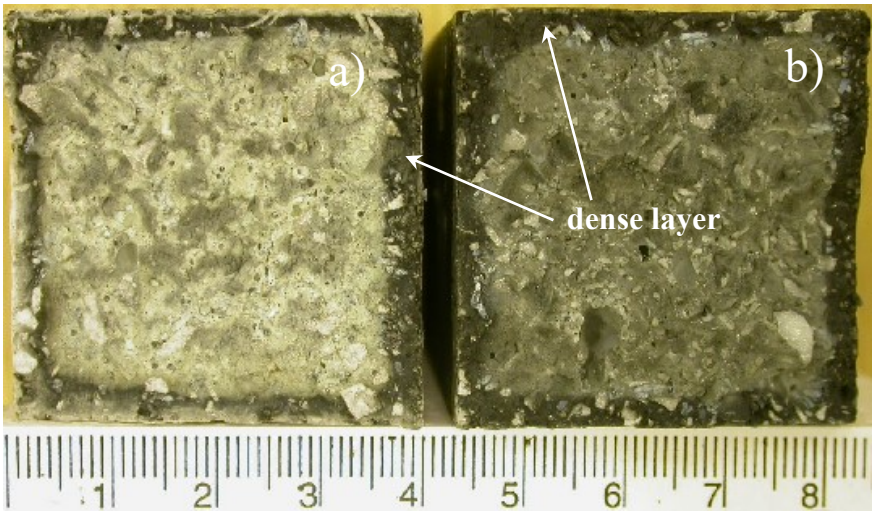

Figure 4.8. Pre-firing in coke protected atmosphere and test a) with argon protection (at 1450°C), b) without argon protection (at room temperature)

4.3. Macrostructural characterization of various castables

This section presents the extensive macrostructural observations carried out on the castables throughout the project. Within the framework of this project, the macrostructural analysis of materials is a key result, since it forms an integral part of the objective.

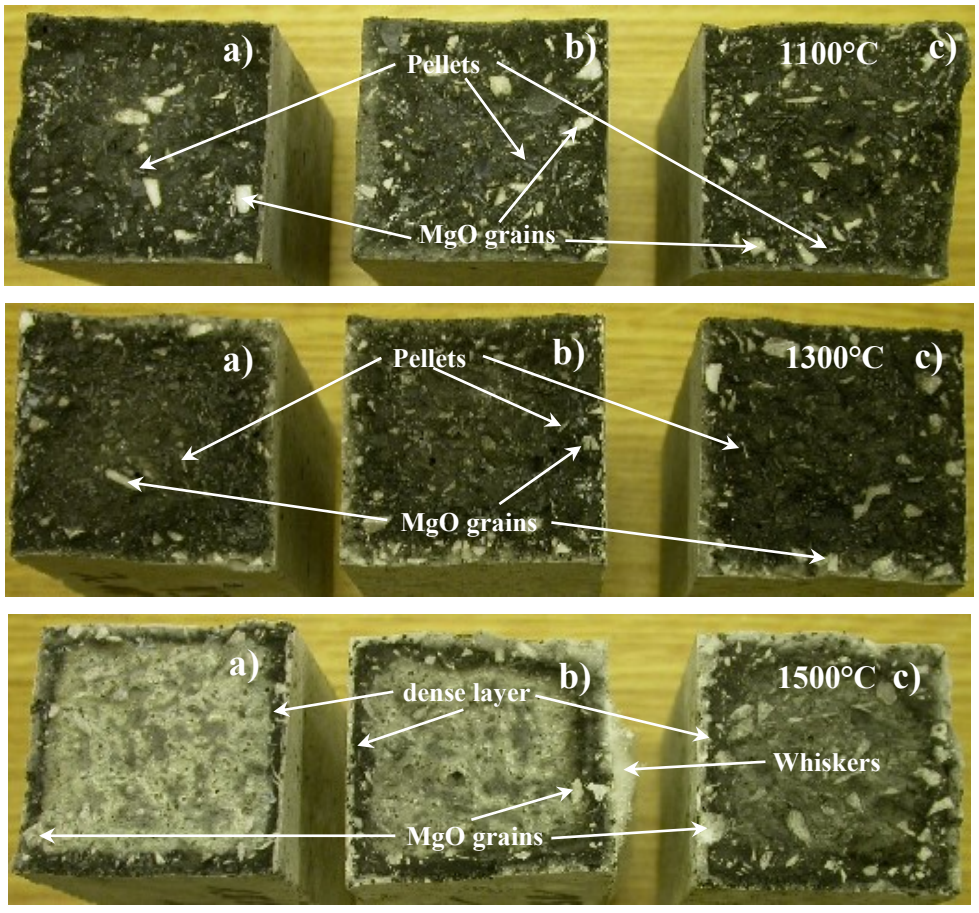

Figure 4.9. Castables pre-fired and tested at 1100, 1300, 1500°C, the holding time was a) 5 hour, b) 10 hours and c) 15 hours

The observations were all made on pre-fired samples after testing either on bars or on wedge splitting test specimen. In the first part differences between the samples pre-fired with different holding times and pre-fired and tested with different temperatures will

be discussed. In the second part a closer look on the four main groups of castables mentioned in chapter 3 will be taken.

As shown in figure 4.5 holding times and pre-firing temperatures as well as testing temperatures have a big influence on the maximum strength of the castables. The macroscopic observations done can give us a rough idea what happens during firing and during testing.

The fracture surfaces presented in figure 4.9 reflect the differences in the oxidation extent due to pre-firing and testing at different temperatures.

An interesting aspect is the formation of MgO whiskers on the outside of the castables. This whiskers can be seen very well in figure 4.9 b) at 1500°C. Figure 4.10 shows a microscopic picture of those MgO whiskers.

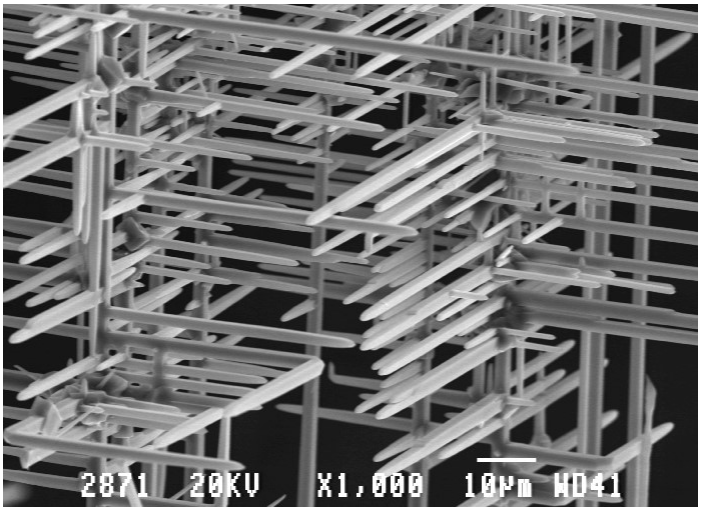

Figure 4.10. MgO whiskers

Part two of this section will take a closer macroscopic look on the four main groups which were examined. Especially the important role of Si as an antioxidant, group one with different amount of EG pellets and the extremes of the other groups compared

to the “reference” sample are compared. For more detailed observation the larger wedge splitting test specimens were used.

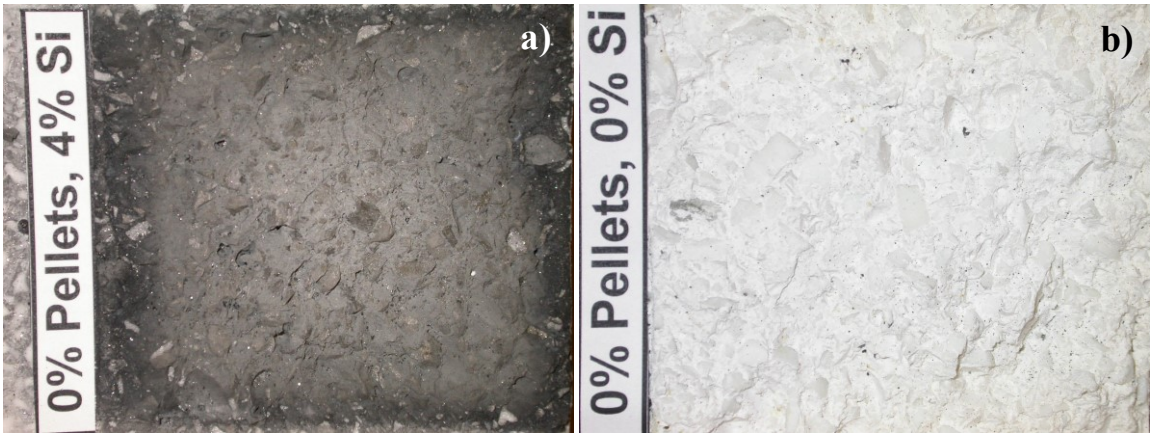

Figure 4.11. a) Castable 1 (0% Pellets, 4% Si), b) Castable 14 (0% Pellets, 0% Si)

Figure 4.11 shows that Si is responsible for the secondary carbon formation: Both samples were fired in coke at 1300°C for five hours, while there was secondary carbon formation in sample a) -with 4% Si, there was no secondary carbon formation in sample b) -without Si. That confirms that Si makes the reduction of carbon containing phases possible.

Figure 4.12 shows an overview of group one. In this group the amount of EG pellets varies from zero to 9%. The degree of oxidation from figure 4.12 a) to d) can be easily seen. While figure 4.12 a) (without pellets) does not show much oxidation, the oxidation increases with increasing amount of pellets and hence increasing porosity. The darker outside layer and the brighter inside layer can be distinguished by visual observation in all the samples.

It is easy to see, that the surface of the pellets is coated with a bright layer in all the samples. It was observed later in SEM that this is due to thin coating on the pellets.

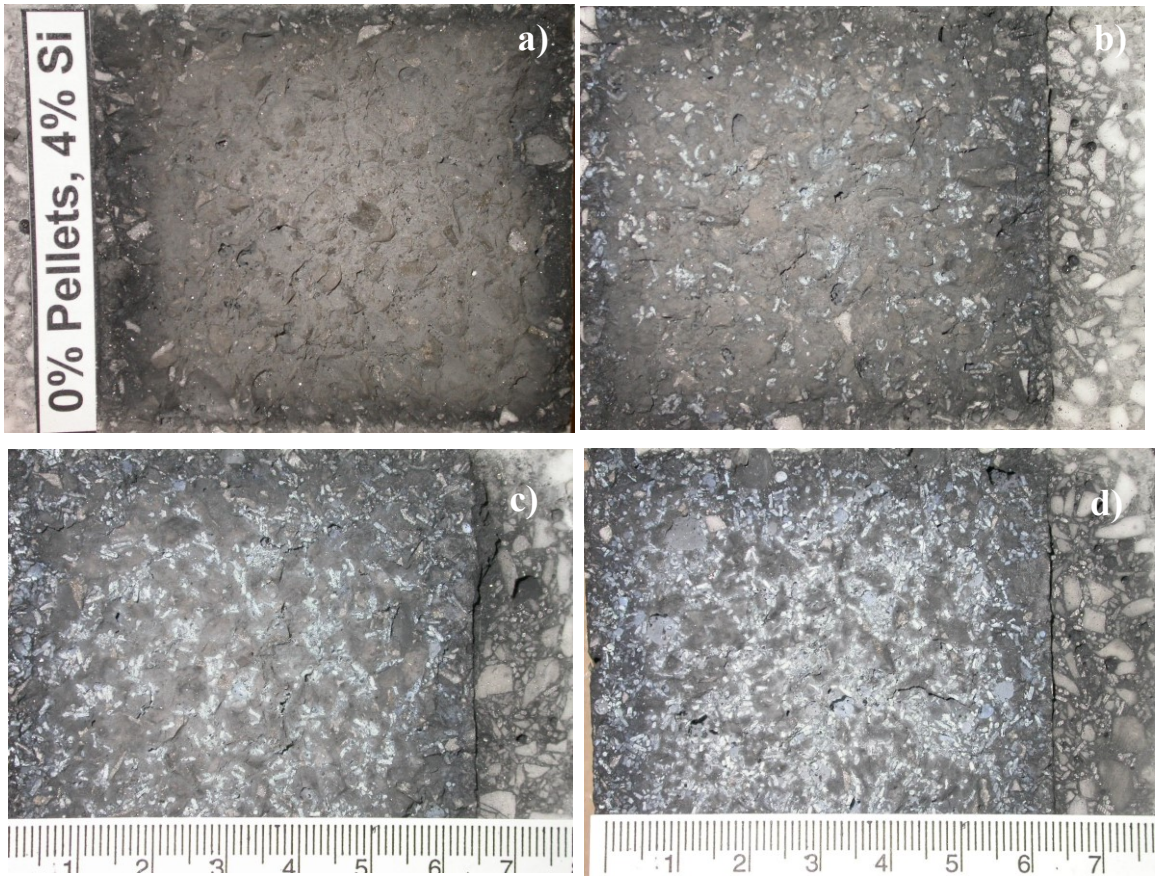

Figure 4.12. a) Castable 1 (0% Pellets, 4% Si), b) Castable 2 (3% Pellets, 4% Si), c) Castable 3 (5% Pellets, 4% Si; reference), d) Castable 5 (9% Pellets, 4% Si)

Figure 4.13 shows the "extremes" produced in the frame work of this thesis compared to each other. Samples a) and c) contain the same amount of pellets (5%) but there is an extra of 4% fine carbon in sample c). It is observed that the pellets in the samples look the same (decohesion). Sample c), with fine C, has a black core while sample a), only pellets, has a whiter core (as C is deposited mostly on the periphery). Samples b) and d) look similar since there is flake graphite in both. Sample b) is a castable and has more pores than sample d), a brick.

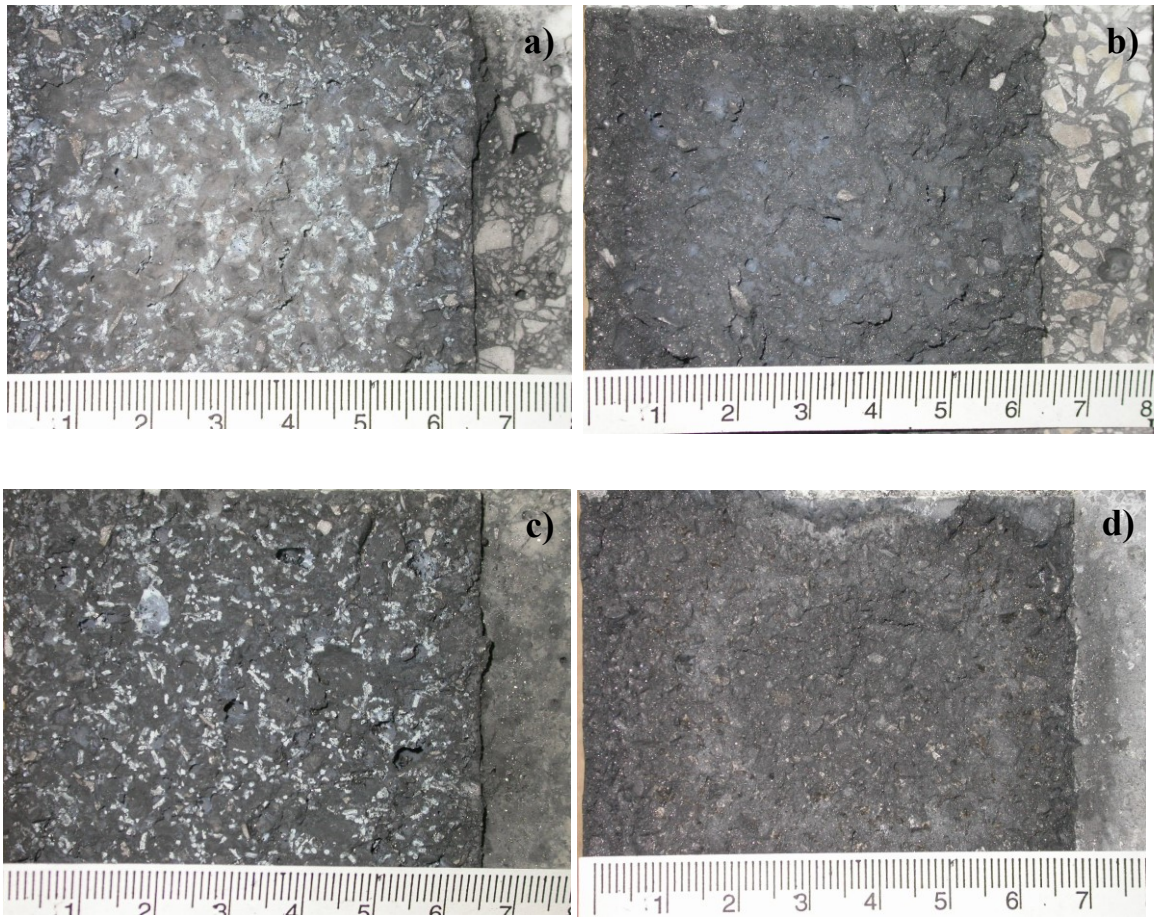

Figure 4.13. a) Castable 3 (5% Pellets, 4% Si; reference), b) Castable 10 (4,5% Flake Graphite, 4% Si), c) Castable 13 (4% fine Carbon, 5% Pellets, 4% Si), d) Brick 16 (5% Carbon)

4.4. Microstructural properties

In parallel with the mechanical properties, several specimens of different compositions were selected for optical microscopy and scanning electron microscopy (SEM) investigations. This included fracture surface after hot modulus of rupture or after wedge splitting test, as well as polished sections after firing. The emphasis was made on the analysis of the castables with EG pellets, as those represent a novel material.

In the figure 4.14, a typical micro structure of the reference castable (5% EG pellets, 4% Si) after firing at 1300°C for 5 hours is shown, as observed by optical microscopy on a polished section. The main features of the micro structure are large MgO aggregates, EG pellets and pores.

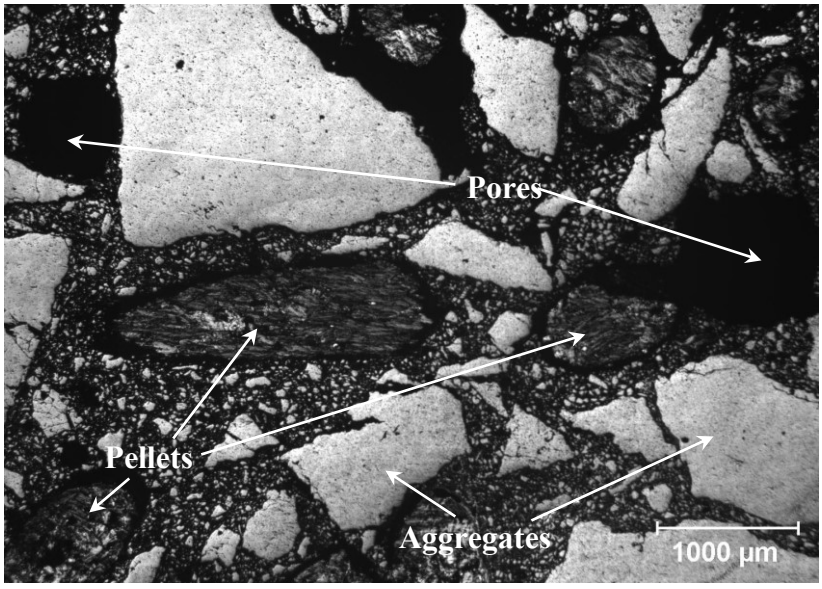

Figure 4.14. Micro structure of the reference castable (5% EG pellets, 4% Si) after firing at 1300°C for 5 hours

Figure 4.15 shows the typical dense layer on the surface of the castables, in this case the reference, fired at 1300°C for 10 hours. It is remarkable, that there is no cohesion with the pellets and the matrix and the pellets are still observable in the dense surface zone.

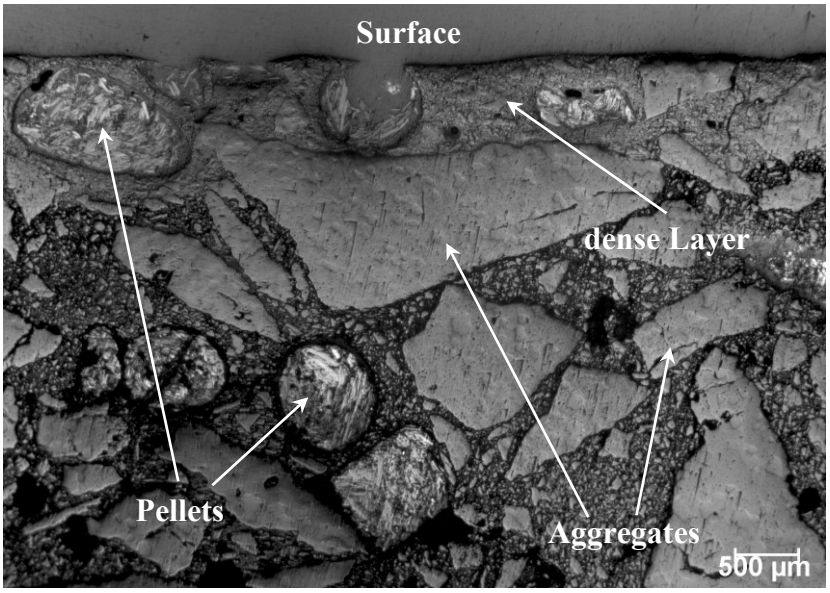

Figure 4.15. Micro structure of the reference castable (5% EG pellets, 4% Si) after firing at 1300°C for 10 hours

Another interesting point, which was mentioned in mineralogy of the castables (see chapter 4.1.1) and shown in the X-ray analysis in figure 4.1, is, that Si particles are still present in the matrix and in the pellets after firing at 1100°C for 10 hours. Figure 4.16 shows the Si particles in the reference castable (5% EG pellets, 4% Si).

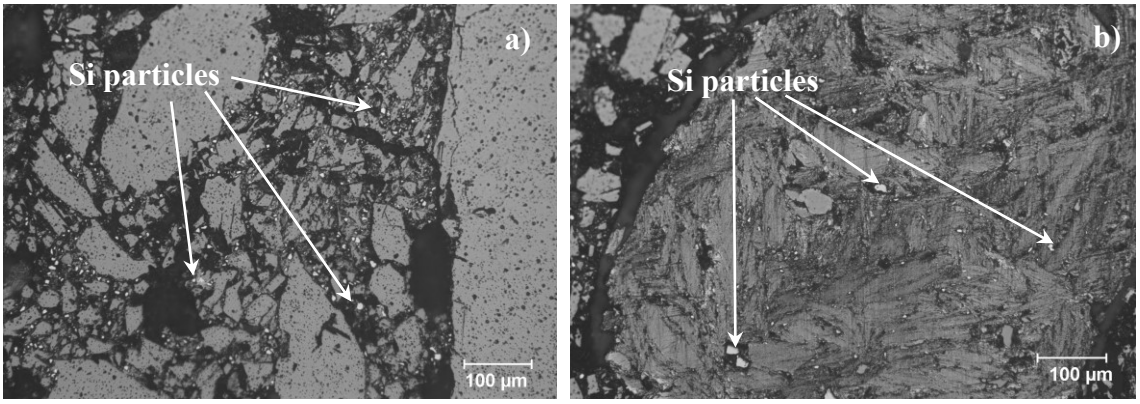

Figure 4.16. Micro structure of the reference castable (5% EG pellets, 4% Si) after firing at 1100°C for 10 hours, a) Matrix, b) EG pellets

The last important observation by optical microscopy on a polished section is shown in figure 4.17, where a void around the pellet can be seen. This void can be observed around all pellets and develops due to bad bonding between the pellets and the matrix.

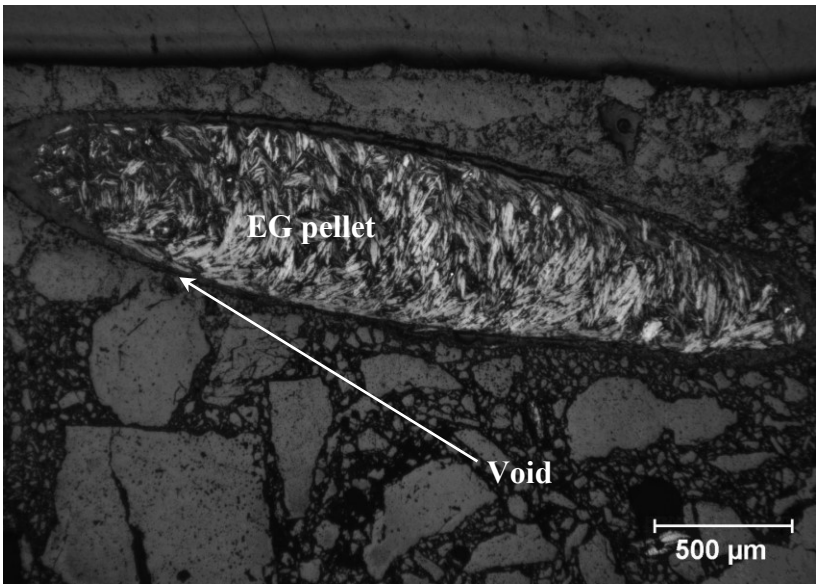

Figure 4.17. Typical EG pellet in the reference castable (5% EG pellets, 4% Si) after firing at 1300°C for 5 hours

In the second part of our microstructural observations we take a closer look on the samples by SEM investigation. First we will take a closer look on the EG pellet itself. Figure 4.18 a) shows the pellets in the castable. The void around the pellets can be easily seen. In addition a coating can be observed on the surface of the EG pellets. Near to the surface of the sample this coating consist of fine forsterite (Mg_2SiO_4) crystals (see figure 4.18 b)). At higher magnification, it can be seen that the coating is made of whiskers, which contend Mg_2SiO_4, according to EDS (see figure 4.18 c)). The difference in the coating structure between b) and c) is due to the oxygen gradient in the sample while firing.

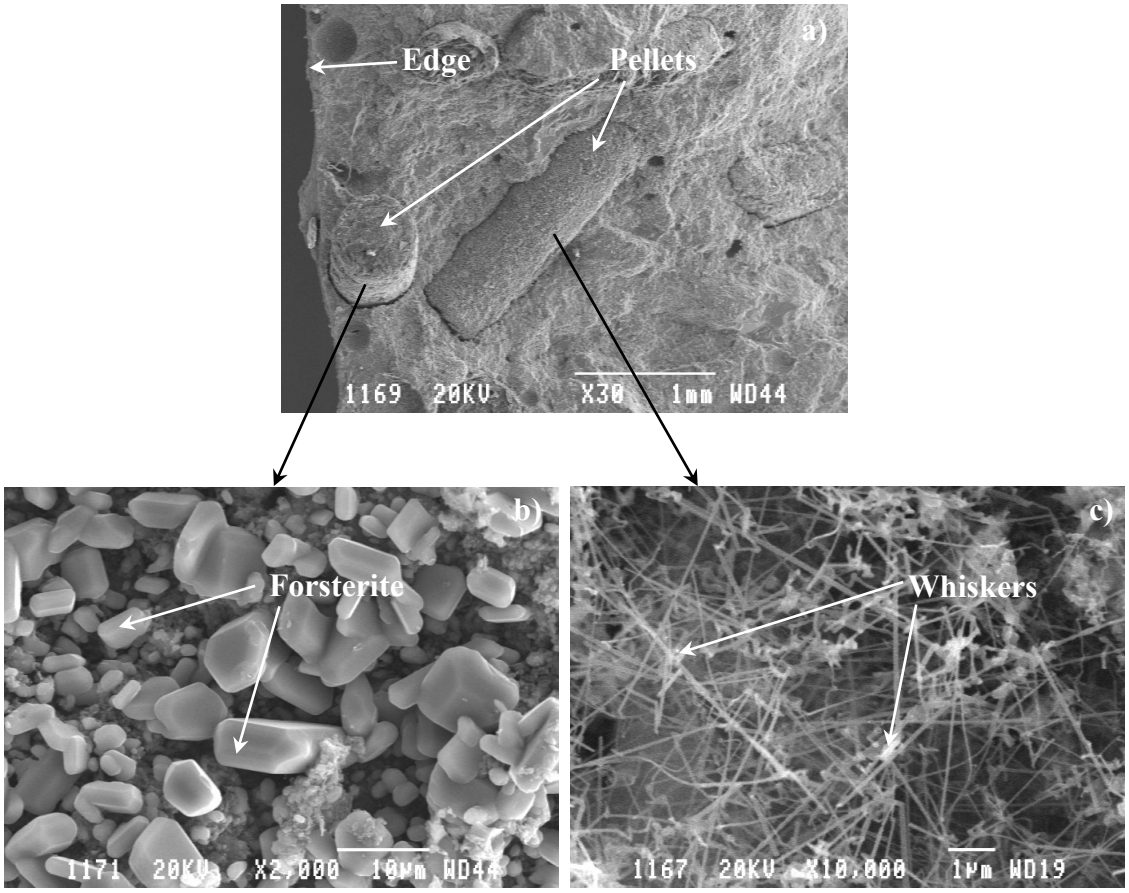

Figure 4.18. Coating of the pellets a) low magnification, b) Forsterite formation near the surface (more oxidation), c) inside, Mg_2SiO_4 whiskers formation

SEM also detected extensive formation of forsterite crystals on the surface of the MgO aggregates (figure 4.19) which promotes bonding between the matrix and the aggregates. Furthermore, the forsterite formation can also be observed at firing temperatures of 1100°C.

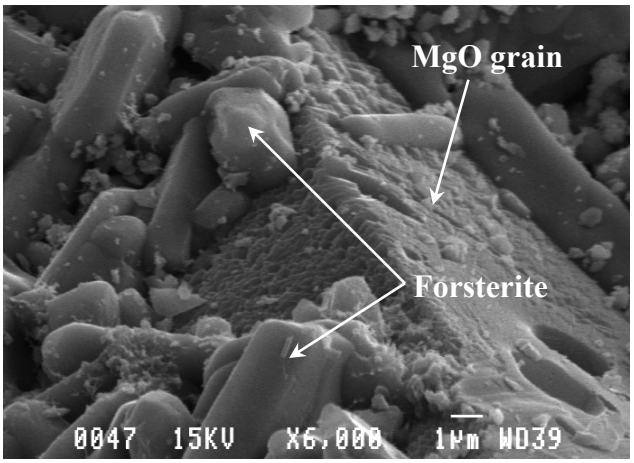

Figure 4.19. Formation of forsterite micro crystals on the surface of the MgO aggregates

We found whiskers in the brick too (figure 4.20). But these were MgO whiskers, not Mg-Si-O. These were identified by EDS, and by comparing their morphology with MgO whiskers found on the outside of the castables (figure 4.21).

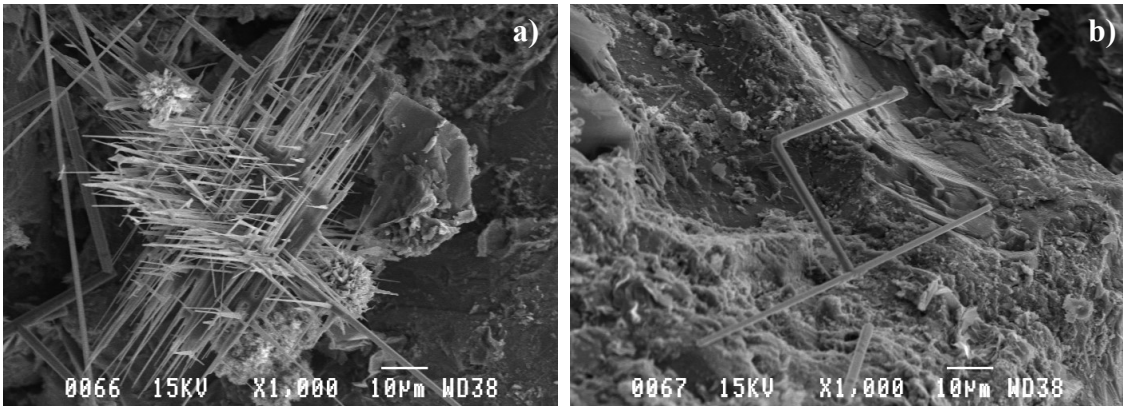

Figure 4.20. Typical appearance of MgO whiskers in a MgO-C brick

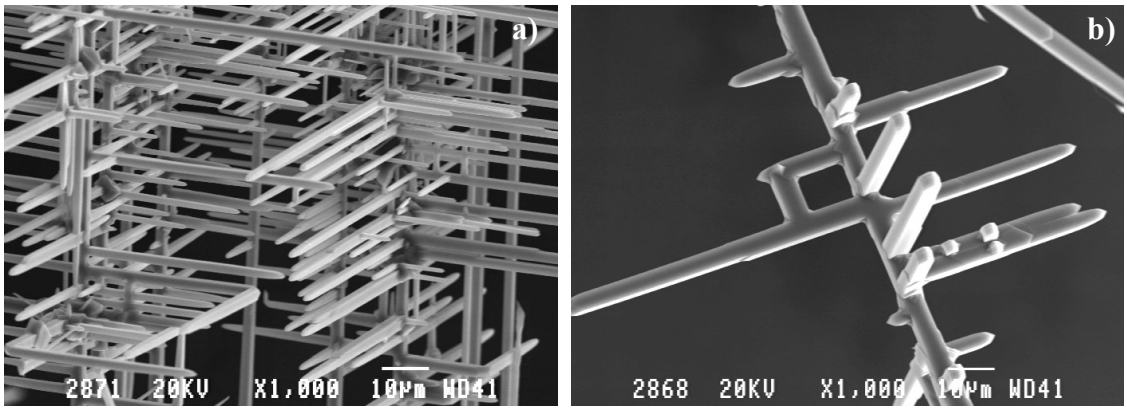

Figure 4.21. Typical MgO whiskers in a castable

Fig. 4.22 shows a SEM image of the flake graphite embedded in the MgO matrix. It is seen that there is a high density of flakes permeating the matrix and hindering the sintering at high temperature, which explains low strength.

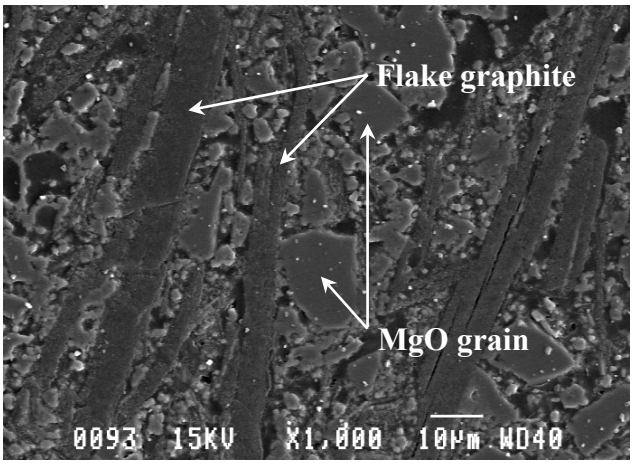

Figure 4.22. Typical appearance of flake graphite in the MgO matrix of a castable

The crack formation while wedge split testing was observed on polished samples, after crack formation when load was applied until 60% of the specimen strength was reached. Figure 4.23 a) shows the crack formation of a sample with EG pellets in comparison to a sample with flake graphite (figure 4.23 b)). It can be observed that in both samples the crack propagates along the bigger aggregates due to the weaker bonding

of aggregates and matrix. Since the sample with EG pellets has a better bonding of the matrix the observed crack is shorter (approx. 3 times) than the one of the sample with flake graphite (see scale).

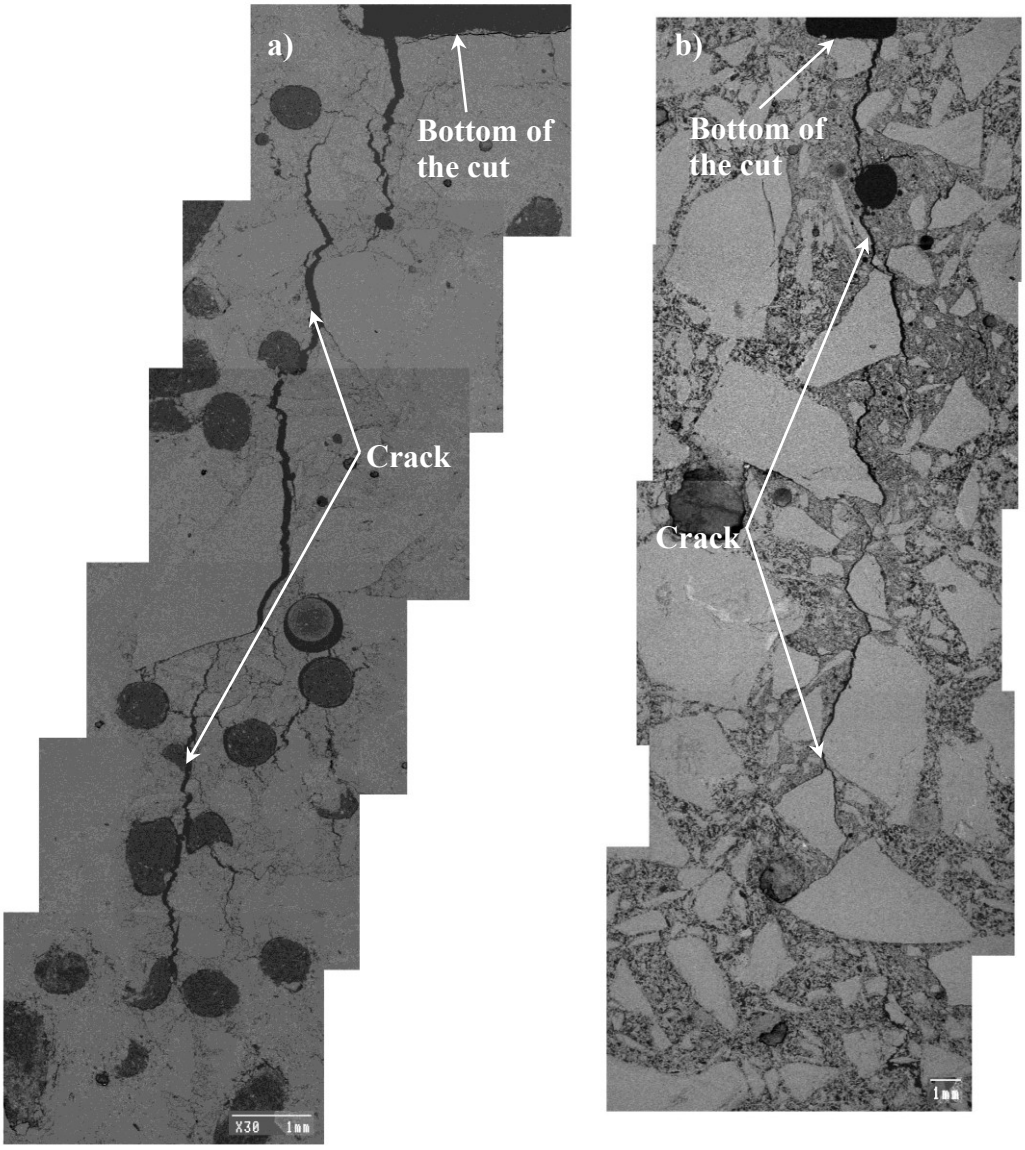

Figure 4.23. Crack formation in a MgO-C castable with a)EG pellets and b) flake graphite as carbon source

4.5. Mechanical and microstructural properties

In this section the mechanical and the microstructural properties of the different castables will be discussed. We will initially present the basic properties, such as the mechanical resistance (modulus of rupture) and the modulus of elasticity followed by the results of the wedge splitting test and the microstructural observations. The modulus of rupture as well as the modulus of elasticity was measured at 1300°C by the 3 point bending test, the work of fracture was determined with the wedge splitting test specimen and the porosity was measured on bars (40x40x160 mm). Since we have sixteen different samples we will first discuss the results in the four main groups and end with some important cross comparisons in between those groups.

4.5.1. Different amounts of Si

Here, we intend to show the important influence of Si as antioxidant.

a) Hot modulus of rupture

In figure 4.24 one can see that Si has a positive influence on the HMOR. With increasing amount of Si the HMOR increases. This is true for samples with and without carbon. In the carbon-free castable, as figure 4.24 shows, Si addition in the matrix has a crucial role in strengthening the castable, increasing the fracture stress from 6,5 to 17,0 MPa. Also, reducing the amount of Si from 4 to 2 wt.% in the castable with 5% pellets leads to 50 % reduction in strength. One can also see that the amount of Si has an influence on the porosity. The porosity is lower for samples with Si.

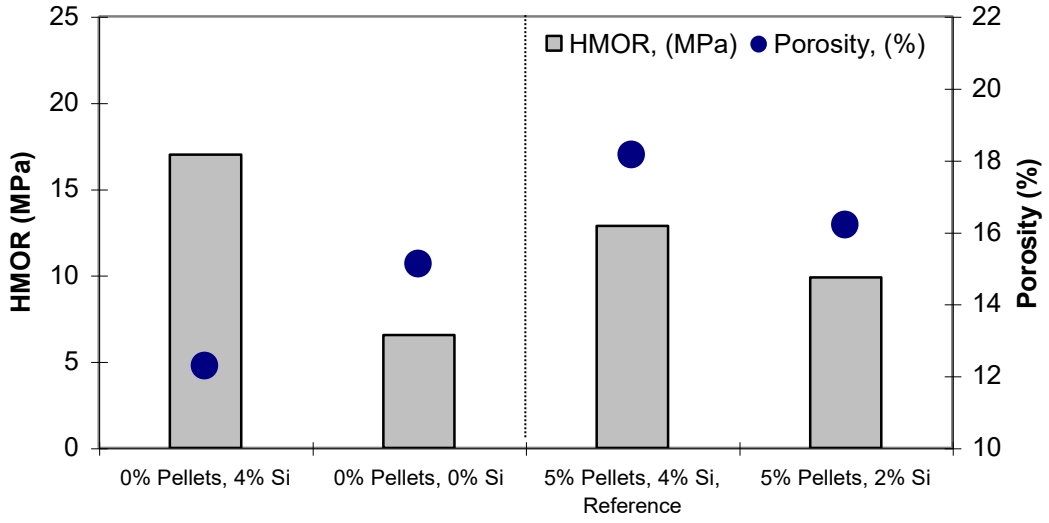

Figure 4.24. Hot modulus of rupture in comparison to the porosity at different amounts of Si

b) Modulus of elasticity

The results of this test are given in table 4.5 and show that within the margin of errors the E-modulus is higher for high Si amounts. All the castables tested have a non-linear behaviour, with the load – displacement relationship deviating from the straight line even at relatively low loads.

Table 4.5. E – Modulus (GPa) of selected castables at 1300°C

Castable	E – Modulus (GPa)	dyn. E – Modulus (GPa)
1 (0%P, 4%Si)	5,1	55
14 (0%P, 0%Si)	3,3	81
3 (5%P, 4%Si)	4,7	46
15 (5%P, 2%Si)	4,0	54

P=Pellets, Si=Silicon

c) Study of the fracture at high temperature (wedge splitting test)

The study of the fracture behaviour is one of the key results of this work. These results were obtained with the wedge splitting test. The test is described in details in chapter 3. In figure 4.25 and 4.26 the curves for the specimens with different amounts of Si are presented. In both cases it can be easily seen that a higher amount of Si increases the work of fracture.

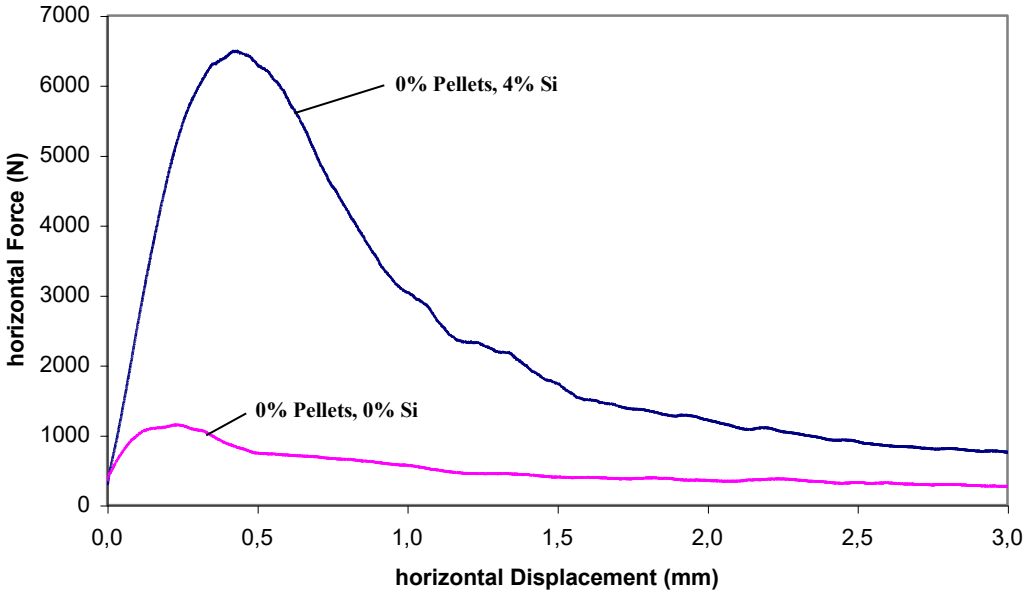

Figure 4.25. Load – displacement curves of castables 1 and 14, at 1300°C

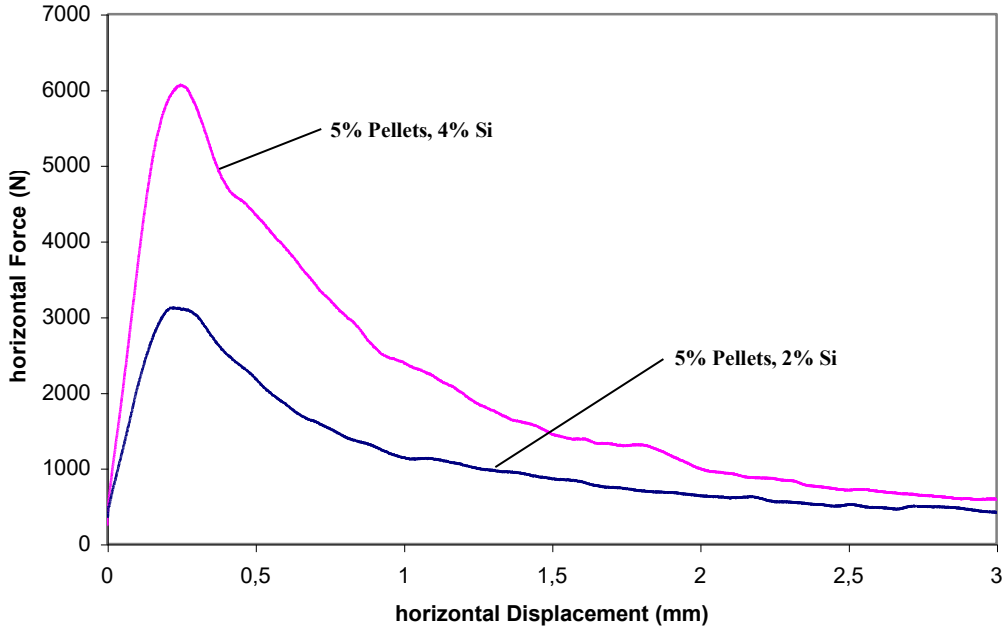

Figure 4.26. Load – displacement curves of castables 3 and 15, at 1300°C

The parameter which is most generally used to characterize the resistance of a material to crack initiation is the critical stress intensity factor (K_{IC}). K_{IC} is proportional to the measured maximum load. The fracture toughness values were calculated for all castables and presented in the appropriate tables. Table 4.6 shows the fracture toughness for different Si content. As can be seen the decrease in Si content results in a considerable decrease of the fracture toughness (in order 50% and 80%).

Table 4.6 Critical stress intensity factor at crack initiation for castables 1, 14, 3, 15

Castable	K_{IC}, (MPa (m)$^{1/2}$)
1 (0%P, 4%Si)	2,3
14 (0%P, 0%Si)	0,4
3 (5%P, 4%Si)	2,2
15 (5%P, 2%Si)	1,1

P=Pellets, Si=Silicon

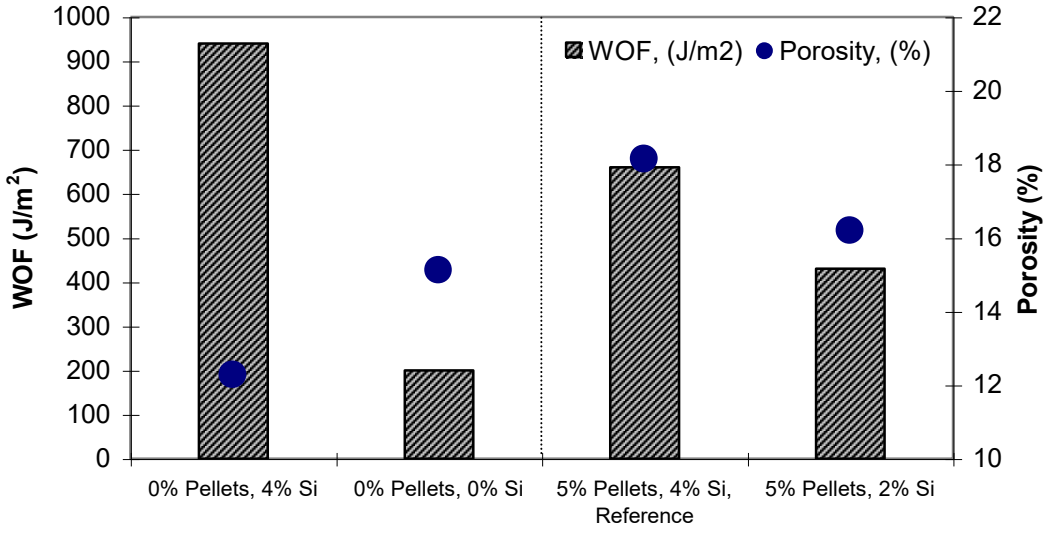

Figure 4.27. Work of fracture in comparison to the porosity at different amounts of Si

In figure 4.27 the work of fracture of carbon free castables with different amount of Si and castables with 5% EG pellets with different Si amount is presented together with their porosity levels. For the carbon-free castable the work of fracture at 935 J/m^2 is five times higher than for the castable without Si addition. For carbon containing castables a higher amount of Si still results in 30% higher work of fracture.

4.5.2. Different amounts of EG pellets

This part highlights the differences of the mechanical properties at varying amounts of EG pellets.

a) Hot modulus of rupture

Figure 4.28 shows that the introduction of carbon has a negative influence on both, the strength and the porosity. However, the strength variations are rather moderate

(from 13 to 11 MPa for 3% to 9% pellets), meaning that a high amount of carbon can be introduced as pellets without significantly loss of strength.

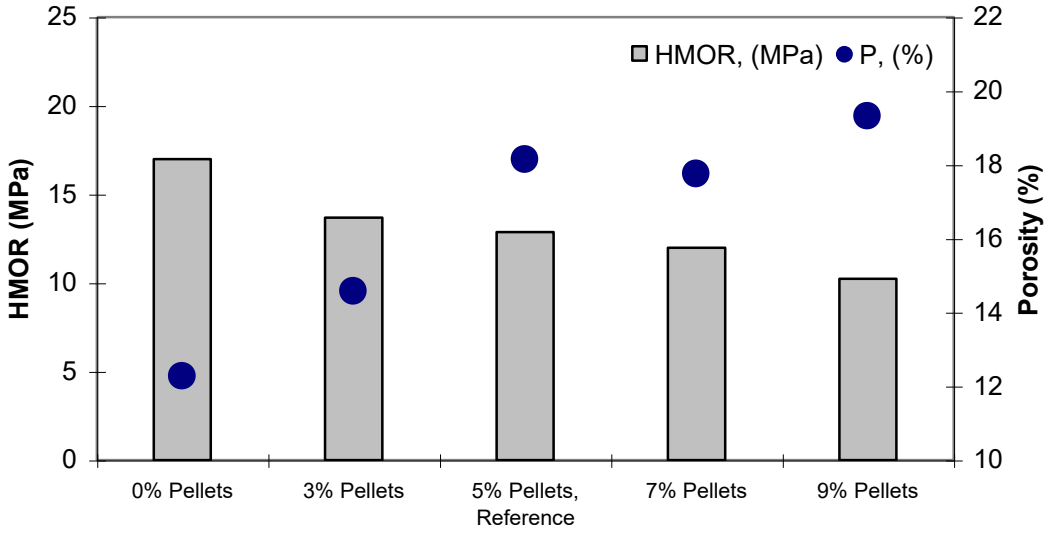

Figure 4.28. Hot modulus of rupture in comparison to the porosity at different amounts of EG pellets

b) Modulus of elasticity

The values of the modulus of elasticity, *E*, evaluated at 1300°C correlate with the porosity levels and development of adequate bonding in the castables. In particular, castables with low carbon (pellet) content exhibit a higher E-modulus value (table 4.7). The introduction of smaller maximum MgO grain size (<3 mm) has a positive effect and increases the E-modulus up to 20% compared with the castable with the same amount of EG pellets but a maximum grain size of 6 mm. The application of long EG pellets slightly increases the E-modulus compared to the castable with the same amount of "normal" EG pellets. The effect of smaller maximum grain size and of the introduction of long EG pellets will be discussed again later in the cross comparison.

Table 4.7. E – Modulus (GPa) of the castables 1 to 7 at 1300°C

Castable	E - Modulus (GPa)	dyn. E - Modulus (GPa)
1 (0%P, 4%Si)	5,1	55
2 (3%P, 4%Si)	4,3	56
3, Reference (5%P, 4%Si)	4,7	46
4 (7%P, 4%Si)	2,8	46
5 (9%P, 4%Si)	3,5	41
6 (5%P, 4%Si, MgO<3)	6,6	59
7 (5%LP, 4%Si)	5,3	47

P=Pellets, LP=Long Pellets, Si=Silicon

c) Study of the fracture at high temperature (wedge splitting test)

The curves presented in figure 4.29 indicate that a difference exists between the castables as for their resistance to crack propagation. The difference is expressed by the width of the peak and the slope of the curve at its maximum. Thus it appears clearly that the castable 1 (with 0% EG pellets) presents the highest resistance to crack propagation, since the curve is very wide and falls slowly while the castable 5 (with 9% EG pellets) has the lowest resistance to crack propagation, since the curve falls very quickly. The same behaviour from low to high amount of pellets can be seen from the critical stress intensity presented in table 4.8. It can be seen that the introduction of long EG pellets or the use of MgO aggregates with lower maximum grain size has almost no influence on the stress level necessary for the crack initiation.

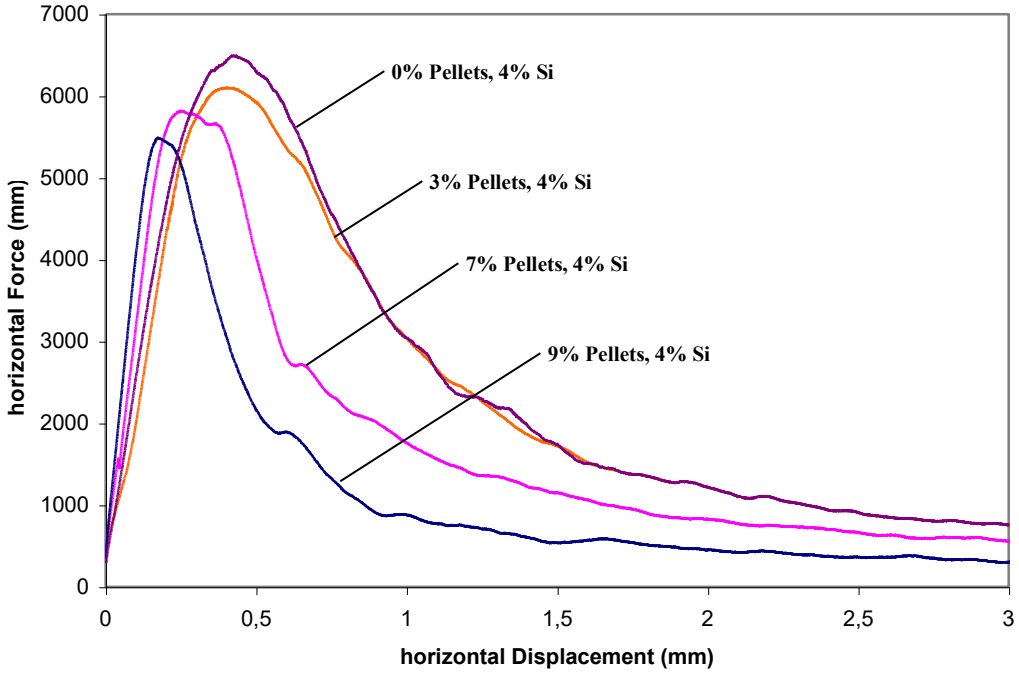

Figure 4.29. Load – displacement curves of castables 1, 2, 4, 5 at 1300°C

Table 4.8. Critical stress intensity factor at crack initiation for castables 1 to 7

Castable	K_{IC}, (MPa (m)$^{1/2}$)
1 (0%P, 4%Si)	2,3
2 (3%P, 4%Si)	2,2
3, Reference (5%P, 4%Si)	2,2
4 (7%P, 4%Si)	2,1
5 (9%P, 4%Si)	1,9
6 (5%P, 4%Si, MgO<3)	2,3
7 (5%LP, 4%Si)	2,2

P=Pellets, LP=Long Pellets, Si=Silicon

The work of fracture shown in figure 4.30, presents in fact the similar trends. Here an explanation can be found in the big change of the porosity level between 0% EG pellets and 9% EG pellets. While the porosity changes from 12% to almost 20%, the work of fracture is decreased by approximately 50%.

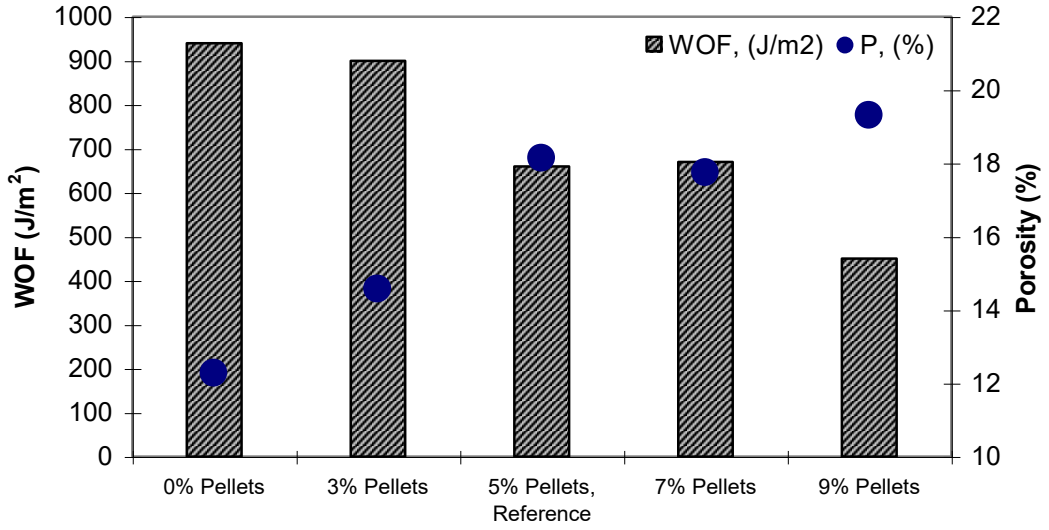

Figure 4.30. Work of fracture in comparison to the porosity at different amounts of EG pellets

4.5.3. Different amounts of flake graphite

The results of the experiments made with different amount of flake graphite are presented in the following section.

a) Hot modulus of rupture

The modulus of rupture is highly affected by the amount of flake graphite. Due to the very bad wettablility of flake graphite, the water content for the castables 9 (2,5% flake graphite) and 10 (4,5% flake graphite) was 2,5% higher than for all the other castables (figure 4.31). This higher water content and hence a higher porosity as well as the bad bonding of the graphite flakes lead to very low values for the HMOR. Compared to the castables 1 (0% flake graphite) and 8 (1% flake graphite) the porosity is 30% to 50% higher for the two castables with the higher flake graphite content and the HMOR is 30% to 70% lower.

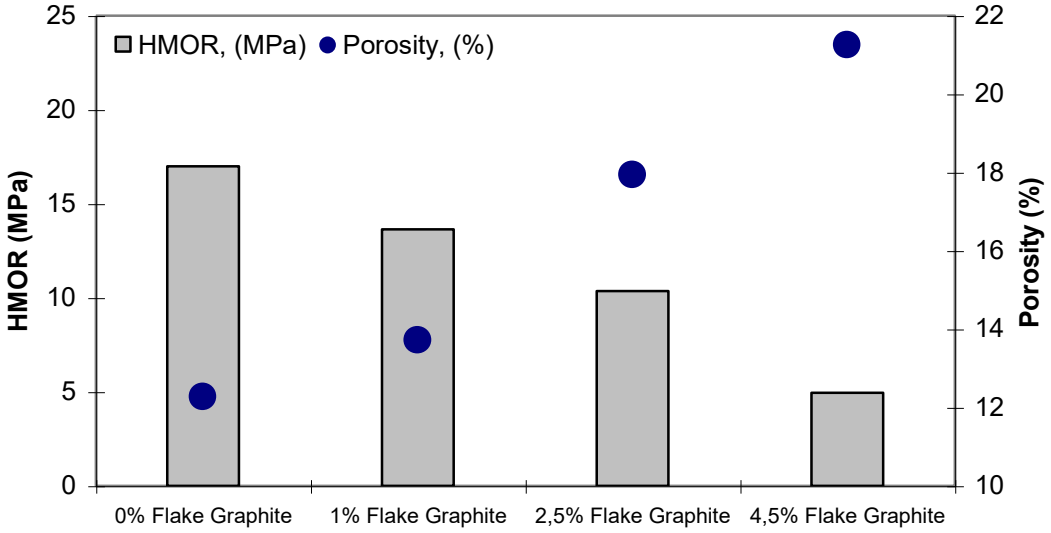

Figure 4.31. Hot modulus of rupture in comparison to the porosity at different amounts of graphite

b) Modulus of elasticity

The modulus of elasticity shows a similar behaviour as the HMOR and decreases from low to high amount of flake graphite. The values of the results of this test are given in table 4.9.

Table 4.9. E – Modulus (GPa) of castables 1, 8, 9, 10 at 1300°C

Castable	E - Modulus (GPa)	dyn. E - Modulus (GPa)
1 (0%FG, 4%Si)	5,1	55
8 (1%FG, 4%Si)	5,5	52
9 (2,5%FG, 4%Si)	3,5	38
10 (4,5%FG, 4%Si)	2,0	32

FG=Flake Graphite, Si=Silicon

c) Study of the fracture at high temperature (wedge splitting test)

Again, due to poor binding of graphite and high porosity, the crack initiation resistance decreases with increasing amount of flake graphite which is shown in figure 4.32 and table 4.10.

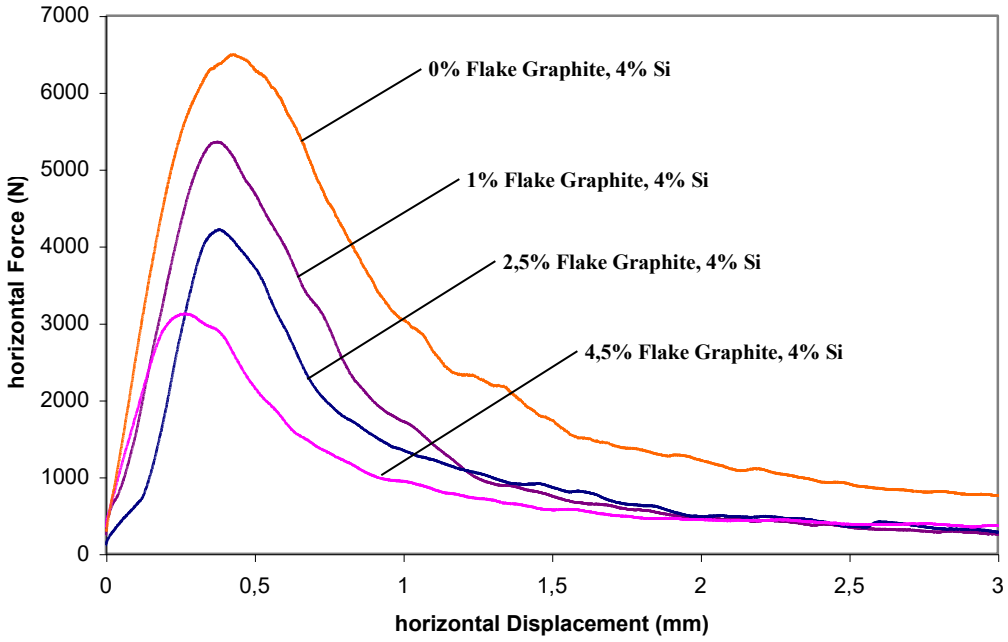

Figure 4.32. Load – displacement curves of castables 1, 8, 9, 10 at 1300°C

Table 4.10. Critical stress intensity factor at crack initiation for castables 1, 8, 9, 10

Castable	K_{IC} (MPa $(m)^{1/2}$)
1 (0%FG, 4%Si)	2,3
8 (1%FG, 4%Si)	1,9
9 (2,5%FG, 4%Si)	1,5
10 (4,5%FG, 4%Si)	1,1

FG=Flake Graphite, Si=Silicon

For the work of fracture, both the high level of porosity and the bad bonding between the matrix and the graphite flakes have an impact on the results shown in figure 4.33. It can be seen that if one compares castable 1 (0% flake graphite) with castable 9

(2,5% flake graphite), the work of fracture is almost 50% lower for the flake graphite containing castable. This result becomes even more distinctive if one compares 0% flake graphite with castable 10 (4,5% flake graphite).

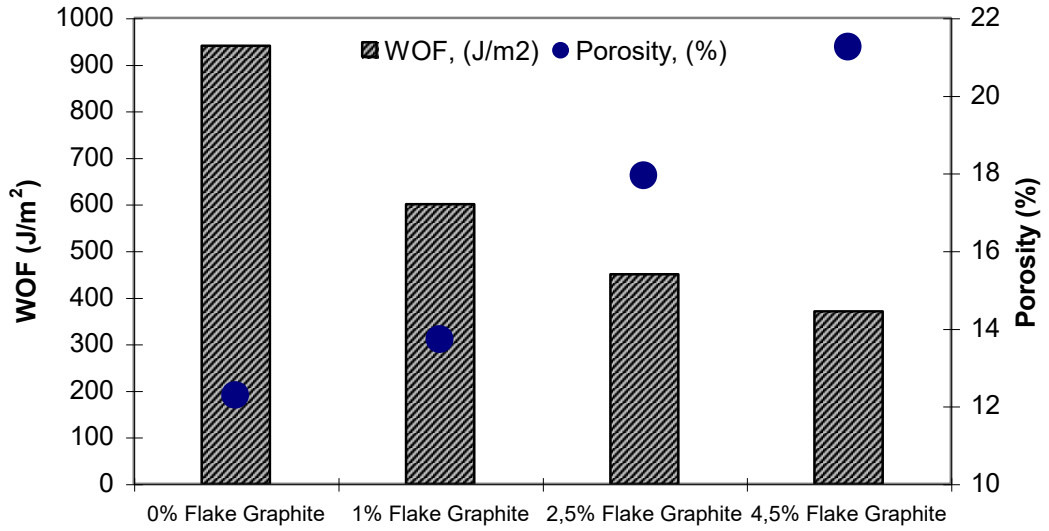

Figure 4.33. Work of fracture in comparison to the porosity at different amounts of flake graphite

4.5.4. Different amounts of fine carbon

The different mechanical properties after fine carbon addition to the "reference" castable are discussed in this section.

a) Hot modulus of rupture

As shown in figure 4.34 the hot modulus of rupture does not change very much with the addition of fine carbon. The same is applicable for the porosity which changes between 18% for castable 3 (reference with 5% EG pellets) to 16,5% for castable 12 (5% EG pellets with 2% fine carbon). The more or less constant level of porosity can be explained in that way, that one does not need more water for the addition of fine carbon.

The porosity for the two castables with 2% and 4% fine carbon addition is even smaller than for the castables with no or just 1% fine carbon addition.

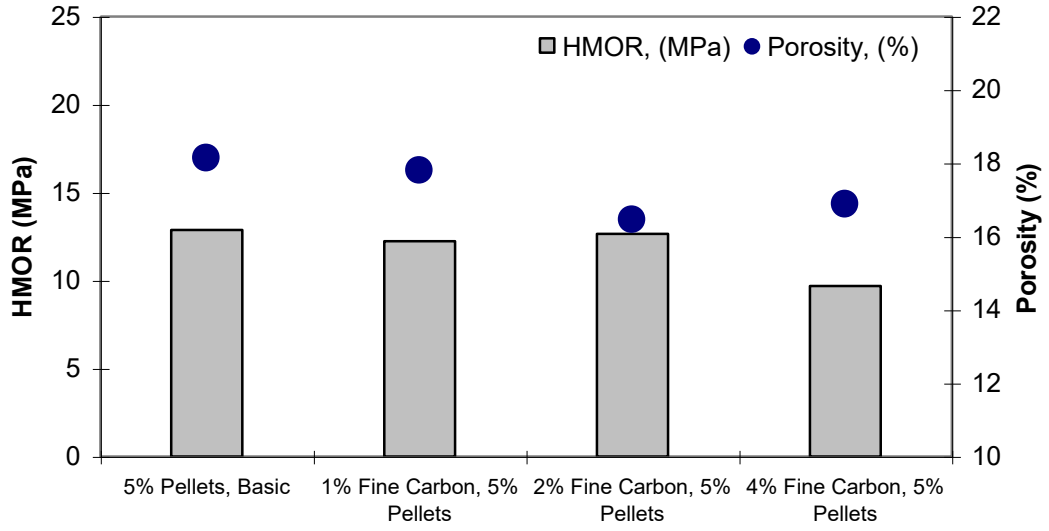

Figure 4.34. Hot modulus of rupture in comparison to the porosity at different amounts of fine carbon addition

b) Modulus of elasticity

The modulus of elasticity, given in table 4.11, shows also a more or less constant behaviour between the margins of errors.

Table 4.11. E – Modulus (GPa) of castables 3, 11, 12, 13 at 1300°C

Castable	E - Modulus (GPa)	dyn. E - Modulus (GPa)
3 (5%P, 4%Si)	4,7	46
11 (5%P, 1% fc, 4% Si)	4,9	44
12 (5%P, 2% fc, 4% Si)	5,0	49
13 (5%P, 4% fc, 4% Si)	3,1	35

P=Pellets, fc=Fine Carbon, Si=Silicon

c) Study of the fracture at high temperature (wedge splitting test)

For the crack propagation shown in figure 4.35 one can see that the curves are very wide and hence a good resistance against cracking can be expected. Since the critical stress intensity, shown in table 4.12 decreases with increasing amount of fine carbon addition it is not surprising that the work of fracture (figure 4.36) decreases also from castable 3 (0% fine carbon addition) to castable 14 (4% fine carbon addition)

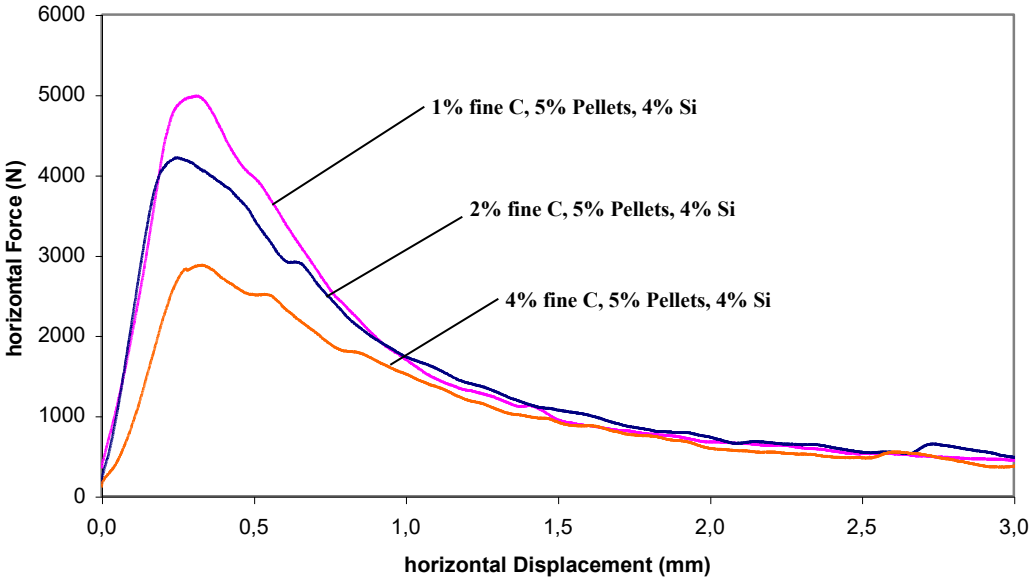

Figure 4.35. Load – displacement curves of castables 11 to 13, at 1300°C

Table 4.12. Critical stress intensity factor at crack initiation for castables 3, 11, 12, 13

Castable	K_{IC}, (MPa (m)$^{1/2}$)
3 (5%P, 4%Si)	2,2
11 (5%P, 1% fc, 4% Si)	1,8
12 (5%P, 2% fc, 4% Si)	1,5
13 (5%P, 4% fc, 4% Si)	1,0

P=Pellets, fc=Fine Carbon, Si=Silicon

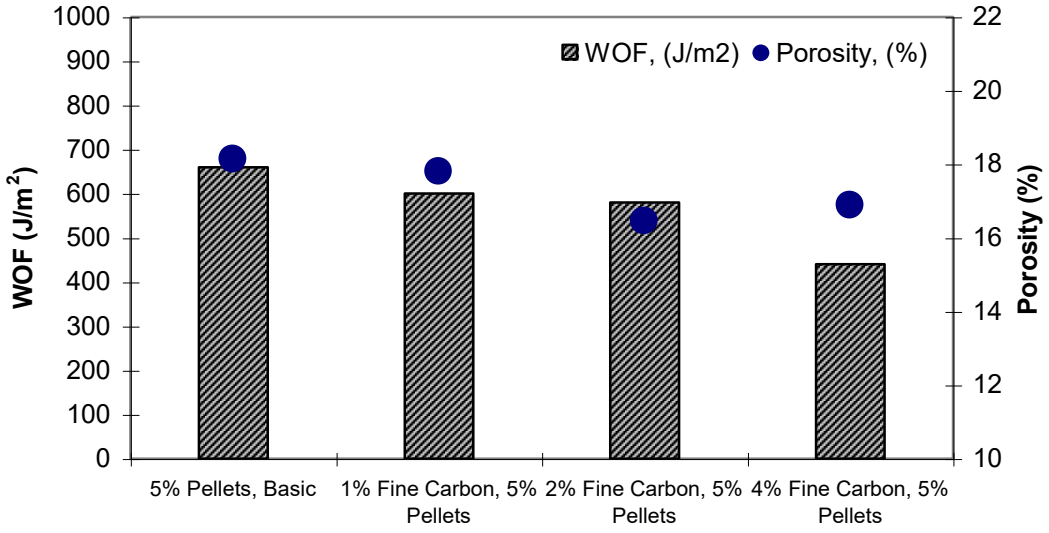

Figure 4.36. Work of fracture in comparison to the porosity at different amounts of fine carbon addition

4.5.5. Cross comparisons

This section serves for comparisons between the different groups, to show some extremes and to show some advantages and disadvantages of the different carbon sources.

a) Castable with 5% EG pellets – MgO-C brick (5% Carbon)

Here, the comparison is done for different castables and a MgO-C brick with approximately the same carbon amount. Figure 4.37 shows the HMOR in comparison to the porosity of three castables and one brick. It can be seen easily that there is a high difference between the porosity, which is around 11% for the brick and between 16% and 18% for the castables. The HMOR on the other side does not show extreme differences. In fact castable 6, with a smaller maximum grain-size (<3 mm) and a much higher level of porosity, has the same strength as the MgO-C brick. Overall one can say that the

values of the HMOR of the tested samples are very high and hence almost in the range of modern MgO-C bricks (like the tested one).

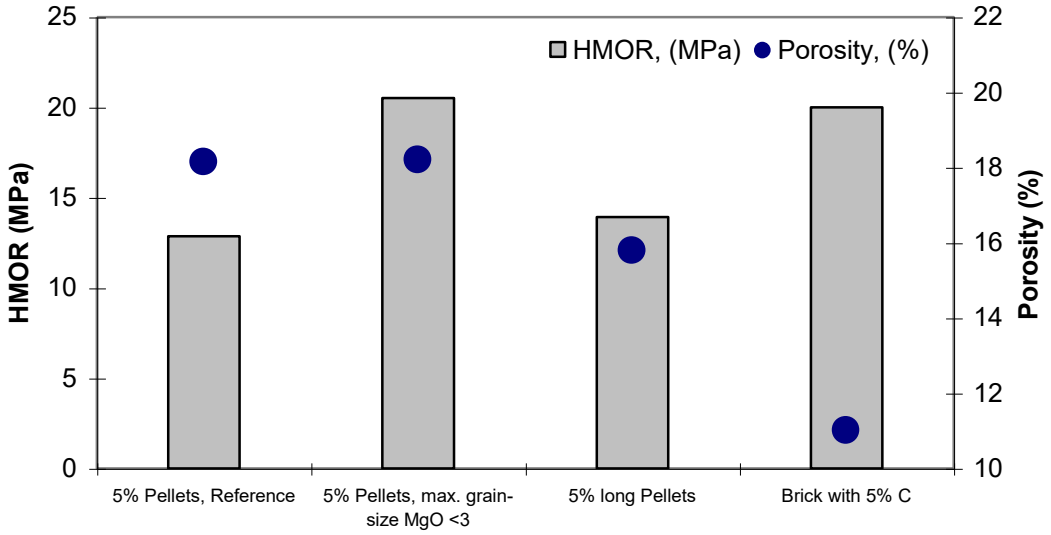

Figure 4.37. Hot modulus of rupture at 1300°C in comparison to the porosity of castables with EG pellets compared to a MgO-C brick

That the difference between the work of fracture of MgO-C castables with EG pellets and MgO-C bricks is very small is shown very well in figure 4.38. Again, even with huge differences between the porosity levels the work of fracture is almost the same for all those samples. The critical stress intensity factor, in table 4.13, also shows a more or less constant level between the castables and the brick.

Table 4.13. Critical stress intensity factor at crack initiation for castables 3, 6, 7, 16

Castable	K_{IC} (MPa $(m)^{1/2}$)
3, Reference (5%P, 4%Si)	2,2
6 (5%P, 4%Si, MgO<3)	2,3
7 (5%LP, 4%Si)	2,2
16, Brick (5% C)	2,3

P=Pellets, LP=Long Pellets, C=Carbon, Si=Silicon

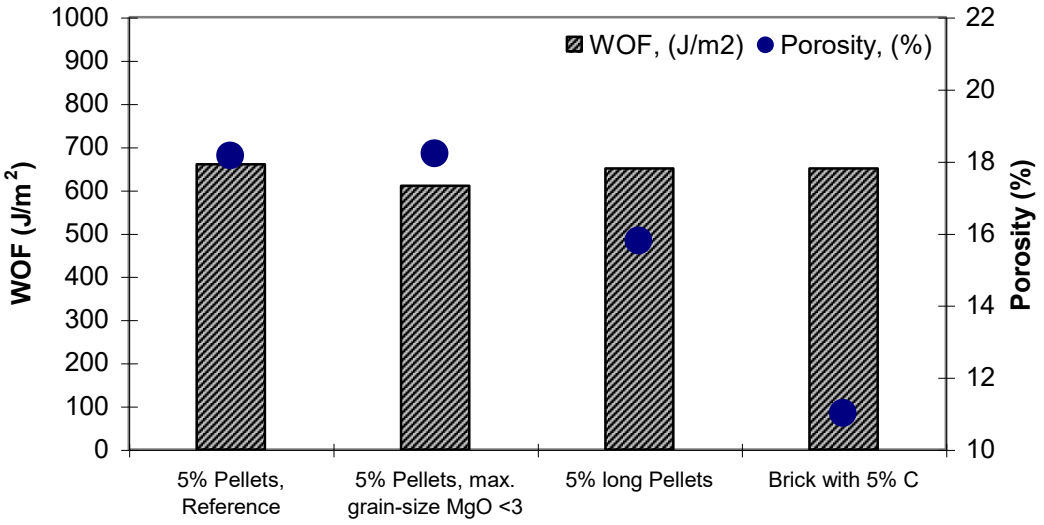

Figure 4.38. Work of fracture in comparison to the porosity of castables with EG pellets compared to a MgO-C brick

b) EG pellets – flake graphite with approximately the same carbon content

This comparison should show the advantages of the EG pellets to flake graphite. Two cases were examined and in each case a castable with 5% and 3% EG pellets was compared to a castable with flake graphite corresponding to approximately the same carbon content. Figure 4.39 compares the HMOR and the porosity values of these castables. It can be easily seen that castables with the same carbon content have huge differences in both, the strength and the porosity. The samples with flake graphite as a carbon source are much weaker and show higher porosity than the samples with EG pellets. It can also be seen that with increasing carbon content the differences in strength and porosity are growing between EG pellets and flake graphite.

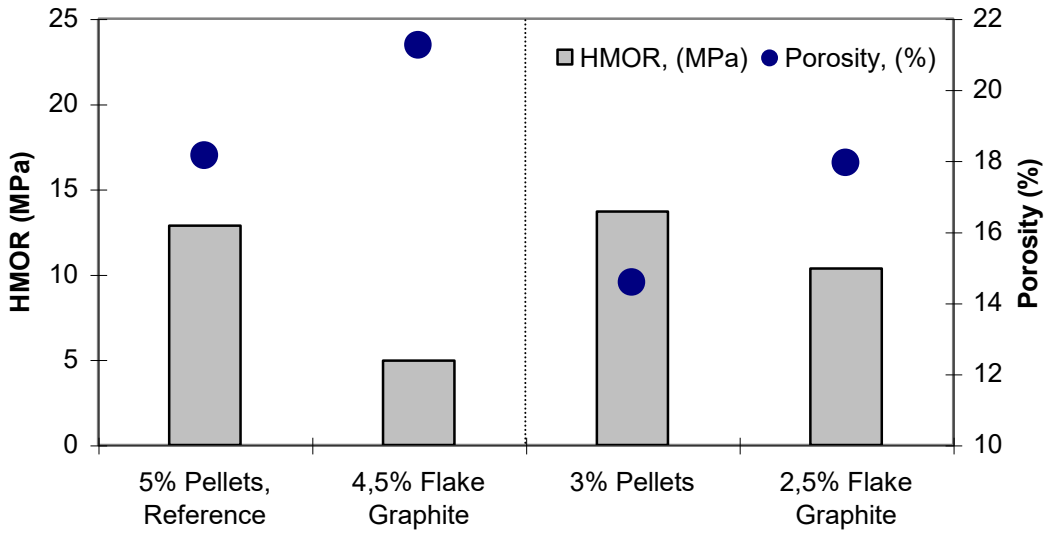

Figure 4.39. Hot modulus of rupture in comparison to the porosity of castables with EG pellets compared to castables with flake graphite

Almost the same results are shown in figure 4.40 were the work of fracture is compared with the porosity. Again, the differences between the flake graphite samples and the EG pellets are enormous.

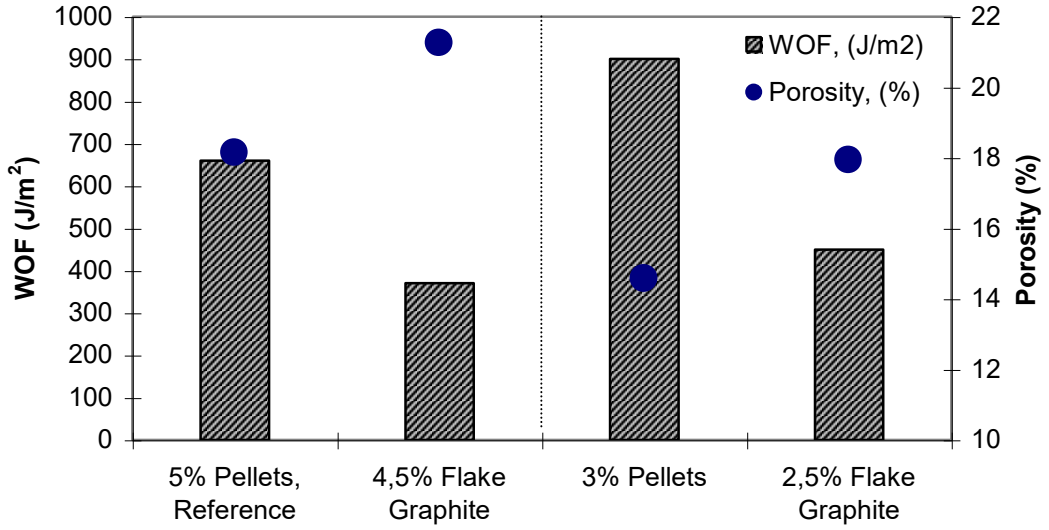

Figure 4.40. Work of fracture in comparison to the porosity of castables with EG pellets compared to castables with flake graphite

c) 2,5% flake graphite – 5% EG pellets with 2% fine carbon addition

To highlight the difference between flake graphite and EG pellets even more, this comparison shows that even castables with an approximate carbon content of 6,5% (5% EG pellets plus 2% fine C) have a higher maximum strength, lower porosity and a better work of fracture (figure 4.41 and figure 4.42) than castables with just 2,5% flake graphite.

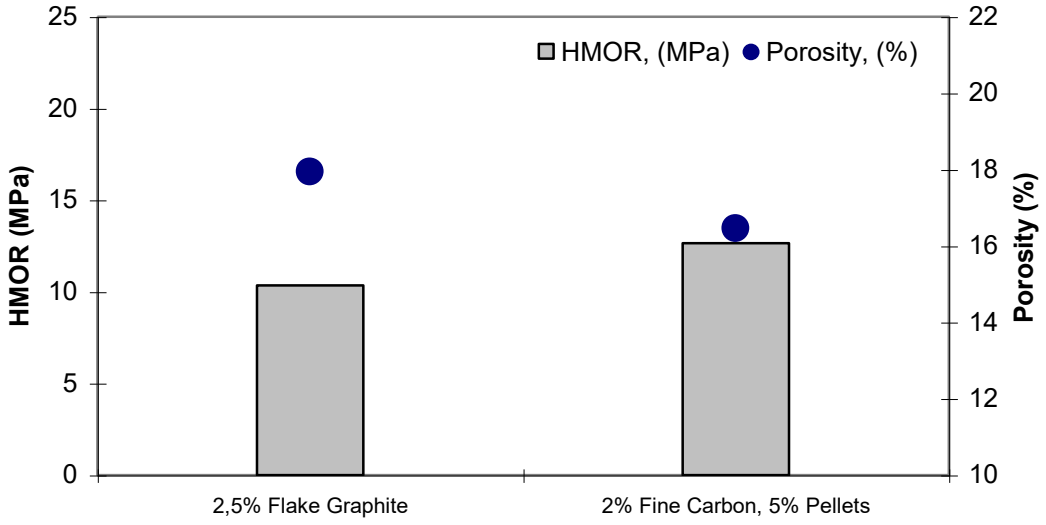

Figure 4.41. Hot modulus of rupture in comparison to the porosity of castables with flake graphite compared to castables with EG pellets with 2% fine carbon addition

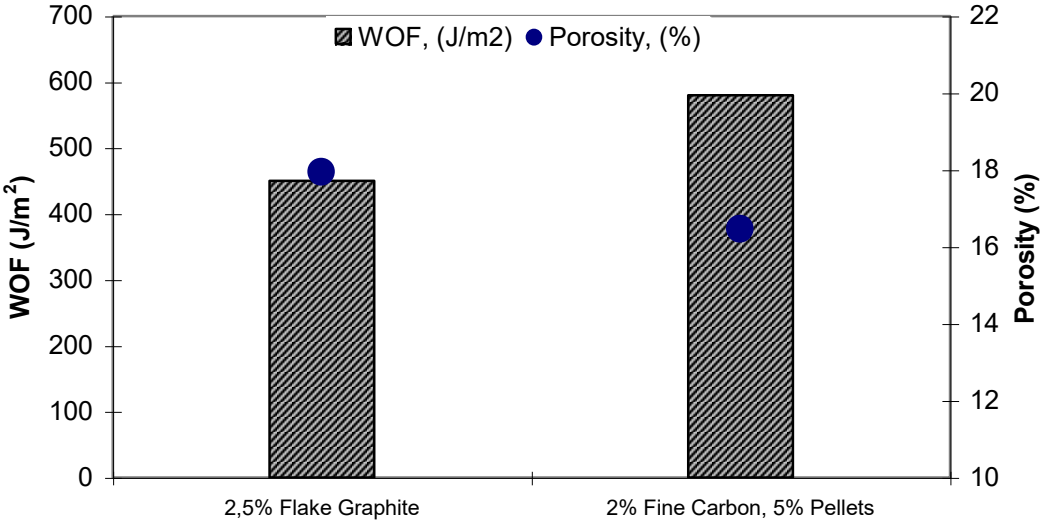

Figure 4.42. Work of fracture in comparison to the porosity of castables with flake graphite compared to castables with EG pellets with 2% fine carbon addition

Chapter 5. Interpretation and recommendations

This chapter is a last overview about the whole project. It shows once more the object of the thesis, the methodology of the testing, it presents the achievements and the results which could be made during the work and it shows the meaning and the limitations of the achieved results.

5.1. The objective of the thesis

Incorporating carbon into castables has long been considered a controversial challenge. Among many different carbon types, the flake graphite is thought to be the most desirable source of carbon, as it has the largest crystal size and the highest oxidation resistance. However, the principles used in the design of resin-bonded magnesia-carbon brick with the addition of natural flake graphite could not be simply transferred to castables because the properties of flake graphite are not compatible with a water based castable system. Adding flake graphite into castables leads to a radical deterioration of rheological properties, and subsequently to an increased water demand, higher porosity and lower strength, resulting in the total loss of any advantage expected from incorporating graphite in the castable (Teranishi, 1998).

In order to avoid the problems caused by the addition of flake graphite, other types of carbon sources - such as pitch, carbon black, amorphous graphite, and needle coke, have been used in castables, but with unsatisfactory results. Low oxidation resistance of these carbons, as compared to the flake graphite, ultimately results in the high apparent porosity and low strength. Therefore, recent studies in carbon-containing castables attempt various approaches to modify flake graphite for use in castables (Rigaud, 2002; Zhang, 2002). However, in most cases, the high porosity, high oxidation, and low strength of these castables have prevented them from being used in severe conditions such as in the steel-making industry.

Newly employed extruded micro-pellets were developed in CIREP as an efficient strategy for incorporating flake graphite into castables. The advantages of using EG pellets in castables have been documented in terms of water addition and flowability, oxidation and corrosion resistance of the castables (Rigaud, 2002 and 2003). These key issues notwithstanding, thermo-mechanical stresses are another main factor strongly affecting the performance of refractory products. The dynamic stresses and thermal shock conditions in service require materials with high resistance to thermo-mechanical failure and crack propagation. Therefore, achieving a high level of mechanical properties becomes a very important issue. In this paper, thermo-mechanical properties of new carbon-containing castables are reported. While the emphasis is on the castables, incorporating extruded graphite (EG) pellets, comparison with other carbon sources are also presented.

To tackle the problem of adding flake graphite (FG) into castables, the agglomeration of flake graphite with an organic binder was employed in order to obtain elongated filaments by extrusion. After curing and milling, micro-pellets of 0.5mm in diameter and 2-4mm in length were obtained (EG-1). The improvements were then gradually introduced to each new generation of pellets – both in the composition design and in the surface treatment. Whereas the EG-1 pellets contained only flake graphite and binder, several antioxidants were added in the EG-2 pellets in the initial mixing step. In the EG-3 pellets, the pelletized packages contained flake graphite, binder, antioxidants and oxide fillers.

Characterization of EG pellets was carried out in full through measurements of physical properties, pore size distribution, oxidation resistance, mechanical properties and microstructural analysis. In particular, it was found that the bulk density of the extruded pellets increased from 1.31 g/cm^3 in the first generation of pellets (EG-1) to 1.54 g/cm^3 in the third generation (EG-3). At the same time, the median pore size in those two groups of EG pellets dropped from 8.8μm to 1.5μm, and it was possible eventually to produce

pellets with median pore size of 0.5µm. Furthermore, EG-4 pellets were obtained by adding a surface treatment step to the EG-3 pellets. As the result, the porosity of the new pellets was reduced by approximately 50 % as compared to the EG-3 pellets.

From EG-1 to EG-4, not only density and porosity, but also pore size, oxidation resistance, and the strength of the pellets were improved. The positive role of EG pellets, which contribute to improved oxidation resistance of the castables, was effectively exhibit. This is mainly due to decrease in the water addition from 8% (FG containing castable) to 6% (EG-1 to EG-3 containing castables). Even more encouraging results were obtained for EG-4 containing castable by further decreasing the water addition to 4.8%. It is important to note that no decrease in the flow rate as a function of mixing time was observed, which demonstrates the strength improvement of EG pellets, and shows that EG pellets can be used to withstand long-time mixing for big-batch production.

Briefly, it could be summarized that the introduction of graphite into castables in the form of EG pellets indeed brought many advantages as compared to flake graphite and other types of carbon. However, the improvement of the rheology of wet mix, as well as of the oxidation resistance, and hence the corrosion and spalling resistance of carbon containing castables may come at the cost of degradation of mechanical properties due to the presence of carbon. The results, presented in the next paragraphs, show that even those negative effects of carbon addition into castables can be controlled and minimized by using the EG-pellets instead of other carbons.

5.2. Methodology

5.2.1. Design of the mixes

Magnesia based castables were produced using different sources of carbons and various EG pellets. For all of the castables to be considered hereafter, sintered magnesia, with five size fractions of 6.7-3.35mm, 3.35-1.18mm, 1.18-0.3mm and 0.3-0.05mm and ball-mill fines <0.075mm were used. Silica fume, metallic silicium and silicium carbide were used as bonding agents and antioxidants. Carbon sources presented in this paper include fine carbon black (FC), flake graphite (FG) and extruded graphite pellets (EG-4). The castables contained between 0 and 9% carbon of one of those sources, 2% of silica fume, and over 88% of magnesia in total in different size fractions.

5.2.2. Evaluation of thermo-mechanical properties

Hot modulus of rupture (HMOR) was measured by subjecting a rectangular beam specimen with dimensions of 40×40×160mm to 3-point bending test at 1300°C. Cold modulus of elasticity (CMOE) was measured by dynamic technique, using a grindo-sonic system, where the elastic modulus value in flexural vibration mode is measured directly. Hot modulus of elasticity (HMOE) was measured by static technique using the deflection data in 3-point bending test, as measured by LVDT device. Furthermore, fracture behaviour was analyzed employing a wedge splitting test (WST), at a high temperature of 1300ºC.

WST technique was introduced recently as a way to evaluate fracture behaviour of refractories (Harmuth, 1997). This method enables stable crack propagation even for relatively large specimen dimensions that are necessary to eliminate the size effect. In this set-up, load transmission equipment consisting of a wedge, two roll bodies, and two loads transmission pieces which are inserted into the groove. For small angles of the wedge, the machine force, $F_{M,}$ of the testing machine applies a larger horizontal force, F_H, as the splitting force acting to separate the specimen into two pieces. The WST tests

were carried out on an Instron testing machine with a speed of 0.5mm/min during the loading.

The force F_H was calculated by $F_H = F_M / (2\tan \frac{\beta}{2})$, where β is 10^o. Based on the recorded load-displacement curves for the specimen, work of fracture was calculated as follows: $\gamma_{wof} = \frac{\int_\delta Fd\delta}{2A}$, where $\int_\delta Fd\delta$ is the total area under the load-displacement curve, and 2A is the total projected fracture area.

5.3. Achievements and results

Apart from oxidation, corrosion and penetration phenomena, the degradation of MgO-C castables in service conditions is strongly dependent on their resistance to thermo-mechanical stresses. To fully understand thermo-mechanical properties and fracture behaviour of carbon-containing castables, the samples were first fired at different temperatures in coke protection. The hot mechanical properties are characterized by hot modulus of rupture, hot modulus of elasticity and hot wedge-splitting tests at a temperature of 1300^{o}C.

Carbon sources used in castables are divided into two groups: 1) graphitic materials such as flake graphite and extruded graphite pellets; and 2) the combination of extruded graphite with fine carbon black.

5.3.1. Mechanical properties at high temperature

The influence of fine carbon on mechanical properties was studied further in MgO-SiO_2-C castables. The hot modulus of rupture (HMOR) and hot modulus of elasticity (HMOE) at 1300°C were measured, where the castables contained 5% EG pellets and the fine carbon content varied from 0 to 4%. All castables contained metallic silicon as bonding and oxidation agent.

With the addition of fine carbon from 0 to 4%, the HMOR values of castables decreased from 12.9MPa to 9.7MPa. The HMOR value of castable with the combination of 5% EG and 2% fine carbon can be preserved at a level of 12.4MPa, which is quite acceptable. Evolution of HMOE is similar to the HMOR evolution, where the addition of carbon black reduces HMOE values, although not as sharply as HMOR values.

Metallic antioxidant plays a multi-functional role in carbon containing castables. It is not only efficient in reducing pore size and increasing oxidation resistance but also improves the microstructure and the mechanical properties. The antioxidant acts locally

in extruded graphite pellets and overall in the matrix of the castables as well (Rigaud, 2002). The castables containing EG pellets and metallic antioxidant were found to exhibit HMOR values in excess of 10 MPa (Rigaud, 2003). Subsequently, several grades of castables with EG-pellets, flake graphite, and fine carbon, after firing in coke were subjected to WST at 1300°C in argon.

The increase in the strength of castables that results from the presence of metallic silicon addition into the matrix is to a large extent preserved when EG pellets are added, even though the porosity is somewhat increased (Rigaud, 2001). Under the same condition, however, when a non-agglomerated flake graphite or fine carbon is used, the increase in porosity and deterioration of strength is quite significant. The increase of the content of pellets from 3 to 9% resulted in only a slight decrease in strength.

The effect of metallic silicon and EG-pellets on their strength and work of fracture of castables originates from the promotion of bonding and development of porosity upon firing. As the results of both XRD and SEM/EDS indicated, there was a considerable amount of forsterite formed in the castables fired at 1100°C for 5h, and even higher amounts of forsterite (complete disappearance of unreacted Si) after firing at 1300°C. SEM observations of fracture surfaces suggest that the forsterite formation in the castables was substantially promoted by vapour-phase reactions.

Faceted Mg_2SiO_4 crystals reaching in size up to 10-15μm are abundant on the fracture surfaces in the matrix, as well as on the pellets. Reactions involving Mg, SiOx and CO gaseous phases upon firing at 1100-1500°C also resulted in formation of very fine Mg-Si-O-C fibers, primarily as a coating on the surface of the pellets, but also inside the pellets and in the matrix,.

These fibers do not seem to contribute to the cohesion between the matrix and the pellets, as most of the pellets appear to be circumvented by the propagating crack on the

fracture surface. The easy advance of the crack through the essentially porous matrix-pellet interfaces leads to the decrease of the work of fracture values with increasing pellets content in the castables. On the other hand, the well-bonded forsterite layer, typically found around large magnesia grains, contributes to the retention of high-temperature strength, even as the porosity of the castable increases with higher pellets content. Consequently, as compared to the castable containing non-agglomerated flake graphite, the castables with the same amount of carbon in pellets exhibit lower porosity and much higher strength and work of fracture values.

5.4. Interpretation and limitations of the conducted research

In order to better understand the significance of the obtained results both, for further scientific research and for the industrial practice, the following aspects of the experiments carried out in this work have to be considered:

1. All experiments were made within the $MgO – SiO_2 – C$ system. In this system, further optimization of castable compositions, finding the optimal combination of pellet content, antioxidant amount and MgO grain size distribution would be recommended. Also, exploring the use of pellets in different refractory systems, using for example the $MgO – Al_2O_3 – C$ system would be interesting in terms of scientific research. Combining pellets for corrosion resistance and steel fibers for intermediate temperature strength, with possible benefit of fiber protection by the carbon in the pellets would be another way to go.
2. All the results were obtained after prefiring the samples under coke protected atmosphere.
3. The tests at high temperature were made under Argon protection.
4. The temperature was the same everywhere in the sample during testing.

Points 2, 3 and 4 allowed us to produce comparable and reproduceable results in laboratory research. Of course in an industrial trial we would not have the same overall conditions (atmosphere, humidity, outside temperature) as in the laboratory research. There would be no chance to prefire castables under coke protected atmosphere, which would mean that the surface oxidation effects may be more severe. Also there would not be any secondary carbon formation due to the absent of coke protection. The oxidation would be gradual from the outside to the inside of the castable, so that we would have different compositions at different layers of the castable.

Furthermore for industrial practice we would need to consider a thermal gradient in the castable (which, like the gradient of oxidation, would be different from the inside to the outside).

In summary one can see that the conducted research carries different messages for industrial practice and for further scientific research:

In terms of scientific research, recommendations for further testing can be made, using the obtained results to compare them to experiments made at other temperatures, in other systems or with other additives.

For industrial practice the obtained results might not be very interesting in themselves since industrial environments are not quite similar to model environment created in laboratory testing. Here we can make suggestions of promising compositions for in-plant tests. With further scientific research and some results from in-plant trials, we should be able to discover the weak points of selected compositions and improve them further.

Conclusions

1. X-ray, optical microscope and SEM analysis have shown that after firing at 1300°C the microstructure of the castables containing Si as an antioxidant consist of MgO, Mg_2SiO_4, C, SiC and SiO_2 phases. The inner layer is mostly MgO, Mg_2SiO_4, SiC and SiO_2; the outer layer is mostly MgO, Mg_2SiO_4, SiC and C.

2. The porosity of the castables is increasing with increasing carbon content. However, castables with EG pellets show an overall lower porosity than castables with flake graphite as carbon source. This shows that the non-wetting behaviour of graphite was effectively countered through the use of pellets.

3. The HMOR tests at 1100°C, 1300°C and 1500°C and 5, 10 and 15 hours holding time of the reference castable showed that the strength variations between 5 and 10 or 15 hours of firing are rather small and that good strength values can be achieved up to 1300°C. By testing the hot modulus of rupture for all castables it could be observed that increasing the amount of Si increases the HMOR. This is true for samples with and without carbon. Introduction of carbon has a small, but negative influence on the strength. The HMOR is highly impacted by flake graphite due to the very bad wettablility of flake graphite and hence the higher water content. This higher water content and hence a higher porosity as well as the bad bonding of the graphite flakes lead to very low values for the HMOR. The addition of fine carbon has almost no influence on the HMOR.

4. The values of the modulus of elasticity, *E*, evaluated at 1300°C correlate with the porosity levels and development of adequate bonding in the castables. In particular, castables with 4% Si have a higher E-modulus than castables with 2% Si; castables with low carbon (pellet) content exhibit a higher E-modulus value; castables containing a high amount of flake graphite have the lowest E-modulus due to poor bonding in the matrix and high porosity.

5. The wedge-splitting test proved itself as an efficient and reliable tool for the evaluation of mechanical properties at elevated temperatures. In this work, the test allowed in first place to measure the work of fracture values of castables and to analyse the influence of different factors on the work of fracture. It was also used to estimate the E-modulus of castables and to expose the non-linear mechanical response at high temperature. It showed that a higher amount of Si increases the work of fracture. With increasing amount of EG pellets, the work of fracture decreases. A similar behaviour as with increasing amount of EG pellets can be observed with increasing amount of flake graphite, but flake graphite decreases the work of fracture more than pellets. The introduction of fine carbon to 5% pellets also decreases the work of fracture, but not as strongly as high amounts of flake graphite.

6. The observed differences in high temperature properties of different castables evaluated in this work follow from the different microstructures formed in those castables upon firing. The high strength levels (especially in castables with EG pellets and 4% Si) are due to extensive formation of Mg_2SiO_4 bonding phase, in part through reactions in vapour phase. The overall negative influence of carbon in the matrix on the bonding and, consequently, the strength, is significantly reduced when carbon is agglomerated in pellets without sacrifice in oxidation resistance.

7. Overall one can say that the introduction of EG pellets have a positive effect on the properties of MgO-C castables compared to castables with flake graphite as carbon source.

Recommendations:

Since the results with EG pellets are satisfying in laboratory size experiments the main recommendation therefore to be made are:

1. Further optimization of castables composition: finding the optimal combination of pellet content, antioxidant amount and MgO grain size distribution.

2. Evaluation of thermal shock resistance; testing at different temperatures (i.e. 1400°C, 1450°C).

3. Test magnesia carbon castables in a steel making ladle under monitoring and documenting this in-plant trial.

References

BRADT, R. C. (1993), Elastic Moduli, Strength and Fracture Characteristics of Refractories. *Key Engineering Materials*, Trans Tech Publications, Vol. 88, pp. 165-192.

BRISSON, P-Y. (2002), Influence de la microstructure sur le comportement mécanique de bétons alumineux, Mémoire de Maîtrise ès Sciences Appliquées, École Polytechnique de Montréal

CARNIGLIA, S. C., BARNA, G. L. (1992). Handbook of Industrial Refractories Technology. Noyes Publication, 627 pages.

COOPER, C. F. (1994), Graphite, Natures unique Raw Material, *J. Can. Ceram. Soc*. Vol. 63, No. 3, pp. 197-208.

COOPER, C. F. (1987), The Charaterisation and Evaluation of Graphitic Continuous Casting Refractories, *Interceram, Special Issue* Vol. 36*,* pp. 1-6.

COOPER, C. F. (1986), Graphite in Refractories, *Special Publication,* pp. 1-11.

COOPER, C. F. (1984), Refractory Applications of Carbon, Flake Graphite, its Function in modern Refractories, *Br. Ceram. Trans. J.* Vol. 84, pp. 57-62.

COOPER, C. F. (1980), Graphite containing Refractories, *Refractories Jornal*. No. 6, pp. 11-21.

HARMUTH, H., TSCHEGG, E. K. (1997), A fracture mechanics approach for the development of refractory materials with reduced brittleness, *Fatigue and Fracture of Engineering Materials and Structures,* Vol. 20 (11), pp. 1585-1603.

HARMUTH, H., RIEDER, K., KROBATH, M., TSCHEGG, E. (1996), Investigation of the nonlinear fracture behaviour of ordinary ceramic refractory materials, *Materials Science & Engineering*, A214, pp. 53-61.

HARMUTH, H. (1995), Stability of Crack Propagation Associated with Fracture Energy Determined by Wedge Splitting Specimen, *Theoretical and Applied Fracture Mechanics*, Vol. 23, pp. 103-108.

HASSELMAN, D. P. H. (1969), Unified Theory of Thermal Shock Fracture Initiation and Crack Propagation in Brittle Ceramic. *J. Am. Ceram. Society.* Vol. 52, No. 11, pp. 600-604.

KINGERY, W. D. (1955), Factors Affecting Thermal Stress Resistance of Ceramic Materials, *J. Am. Ceram. Soc*. Vol. 38, No. 1, pp. 3-14.

LEE, W. E., MOORE, R. E. (1998), Evolution of in situ Refractories in the 20th Century, *J. Am. Ceram. Soc*, Vol. 81, No 6, pp. 1385-1410.

PARANSKY, Y. (2000), Non-published work.

RIEDER, K. A., TSCHEGG, E. K., HARMUTH, H. (1998), Notch Sensitivity of Ordinary Ceramic Refractory Materials, Chapman et Hall, pp. 675-678.

RIGAUD, M., HE, H., PALCO, S., PARANSKY, E. (2003), Graphite Pellets: A new Source of Carbon Designed for Castables, *Proceedings of UNITECR 2003, Osaka,* Japan, pp. 445-448

RIGAUD, M., HE, H., PALCO, S., PARANSKY, E., PASCHEK, G. (2004), Role of graphite pellets on thermo mechanical properties of basic castables, *Proceedings of the 4th International Symposium on Advances of Refractories for the Metallurgy Industry, Conference of Metallurgists 2004, Hamilton, Canada, Published by the Canadian Institute of Mining and Metallurgy, Montréal, Canada,* Accepted for publication, April 19th, 2004

RIGAUD, M., HE, H., PALCO, S. (2003), Magnesia-Graphite Cement-free Castables, *Proceedings of the 4th international symposium on refractories, Dalian, China*, pp. 21-29

RIGAUD, M., HE, H., PALCO, S. (2003), Extruded graphite pellets in magnesia-based castables, *Canadian Metallurgical Quarterly,* Vol. 42, pp. 149-156

RIGAUD, M., HE, H., PALCO, S., PARANSKY, E. (2002), Packaging Carbon into Castables, *Proceedings of the 31st Conference of ALAFAR, Bahia, Brazil*, pp. 45-56

RIGAUD, M., PALCO, S., ZHOU, N. (2002), Alumina and Magnesia based castables containing graphite: A comparison, *Iron and Steel Maker,* Vol. 10, pp. 45-51

SAKAI, M., BRADT, R. C. (1993), Fracture toughness testing of brittle materials, *International Materials Reviews*, Vol. 38, No. 2, pp. 53-78.

SAKAI, M., ICHIKAWA, H. (1992), Work-of-fracture of Brittle Materials with Microcracking and Crack Bridging. *Int. J. of Fracture*, Vol. 55. pp. 65-79.

SAKAI, M., INAGAKI, M. (1989), Dimensionless Load-Displacement Relation and Its Application to Crack Propagation Problems, *J. Am. Ceram. Soc*, Vol. 72, No. 3, pp. 388-394.

SAKAI, M. (1988), Fracture Mechanics of Refractory Materials, *Taikabutsu Overseas*, Vol. 8, No. 2, pp. 4-12.

SAKAI, M., YOSHIMURA, J., GOTO, Y., INAGAKI, M. (1988), R-Curve Behavior of Polycrystalline Graphite: Microcracking and Grain Bridging in the Wake Region, *J. Am. Ceram. Soc*., Vol. 71, No. 8, pp. 609-616.

SCHACHT, C. A. (1993), Thermomechanical Behavior of Refractories, *Key Engineering Materials*, Trans Tech Publications, Vol. 88, pp. 193-218.

SHAH, S. P., SWARTZ, S. E., OUYANG, C. (1995), Fracture Mechanics of Concrete, John Wiley & Sons, New-York, 552 pages.

SIMONIN, F. (2000), Comportement thermomécanique de bétons réfractaires alumineux contenant du spinelle de magnésium, *PhD thesis*, INSA de Lyon

TANIGOCHI, T., ISHIKAWA, M. (1988), Deformation and Fracture of Monolithic Refractories, *Taikabutsu Overseas*, Vol. 8, No. 2, pp. 19-25.

TERANISHI, H., KAWAMURA, T., YASUI, K.,IMAI, I. (1998), Applications of MgO-C castables to ladle furnace slag line, *Taikabutsu Overseas*, Vol. 18, No. 1, pp. 38-42.

TSCHEGG, E. K. (1991), New Equipment for Fracture Test on Concrete. *Materialprüfung* Vol. 33, pp. 338-342.

VENKATESWARAN, A., DONALDSON, K. Y., HASSELMAN, D. P. H. (1988). Role of Intergranular Damage-Induced Decrease in Young's Modulus in the Nonlinear Deformation and Fracture of an Alumina at Elevated Temperature. *J. Am. Ceram. Soc*. Vol. 71. No. 7. pp. 565-576.

ZHANG, S., LEE, W. (2002), Carbon containing castables: Current status and future prospects, *British Ceramic Transactions,* Vol. 101, pp. 1-8.

Appendix 1

Form factors of dimensionless compliance for various crack lengths

Table A1.1. Form factors of dimensionless compliance obtained by finite elements simulation. (Thanks to Prof. H. Harmuth, Montanuniversität Leoben)

a	Y(a)	λ(a)
0.00	6.70622146	15.12504015
2.17	6.96840477	16.41777264
4.33	7.31982679	18.21863929
6.50	7.70695179	20.24837629
8.67	8.12090868	22.50208426
10.83	8.58459528	25.01825822
13.00	9.09545541	27.83014387
15.17	9.66502279	30.99198417
17.33	10.3028814	34.56852073
19.50	11.0249602	38.63499381
21.67	11.8468825	43.35938164
23.83	12.7925061	48.74868332
26.00	13.8861901	55.08286256
28.17	15.1601471	62.60688762
30.33	16.6587238	71.6357177
32.50	18.4350053	82.58929837
34.67	20.562628	96.09754802
36.83	23.139387	113.0353533
39.00	26.2932183	134.7325418
41.17	30.0431536	163.0788688
43.33	35.2004633	200.9264647
45.50	41.5695459	253.0872058
47.67	50.2096518	328.1874746
49.83	61.9874314	438.2482133
52.00	78.9727557	612.4206447
54.17	104.928054	907.6773863

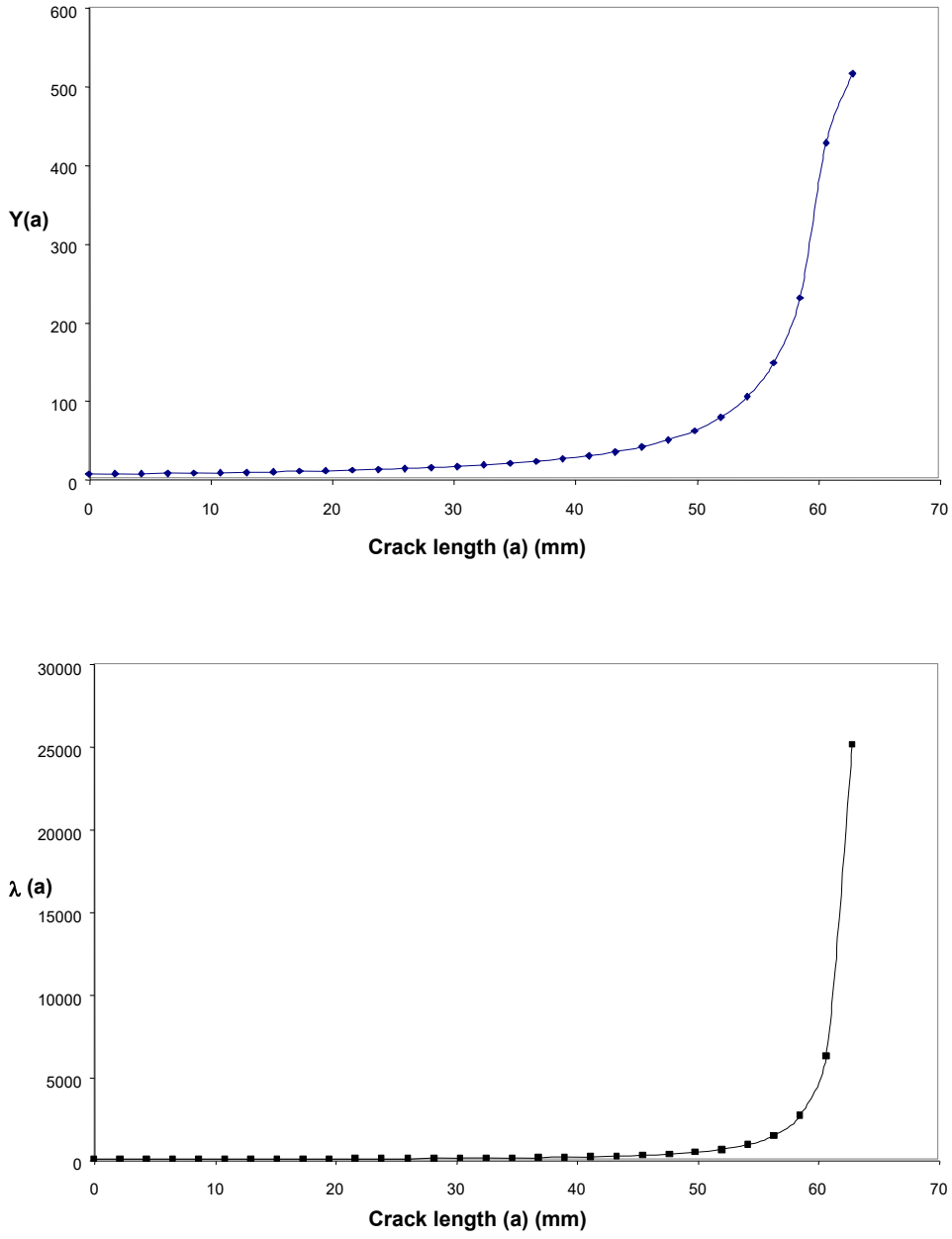

Figure A1.1. Variations of *Y(a)* and *λ(a)* as function of the crack length *a*.

Appendix 2

Comparison of the test results

Table A2.1. Comparison of the mechanical properties of group 1's castables

Castable	1	2	3	4	5	6	7
Note	0% Pellets	3% Pellets	5% Pellets, Reference	7% Pellets	9% Pellets	5% Pellets, max. Grainsize MgO <3	5% Long Pellets
E-Modulus/HMOR							
max. Load, (N)	5714,66	4570,04	4325,36	4156,43	3535,29	6962,09	4682,27
max. Stress, (MPa)	16,99	13,69	12,87	11,99	10,23	20,52	13,93
E-Modulus, (GPa)	5,13	4,34	4,73	2,75	3,48	6,61	5,33
WST							
max. Load, (N)	1137,67	1068,51	1077,55	1018,21	961,46	1150,90	1106,3
max. Stress, (MPa)	11,6	10,9	11,0	10,4	9,8	11,8	11,3
K_{IC}, (MPa $(m)^{1/2}$)	2,3	2,2	2,2	2,1	1,9	2,3	2,2
WOF, (J/m^2)	935	901	662	673	448	614	653
Porosity							
P, (%)	12,27	14,57	18,14	17,74	19,30	18,20	15,78
BD, (g/cm^3)	3,01	2,90	2,75	2,74	2,66	2,74	2,83
dyn. Elasticity							
E-Flexure, (GPa)	55	56	46	46	41	59	47
E-Longitudinal, (GPa)	56	51	42	42	36	43	47
G-Torsion, (GPa)	27	26	19	21	14	26	22
linear Variation							
LV, (%)	0,21	0,11	-0,03	0,09	-0,19	0,08	0,04

Table A2.2. Comparison of the mechanical properties of group 2 and group 3's castables

Castable	8	9	10	11	12	13
Note	1% Flake Graphite	2,5% Flake Graphite	4,5% Flake Graphite	1% Fine Carbon, 5% Pellets	2% Fine Carbon, 5% Pellets	4% Fine Carbon, 5% Pellets
E-Modulus/HMOR						
max. Load, (N)	4473,09	3426,59	1667,74	4149,58	4144,10	3264,92
max. Stress, (MPa)	13,64	10,35	4,95	12,24	12,65	9,69
E-Modulus, (GPa)	5,47	3,52	1,99	4,87	4,97	3,10
WST						
max. Load, (N)	938,80	739,11	547,65	872,84	739,70	504,90
max. Stress, (MPa)	9,6	7,6	5,6	8,9	7,6	5,2
K_{IC}, (MPa (m)$^{1/2}$)	1,9	1,5	1,1	1,8	1,5	1,0
WOF, (J/m^2)	576	454	367	599	581	437
Porosity						
P, (%)	13,71	17,93	21,24	17,80	16,45	16,88
BD, (g/cm^3)	2,95	2,76	2,63	2,75	2,77	2,71
dyn. Elasticity						
E-Flexure, (GPa)	52	38	32	44	49	35
E-Longitudinal, (GPa)	50	34	31	40	43	30
G-Torsion, (GPa)	24	17	15	21	23	16
linear Variation						
LV, (%)	0,07	-0,18	0,12	-0,11	0,01	0,04

Table A2.3. Comparison of the mechanical properties of group 4's castables and the brick

Castable	14	15	16
Note	0% Pellets, 0% Si	5% Pellets, 2% Si	Brick: 5% Carbon
E-Modulus/HMOR			
max. Load, (N)	2052,11	3360,60	n.a.
max. Stress, (MPa)	6,55	9,87	20,01
E-Modulus, (GPa)	3,25	3,99	n.a.
WST			
max. Load, (N)	201,44	546,92	1120,40
max. Stress, (MPa)	2,1	5,6	11,5
K_{IC}, (MPa (m)$^{1/2}$)	0,4	1,1	2,3
WOF, (J/m^2)	195	427	654
Porosity			
P, (%)	15,11	16,19	11,00
BD, (g/cm^3)	2,97	2,81	2,94
dyn. Elasticity			
E-Flexure, (GPa)	81	54	n.a.
E-Longitudinal, (GPa)	88	51	n.a.
G-Torsion, (GPa)	40	24	n.a.
linear Variation			
LV, (%)	0,06	0,02	n.a.